

THE MECHANICAL PROPERTIES OF DILUTE ZINC - TITANIUM ALLOYS

by

ROBERT JAMES WALDRON

B.A.Sc., University of British Columbia, 1965

A THESIS SUBMITTED IN PARTIAL FULFILMENT OF
THE REQUIREMENTS FOR THE DEGREE OF
DOCTOR OF PHILOSOPHY

in the Department
of
METALLURGY

We accept this thesis as conforming
to the required standard

THE UNIVERSITY OF BRITISH COLUMBIA
April, 1970

In presenting this thesis in partial fulfilment of the requirements for an advanced degree at the University of British Columbia, I agree that the Library shall make it freely available for reference and study.

I further agree that permission for extensive copying of this thesis for scholarly purposes may be granted by the Head of my Department or by his representatives. It is understood that copying or publication of this thesis for financial gain shall not be allowed without my written permission.

Department of

Metallurgy

The University of British Columbia
Vancouver 8, Canada

Date

May 8, 1970

ABSTRACT

Zinc-titanium alloys (0.07-0.6 wt.%Ti.) in the form of compacted powder and chill castings have been extruded at temperatures between 150°C and 350°C. The mechanical properties of these alloys have been studied as a function of temperature, strain rate, grain size and intermetallic ($Zn_{15}Ti$) distribution.

Due to a high value of "k" in the Hall-Petch relationship, maximum strengthening is obtained by a reduction in grain size. However because of an increasing amount of grain boundary shear, this potential is not realized. The operation of dynamic recovery mechanisms at 20°C and higher also results in limitations upon the development of high strength.

The use of powder metallurgical techniques gives rise to the formation of intermetallic distributions which inhibit these processes and results in high strength (>60,000 p.s.i.) and low strain rate sensitivity ($m \sim 0.02$). The mechanical properties are not a function of initial powder size. The properties obtained using chill castings do not reach these levels due to the difficulty associated with forming a fine second phase on solidification. Such a distribution is required to obtain a small stable grain size during subsequent extrusion.

To satisfy compatibility requirements deformation modes other than the two supplied by basal slip must be invoked. High strengths are observed when grain boundary shear and migration are inhibited by the distribution of the second phase or by orientation effects. Under such conditions, non basal slip and basal slip are the operative deformation mechanisms. Significantly lower strengths result if grain boundary shear and basal slip satisfy the conditions necessary for ductile behaviour.

The strain rate sensitivity parameter at 20°C lies in the range 0.02–0.07. Varying amounts of grain boundary shear occur, nevertheless deformation is slip controlled.

Increased strain rate sensitivities are observed at high temperatures, but failure by cavitation limits ductility. The strain rate sensitivity is not a function of titanium concentration. Under constant fabrication conditions the strength generally increases with increased Zn₁₅Ti content.

The thermal stability of the intermetallic distribution prescribes the fabrication conditions which must be used to develop high strength, and the temperature to which the mechanical properties can be retained. The high strength microstructures appear to be stable up to at least 150°C for short periods of time.

ACKNOWLEDGEMENTS

The author is grateful for the advice and encouragement given by his director, Dr. N.R. Risebrough. Many of the faculty, staff and students of the Department of Metallurgy contributed helpful suggestions. The author also wishes to thank two great families for their support - the Waldrons and the Cramonds.

Financial assistance provided by the Aluminum Company of Canada and the National Research Council of Canada is gratefully acknowledged.

TABLE OF CONTENTS

	<u>PAGE</u>
1. INTRODUCTION	1
2. PROCEDURE	7
2.1 Starting Materials	7
2.2 Melting Procedures	7
2.3 Atomizing	9
2.4 Construction of the Atomizer	11
2.5 Compaction	11
2.6 Extrusion	12
2.7 Tensile Specimen Preparation	15
2.8 Metallography	16
2.9 Testing Procedures	17
3. ZINC - TITANIUM PHASE DIAGRAM	21
4. RESULTS	25
4.1 Reproducibility	25
4.2 Effect of Extrusion Temperature	25
4.3 Chill Cast and Powder Microstructures	31
4.3.1 Microstructure of Cast Billets	31
4.3.2 Microstructure of Powder	34
4.3.3 Extent of Oxidation of Atomized Powder	38
4.4 Microstructural Characteristics of Extruded Alloys	42
4.4.1 Stringering During Extrusion of Powders	42
4.4.2 Cast Material	45
4.5 The Effect of Extrusion Ratio	52
4.6 Importance of Preferred Orientation	52

	<u>PAGE</u>
4.7 Thermal Stability	54
4.7.1 Introduction	54
4.7.2 Effect of Extrusion Temperature	55
4.7.3 Effect of Annealing Temperature	59
4.7.3.1 Powder Material	59
4.7.3.2 True Stress - Strain Curves	65
4.7.3.3 Annealed Cast-Extruded Zn-Ti Alloys	69
4.8 The Effect of Titanium Concentration	70
4.8.1 Powder Material	70
4.8.2 Cast Material	76
4.8.3 Ductility	76
4.9 Deformation Characteristics	77
4.9.1 Introduction	77
4.9.2 Deformation Mechanisms	77
4.9.2.1 Slip	77
4.9.2.2 Twinning	77
4.9.2.3 Grain Boundary Shear	79
4.9.3 Recovery Mechanisms	80
4.9.3.1 Introduction	80
4.9.3.2 Grain Boundary Migration	80
4.9.3.3 Dislocation Climb	82
4.9.4 The Occurrence and Importance of Substructure in Zinc	82
4.10 Strain-Rate Sensitivity	83
4.10.1 Introduction	83
4.10.2 Deformation of Pure Zinc	85
4.10.3 Deformation of Zinc-Titanium Alloys	88
4.10.3.1 Strain-Rate Sensitivity	88

	<u>PAGE</u>
4.10.3.2 Ductility	94
4.11 High Temperature Deformation Characteristics	95
4.11.1 Deformation of Zinc-Titanium and Zinc-Aluminum Alloys	95
4.11.1.1 Introduction	95
4.11.1.2 Effect of Temperature on the Flow Stress - Strain-Rate Relationship	96
4.11.1.3 Ductility and Fracture Mechanisms	99
4.11.1.4 Activation Energy Analysis	104
4.11.2 Yield Stress Dependence on Temperature	106
4.12 Hall-Petch Analysis	110
4.12.1 Introduction	110
4.12.2 Petch Equation and Hexagonal Metals	111
4.12.3 Modifications of the Petch Analysis	112
4.12.4 Petch Analysis and Zinc-Titanium Alloys	113
4.12.4.1 Flow at -100°C	113
4.12.4.2 Flow at 20°C	115
4.12.4.2.1 Stringered Alloys	115
4.12.4.2.2 Unstringered Alloys	116
4.12.5 Value of σ_0	117
5. SUMMARY	119
5.1 Introduction	119
5.2 Deformation Characteristics	119
5.2.1 Strength	119
5.2.2 Strain-Rate Sensitivity	121
5.2.3 Dynamic Recovery	122
5.2.4 Ductility and Fracture	123

	<u>PAGE</u>
5.3 Thermal Stability	124
5.4 Other Considerations	
6. CONCLUSIONS	126
7. BIBLIOGRAPHY	127

LIST OF FIGURES

		<u>PAGE</u>
Fig. 1	Hypothetical phase diagram.	5
Fig. 2	Schematic representation of the atomizing apparatus.	10
Fig. 3	Schematic representation of the extrusion apparatus.	13
Fig. 4	Standardized extrusion time - temperature conditions.	14
Fig. 5	Zn - 0.6 wt.% Ti alloy extruded from -35 + 100 mesh powder at 150°C - transmission technique.	18
Fig. 6	Zn - 0.6 wt.% Ti alloy extruded from -35 + 100 mesh powder at 150°C - replication technique.	19
Fig. 7	Zinc - titanium phase diagrams.	23
Fig. 8	Zinc rich end of the zinc-titanium phase diagram.	24
Fig. 9	The effect of extrusion temperature on the yield strength of Zn - 0.6 wt.% Ti alloys.	28
Fig. 10	The effect of extrusion temperature on the ductility of Zn - 0.6 wt.% Ti alloys.	29
Fig. 11	Zn - 0.36 wt.% Ti alloy chill cast microstructure.	32
Fig. 12	(a) Electron microprobe absorbed electron image of Zn - 0.36 wt.% Ti chill cast microstructure.	33
	(b) Ti X-ray scan of Zn - 0.36 wt.% Ti chill cast microstructure.	33
Fig. 13	Microstructural characteristics of the eutectic in a chill cast Zn - 0.36 wt.% Ti alloy.	35
Fig. 14	Chill cast microstructure of Zn - 0.6 wt.% Ti alloy.	36
Fig. 15	Electron micrograph of the eutectic structure in -35 + 100 mesh Zn - 0.6 wt.% Ti powder.	37
Fig. 16	(a) Absorbed electron image from an electron microprobe analysis of -35 + 100 mesh Zn - 0.6 wt.% Ti powder.	39
	(b) Ti X-ray scan from an electron microprobe analysis of -35 + 100 mesh Zn - 0.6 wt.% Ti powder.	39

	<u>PAGE</u>
Fig. 17 Electron microprobe analysis of Zn - 0.6 wt.% Ti -35 + 100 mesh powder compact: (a) Absorbed electron image	40
(b) Ti X-ray scan	40
(c) O ₂ X-ray scan.	41
Fig. 18 Microstructure of a Zn - 0.6 wt.% Ti alloy extruded at 150°C using -35 + 100 mesh powder.	43
Fig. 19 Microstructure of a Zn - 0.6 wt.% Ti alloy extruded at 250°C using -35 + 100 mesh powder.	43
Fig. 20 Microstructure of a Zn - 0.6 wt.% Ti alloy extruded at 350°C using -35 + 100 mesh powder.	44
Fig. 21 The origin of the stringered structure in a Zn - 0.6 wt.% Ti alloy fabricated from -35 + 100 mesh powder at 175°C.	46
Fig. 22 The origin of the stringered structure in a Zn - 0.6 wt.% Ti alloy fabricated from -35 + 100 mesh powder at 175°C.	47
Fig. 23 Electron microprobe analysis of Zn - 0.6 wt.% Ti alloy extruded at 250°C using -35 + 100 mesh powder:	
(a) Absorbed electron image	48
(b) Ti X-ray scan	48
(c) Zn X-ray scan.	49
(d) O ₂ X-ray scan.	49
Fig. 24 Microstructure of a chill cast Zn - 0.6 wt.% Ti alloy extruded at 150°C.	50
Fig. 25 Microstructure of a chill cast Zn - 0.6 wt.% Ti alloy extruded at 250°C.	50
Fig. 26 Microstructure of a chill cast Zn - 0.6 wt.% Ti alloy extruded at 350°C.	51
Fig. 27 The effect of extrusion ratio on the yield stress of Zn - 0.6 wt.% Ti alloys extruded at 175°C using -35 + 100 mesh powder.	53
Fig. 28 The structure and mechanical properties of a Zn - 0.6 wt.% Ti alloy extruded at 175°C using -35 + 100 mesh powder.	57
Fig. 29 The effect of extrusion temperature on the yield stress of a thermally stabilized Zn - 0.6 wt.% Ti alloy.	58
Fig. 30 (a) The microstructure resulting from extrusion of a -100 + 200 mesh powder billet annealed for 1 hour prior to extrusion at 150°C.	60
(b) The microstructure resulting from extrusion of a -100 + 200 mesh powder billet annealed for 1 hour prior to extrusion at 350°C.	60

Fig. 31	The effect of annealing temperature on the yield strength of Zn - 0.6 wt.% Ti alloy at 20°C.	62
Fig. 32	The effect of annealing temperature on the ductility of Zn - 0.6 wt.% Ti alloy at 20°C.	63
Fig. 33	The microstructure resulting from a short term anneal at 180°C of a Zn - 0.6 wt.% Ti alloy fabricated at 175°C using -35 + 100 mesh powder.	64
Fig. 34	The microstructure of a Zn - 0.6 wt.% Ti alloy fabricated at 175°C from -35 + 100 mesh powder and annealed for 44 hours at 350°C.	66
Fig. 35	The microstructure of a Zn - 0.6 wt.% Ti alloy fabricated at 175°C from -35 + 100 mesh powder and annealed for 94 hours at 400°C.	66
Fig. 36	The effect of annealing temperature on the true stress - strain relationship at 20°C for Zn - 0.6 wt.% Ti alloys extruded at 175°C using -35 + 100 mesh powder.	67
Fig. 37	True stress - strain curves for zinc-titanium extrusions of -35 + 100 mesh powder at 175°C.	72
Fig. 38	True stress - strain curves for zinc-titanium extrusions of -35 + 100 mesh powder at 350°C.	73
Fig. 39	True stress - strain curves for zinc-titanium extrusions of chill castings at 175°C.	74
Fig. 40	True stress - strain curves for zinc-titanium extrusions of chill castings at 350°C.	75
Fig. 41	Metallographic evidence of non-basal slip in a chill cast Zn - 0.32 wt.% Ti alloy extruded at 175°C.	78
Fig. 42	Metallographic evidence of twinning in a chill cast Zn - 0.16 wt.% Ti alloy extruded at 175°C.	78
Fig. 43	Metallographic evidence of grain boundary shear and migration in a chill cast Zn - 0.32 wt.% Ti alloy extruded at 350°C.	81
Fig. 44	Metallographic evidence of grain boundary shear and migration in a chill cast Zn - 0.32 wt.% Ti alloy extruded at 350°C.	81
Fig. 45	Metallographic evidence of substructure in a chill cast Zn - 0.16 wt.% Ti alloy extruded at 175°C.	84

	<u>PAGE</u>
Fig. 46 The flow stress - yield dependence on strain-rate of zinc fabricated from -325 mesh powder at room temperature.	86
Fig. 47 The variation of "m" with strain-rate for pure zinc fabricated from -325 mesh powder.	87
Fig. 48 The strain-rate sensitivity of zinc-titanium alloys fabricated from -35 + 100 mesh powder at 175°C.	89
Fig. 49 The strain-rate sensitivity of zinc-titanium alloys fabricated from -35 + 100 mesh powder at 350°C.	90
Fig. 50 The strain-rate sensitivity of zinc-titanium alloys fabricated from chill castings at 175°C.	91
Fig. 51 The strain-rate sensitivity of zinc-titanium alloys fabricated from chill castings at 350°C.	92
Fig. 52 The microstructure of a Zn - 0.2 wt.% Al alloy, cast and extruded at 150°C.	97
Fig. 53 The microstructure of a Zn - 0.07 wt.% Ti alloy extruded at 350°C using -35 + 100 mesh powder.	97
Fig. 54 The effect of temperature on the flow stress - strain-rate relationship for Zn - 0.07 wt.% Ti alloys extruded at 350°C using -35 + 100 mesh powder.	98
Fig. 55 Cavitation failure at 300°C in a Zn - 0.07 wt.% Ti alloy extruded at 350°C using -35 + 100 mesh powder.	101
Fig. 56 Scanning electron micrograph of cavitation failure at 300°C in a Zn - 0.07 wt.% Ti alloy extruded at 350°C using -35 + 100 mesh powder: (a) Reflected electrons (b) Secondary electrons.	102
Fig. 57 Schematic representation of cavitation due to the presence of second phase particles on a grain boundary.	103
Fig. 58 Arrhenius plot for Zn - 0.07 wt.% Ti alloy extruded at 350°C using -35 + 100 mesh powder.	107
Fig. 59 The dependence of yield stress on temperature of a thermally stabilized Zn - 0.6 wt.% Ti alloy.	108
Fig. 60 The effect of temperature on the flow stress - strain-rate relationship of a thermally stabilized Zn - 0.6 wt.% Ti alloy.	109
Fig. 61 The Hall-Petch plot for zinc-titanium alloys.	114

LIST OF TABLES

	<u>PAGE</u>
Table I. Composition of Extruded Materials.	8
Table II. Summary of the Experimental Investigations of the Zinc Rich End of the Zinc-Titanium Phase Diagram.	22
Table III. Reproducibility of Mechanical Properties Along Extrusions.	26
Table IV. The Effect of Powder Size on the Mechanical Properties of Zn - 0.6 wt.% Ti Alloys.	30
Table V. Mechanical Properties of -35 + 100 Mesh Zn - 0.6 wt.% Ti Powder Extruded at 175°C and Annealed at Various Temperatures.	68
Table VI. The Effect of Titanium Concentration on Mechanical Properties.	71
Table VII. Summary of Strain-Rate Sensitivity Parameters and the Variables Affecting these Parameters for Zn - 0.16 wt.% Ti Alloys.	93

1. INTRODUCTION

Considerable effort has been made to improve the mechanical properties of metals at elevated temperatures through the introduction of one or more secondary phases into the metal matrix. Research along these lines has led to the development of multiphase alloys (dispersion strengthened alloys) which retain their strength at elevated temperatures and have superior creep rupture characteristics.⁽¹⁻³⁾ The definition of dispersion strengthening varies somewhat in the literature. However a dispersion strengthened alloy is generally considered to consist of a structure of fine, non-coherent second phase particles which are randomly distributed in a pure metal matrix or solid solution. Thus conventional strengthening is usually defined in terms of retardation of dislocation motion. As a result, models developed to explain this type of hardening are based on the description of the size, amount, and spacing of obstacles to dislocation motion.⁽¹⁻⁵⁾ This approach describes hardening quite adequately when reasonably large grain sizes are involved, or when the dispersoid spacing is small in comparison with the grain size, but it leads to an incomplete analysis as the grain size is reduced. This suggests that grain boundaries must be considered in order to explain the role of second phase additions.

Although dispersion hardening has been discussed at length in the literature, little is known about the individual contribution of such variables as grain size, mechanical properties of secondary additions, volume fraction, size and distribution of the dispersoid, etc. The basic understanding of the effect of these variables is thought

to be the approach to the development of even more effective alloys.

The dispersion strengthening of zinc presents some rather unique problems as a result of its low melting point and consequent high effective temperature at room temperature. ($T_H = T/T_m = 0.42$) Dynamic recovery mechanisms such as dislocation climb and grain boundary migration occur readily at 20°C. (6) The result is that zinc does not work harden appreciably and has poor creep properties at normal temperatures. Although the mechanical properties have been enhanced markedly by means of alloying, conventional hardening techniques, which are successful in other metal systems, are often ineffective when applied to zinc.

The development of wrought zinc alloys has been inspired by possible commercial competition with aluminum and copper alloys and has led to the industrial use of such alloys as Zn-Cu-Ti and Zn-Ti. (7,8,9) Little is known regarding the basic deformation and recovery characteristics of these alloys, or the role of the dispersoid.

At low temperatures where the grain boundaries may be considered "hard", the strength of zinc is expected to increase as the grain size is decreased. Essentially this behavior has been related to the operation of grain boundaries as effective barriers to dislocation movement. This effect is usually analyzed by means of the Hall-Petch relationship which relates the yield stress and grain size according to the expression:

$$\tau_y = \tau_0 + kd^{-1/2}$$

where τ_y is the yield stress, k and τ_0 are constants, and d is the grain size. The high "k" values observed for zinc suggest high strengthening potential. However at fine grain sizes,

grain boundaries may become the reason for decreased strength rather than increased strength. As a consequence of the high homologous temperature, grain boundary shear can occur readily at ambient temperatures. Thus grain refinement will result in the improvement of the mechanical properties of a metal or alloy only if the boundaries remain immobile. This suggests that the development of high strength alloys is at least in part dependent on achieving a small stable grain structure and a fine stable dispersoid. In terms of zinc alloys it is thought that the microstructure should remain stable up to at least 75°C before the alloy could be of any commercial importance. Increased interest in high temperature creep properties and superplastic deformation has led to an effort to define more clearly the role and characteristics of grain boundary deformation. (10-23)

Many different approaches have been taken in order to develop a small grain size and second phase dispersion. (2) These include:

- a) Solid state transformations
- b) Gas-metal reactions
- c) Precipitation from liquids during solidification
- d) Powder metallurgical techniques.

The use of powder or particulate metallurgical techniques has proved to be applicable to zinc alloys. These techniques have been applied to many dilute zinc alloy compositions with a wide range of mechanical properties. (8,9,25-27)

The development of alloys hardened by dispersed intermetallic compounds through the application of powder metallurgical procedures has been the most successful approach from the point of view of the development of high strength and desirable creep properties. The solidification

or atomization of suitable alloys from a hypothetical system such as is shown in Fig. 1 has been shown to be advantageous.⁽⁸⁾ Solidification of a dilute alloy from this type of system will result in a structure consisting of a dispersion of intermetallic compound in a zinc matrix. Some of the more important features which must be considered when using this approach are:

a) Solid solution effects - The effect of solid solution on recovery processes is not clearly established; however it appears as though little retardation of dynamic recovery processes occurs.

b) Thermal stability - The intermetallic compound must be stable at normal useful temperatures.

c) Intermetallic composition - It is of distinct commercial advantage for the intermetallic to be of a high zinc content so that a large volume fraction of intermetallic is formed with only dilute alloy additions.

d) Mechanical properties of the intermetallic compound - The intermetallic should remain "hard" relative to the matrix at ordinary temperatures; this is thought to be a prerequisite for grain boundary stabilization.

The actual intermetallic dispersion will be a sensitive function of cooling rate and subsequent mechanical working. Rapid cooling rates and large amounts of working promote a finer dispersion. Fragmentation of an alloy melt by means of atomization results in a very rapid solidification rate and usually a fine intermetallic dispersion and grain size.

A system which fulfills these requirements and has received some attention is the zinc-titanium system.^(8,9,27,28,29) The limited

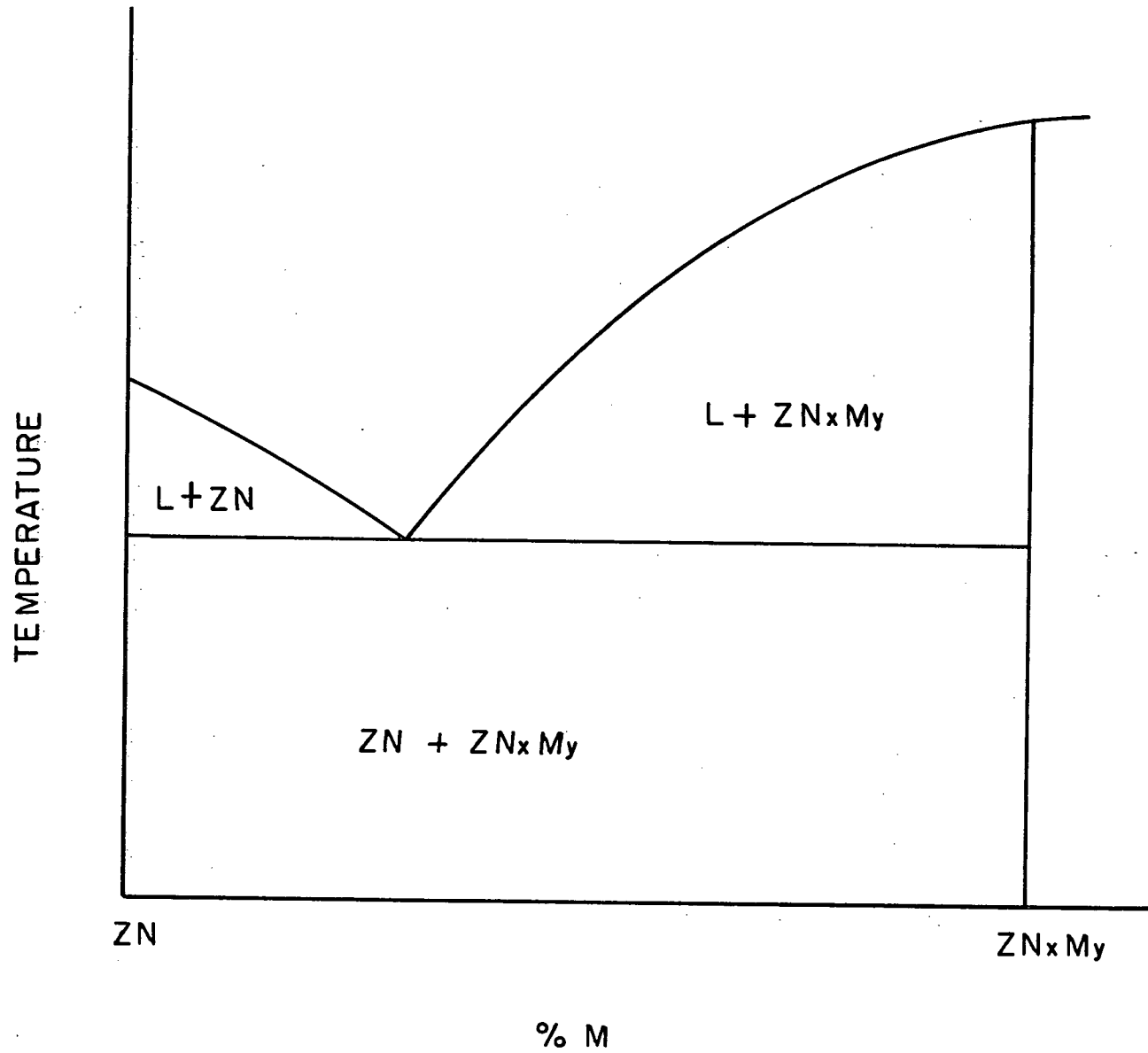


Fig. 1 Hypothetical phase diagram.

amount of investigation which has been carried out using dilute zinc-titanium alloys suggests that high strength and excellent creep properties can be obtained. The work to date suggests that the major requirement is the development of a fine-grained alloy, the potential strength of which may be realized by the selective location of a fine second phase so that the grain boundaries are stabilized. The necessity that the second phase be preferentially located at grain boundaries is a unique requirement in comparison with conventional dispersion-strengthened alloys. The purpose of this work is to attempt to define the microstructural criteria for high strength and good creep resistance in zinc alloys.

The approach involved the correlation of microstructures and mechanical properties in terms of the mechanisms responsible for deformation and recovery. A wide range of solidification and extrusion conditions were used to produce differing combinations of grain size, intermetallic size, and intermetallic distribution with titanium concentrations of up to 0.6 wt.%.

2. PROCEDURE

2.1 Starting Materials

All alloys used in this study were made by dilution of a zinc - 3 wt.% titanium master alloy supplied by Cominco Limited, Sheridan Park, Ontario. Adjustment to the desired alloy composition was carried out using SHG (Special High Grade) zinc. Since one of the purposes of this work was to obtain technical information which could be used in practical applications, this grade of zinc was chosen because of its wide industrial use.

As is shown in Table I, the impurity levels in the extruded materials are low. It is thought that the effect of these impurities on the mechanical properties of the alloys would be negligible in comparison with the effect of the titanium present.

2.2 Melting Procedures

Prior to melting, both the master alloy and the zinc additives were precleaned in a dilute hydrochloric acid solution. The alloys were melted in ten pound batches. The pure zinc component was melted in a silicon carbide crucible heated in a gas-fired furnace. To prevent excessive oxidation of either the zinc or the titanium, a cover consisting of equal weights of potassium chloride and sodium chloride was used on the melt. Additions of the master alloy were made through the molten cover. This procedure proved to be reasonably effective and allowed close control of the final alloy composition. The nominal and final titanium concentrations of the alloys used in this study were:

Material	Extrusion Temperature (°C)	Spec. Analysis (wt. %)				
		Ti	Cu	Ag	Pb	Fe
-35 + 100 mesh powder	350	0.32	0.1*	0.1*	0.001	0.01
Chill Cast	350	0.32	0.1*	0.1*	0.001	0.001

Mg, Be, As, Cr, Ni, Si, Al, Mo, Sn, Sr, Ca, Co, Bi not detected.

* X-ray Fluorescence Analysis indicates these values are high.
The true values are less than 0.01 and probably less than
0.001 wt. %.

TABLE I Composition of Extruded Materials.

Nominal wt.% Ti	Analyzed wt.% Ti
0.10	0.07
0.20	0.16
0.30	0.32
0.60	0.60

The melt was held at 700°C for a minimum of thirty minutes during which time it was agitated at five minute intervals.

After allowing the melt to cool to approximately 600°C and thus freeze the salt cover to prevent contamination during pouring, three chill cast billets were obtained by casting into graphite molds. The remainder of the melt was immediately transferred to a preheated atomizing crucible. Atomization was initiated when the melt stabilized at 600°C.

2.3 Atomizing

The purpose of fragmenting the melt by this procedure was to provide a very rapid cooling rate so as to produce a fine grain size and intermetallic dispersion.

Several atomizer designs were tested; however the common problem was that little control over the product size distribution could be maintained. The final design of the apparatus (Fig. 2) provided the necessary control and allowed for the production of an extremely wide range of particle sizes, ranging from essentially all shotted (+35 mesh) material to approximately 50% -325 mesh .

Basically the nozzle fragments the melt by means of a concentric gas blast around the alloy surface. Argon was used for atomization so that oxidation of the product could be minimized.

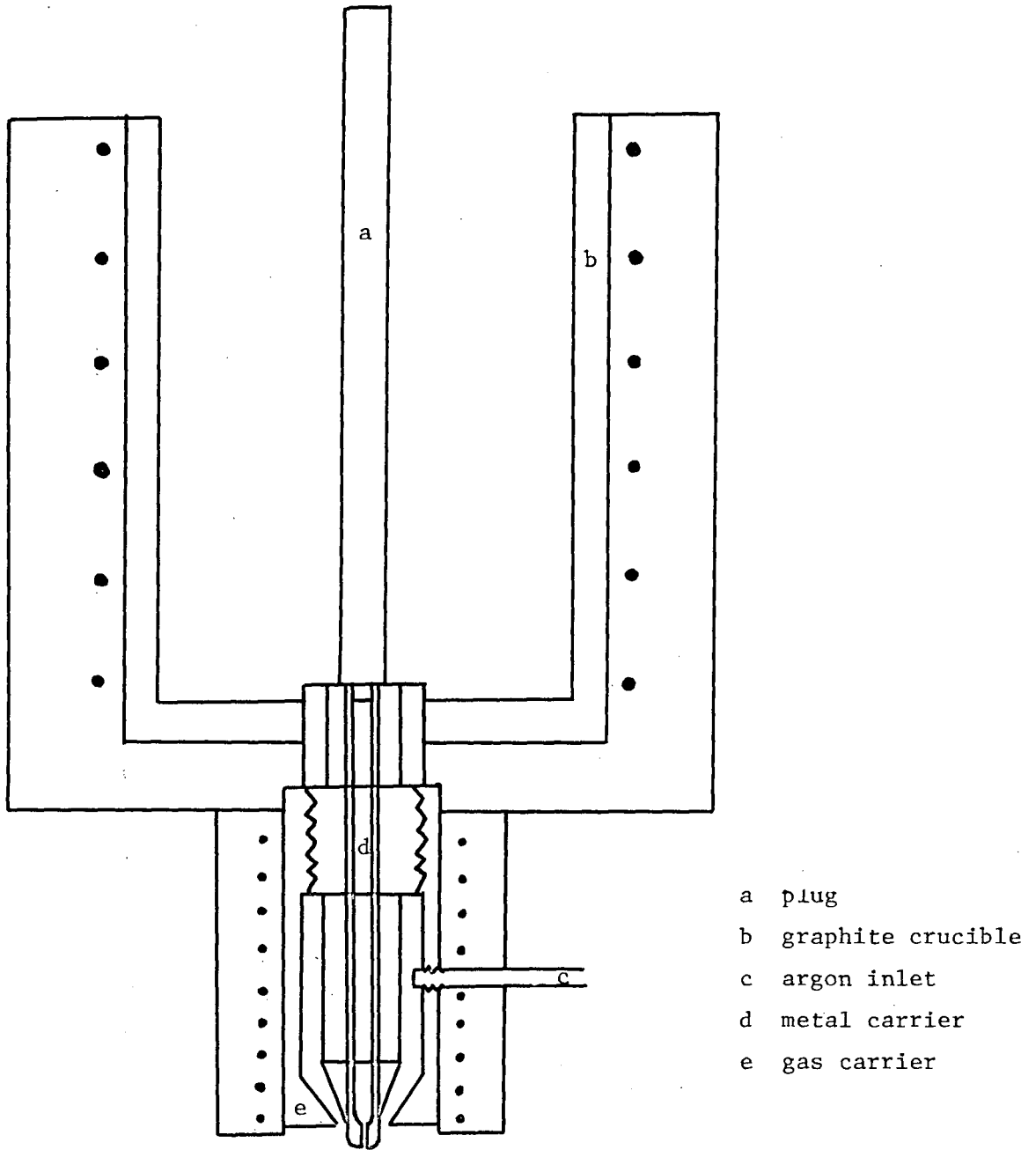


Fig. 2 Schematic representation of the atomizing apparatus.

The product size was controlled by adjustment of one or more of the following:

- a) argon pressure
- b) size of the argon outlet
- c) size of the molten metal orifice
- d) location of the molten metal orifice with respect to the argon outlet.

2.4 Construction of the Atomizer

The apparatus consists of a two piece stainless steel nozzle press fitted into a graphite crucible. The crucible and nozzle were heated and controlled independently. The nozzle itself had two prime functions: one section served as a gas carrier and the other as a molten metal carrier. The inner core of metal-carrying section was lined with a graphite sleeve which was replaced after each atomization.

The atomized melt was impinged onto a cold water bath to facilitate collection, and to ensure complete solidification at a maximum rate.

The product was filtered and then dried for approximately 20 hours at 80°C prior to grading as to size.

2.5 Compaction

Prior to extrusion, all powder was compacted into billets suitable for extrusion. Hydrostatic (isostatic) compaction was used since a sound uncontaminated billet easily accommodated by the extrusion apparatus could be produced at the relatively low pressure of 30,000 p.s.i.

2.6 Extrusion

Fully dense rod of varying diameters was produced by an indirect extrusion technique using the apparatus shown in Fig. 3. Unless otherwise specified, the data in this work pertains to an extrusion ratio of 25:1 and corresponds to an extrusion product 0.150 inches in diameter. The extrusion temperature varied between 150°C and 350°C.

Because of the high extrusion pressures which were required (up to 330,000 p.s.i.), it was considered impractical to place a thermocouple close to the billet cavity as any suitable well would structurally weaken the apparatus and thus put an unnecessary limitation on the operating pressure. It was also desirable to minimize the soaking time of the billet in order to prevent excessive coarsening of the grain size and intermetallic compound. Therefore a series of preliminary experiments were undertaken using a dummy billet containing a thermocouple. The procedure involved plotting the billet temperature after insertion into the preheated extrusion cavity. A series of standard curves for the desired extrusion temperature were plotted in order to establish the minimum soaking time required for the billet to reach the required temperature. An example of such a curve is shown as Fig. 4. It can be seen from this graph that for extrusion at 250°C, the billet should be soaked for at least 7 minutes, and further that the extrusion should be completed within 15 minutes. The purpose of this procedure was to standardize the fabrication conditions. Complex temperature gradients undoubtedly exist in the extrusion apparatus and billet; thus accurate extrusion temperatures per se are difficult to obtain.

Quoted extrusion pressures are of limited quantitative meaning as these pressures depend to a great extent on the condition of

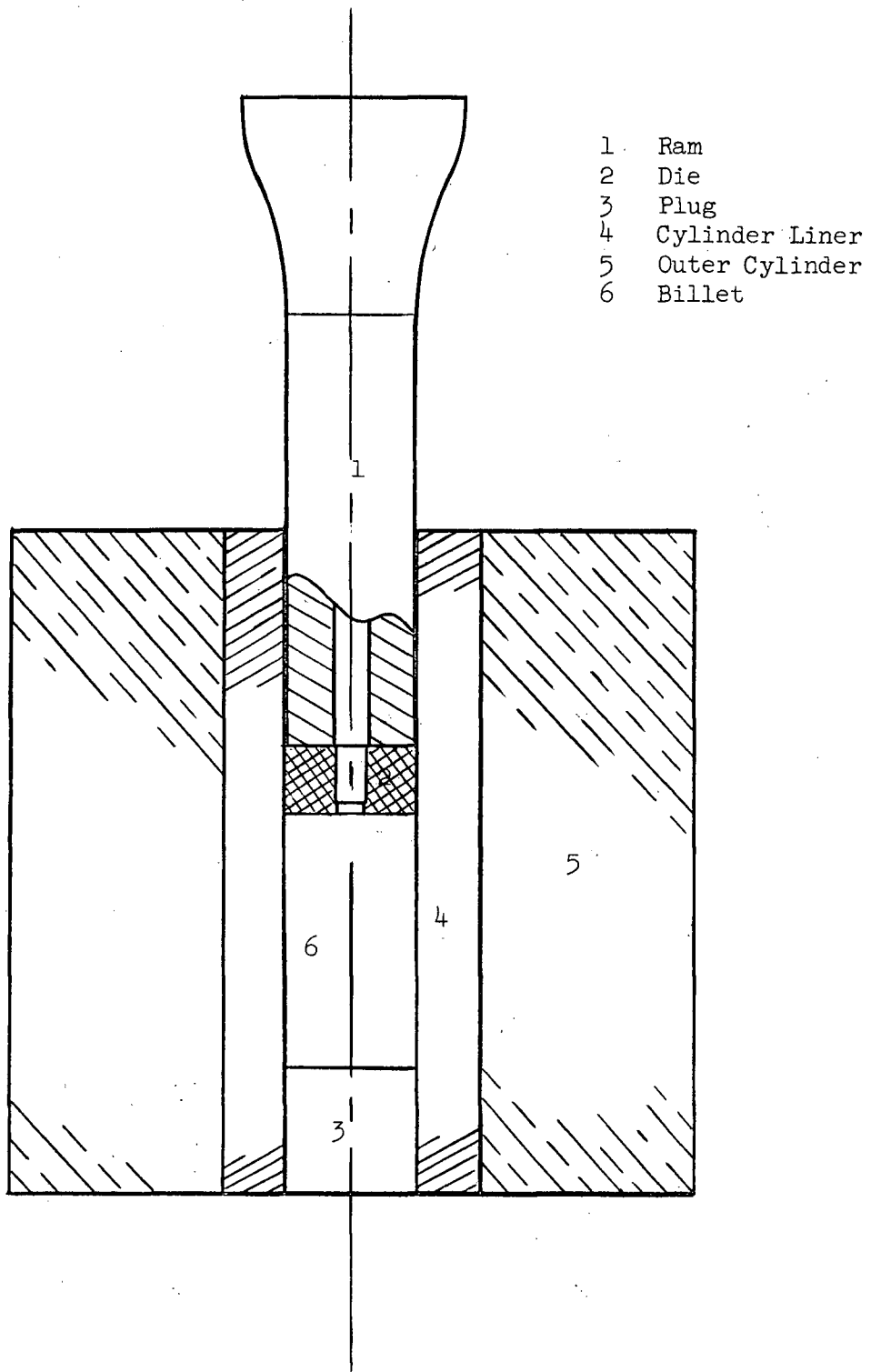


Fig. 3 Schematic representation of the extrusion apparatus.

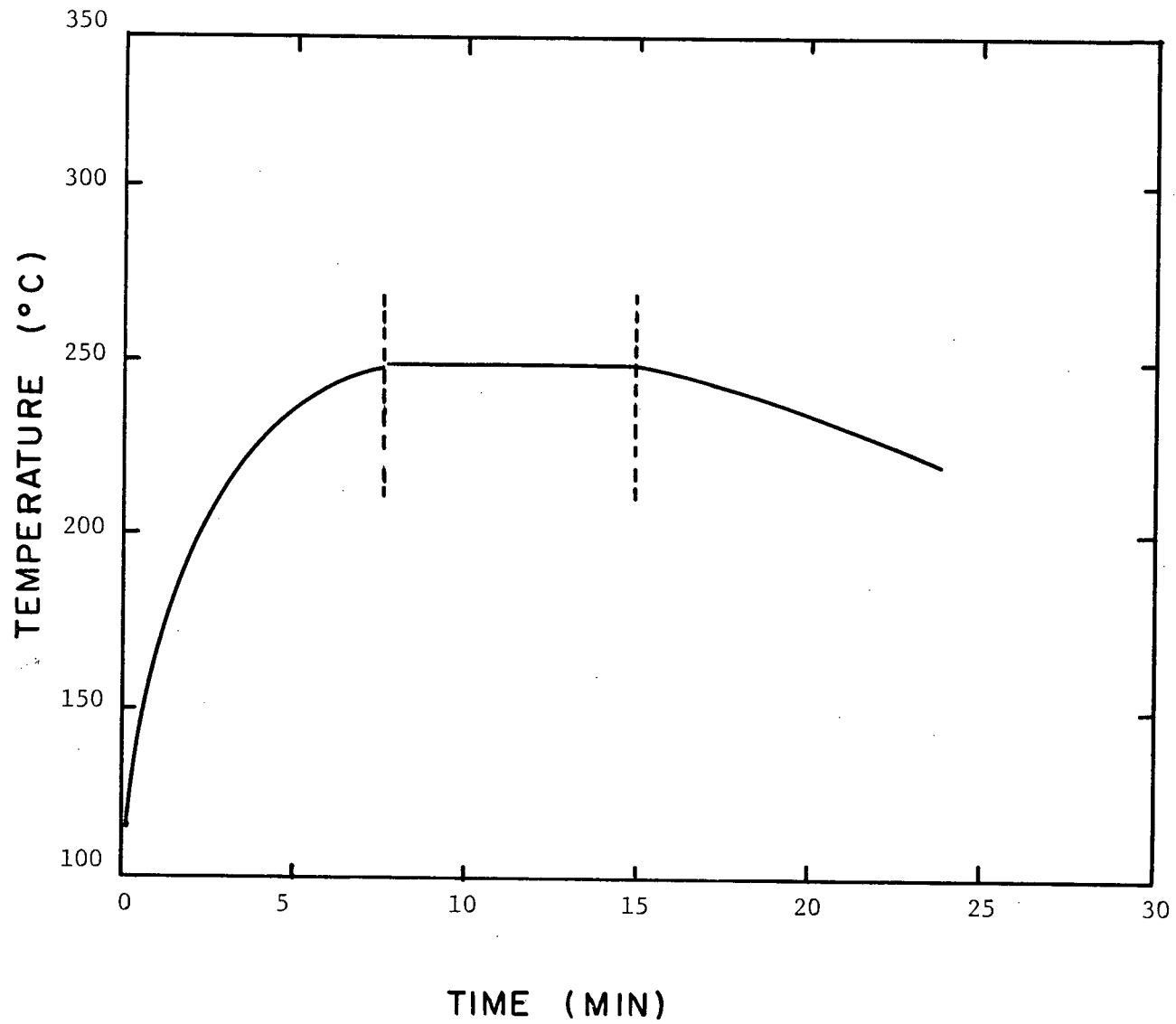


Fig. 4 Standardized extrusion time - temperature conditions.

the die and extrusion cavity. However the trend was for the pressures to be roughly proportional to the tensile strength of the product, with the highest pressures required when extruding the highest alloy powders at the lowest temperatures.

Another consequence of the high extrusion pressures was that the extrusion rates were necessarily kept low in order to keep from exceeding the maximum loading capabilities of the extrusion apparatus.

Attempts were made to lower the required extrusion pressures with the use of lubricants. Liquid lubricants tended to impregnate the powder billets, leading to an unsound product. Cladding the billet with lead was helpful to a limited extent. However at high pressures (> 200,000 p.s.i.), the lead tended to pre-extrude the alloy, leading to lead depletion and/or pinching-off of the zinc extrusion. It was therefore decided to carry out all subsequent extrusions without lubrication.

Four inches of either end of the extrusion were not used for mechanical testing as it was thought that these portions of the extrusion might not be structurally representative of the product.

2.7 Tensile Specimen Preparation

All tensile specimens were machined from extruded rod on a jeweller's lathe to a reduced diameter of approximately 0.075 inches and a gauge length of approximately 0.750 inches. As the grain size and intermetallic compound dispersion were stable at room temperature in both the heat-treated and as-extruded condition, it was not necessary to employ cold machining techniques or to electropolish the surface prior to testing.

2.8 Metallography

Electropolishing was found to be the most successful and convenient method of preparation for metallographic examination.

Electropolishing was preceded by mechanically polishing the specimen on kerosene-wetted emery paper down to 4/0 grit followed by lapping with 5 micron diamond paste.

Several polishing solutions were used, their success varying somewhat with the nature of the microstructure. The most difficult structures to prepare were those having the finest grain size and second phase dispersion. This was thought to be the result of break up of the thin polishing layer adjacent to the specimen surface by the intermetallic.

The most successful electrolyte was found to be:

25 gm. chromium trioxide
133 c.c. glacial acetic acid
7 c.c. distilled water

For coarser structures the following solution was found to be effective and reliable:

800 ml. ethyl alcohol
50 ml. butylcellusolve
60 gm. sodium thiocyanate
20 ml. distilled water

For optical metallography using polarized light, no further preparation was necessary. However, because of the fine microstructures involved, optical microscopy was not particularly useful. Most metallography was accomplished using electron microscopy.

Transmission microscopy was used only to verify the fact that replicas were representative of the structure. Replica techniques have a distinct advantage in that definition of the second phase often is much better, and the technique is rather simple and reliable as

compared with transmission procedures. In all instances a two stage carbon-chromium replica technique was employed. Figures 5 and 6 show electron micrographs of similar microstructures using both techniques in order to illustrate the validity of the replication technique.

Electropolishing did not define the grain boundaries sufficiently to allow a grain size determination. To define the grain boundaries more clearly, all metallographic specimens were deformed slightly by bending prior to replication. The amount of deformation required was dependent on the nature of the microstructure.

Microstructural parameters were determined using a line intercept method. In cases where the structure showed a directional tendency such as intermetallic particle stringing, the grain size was determined by a line intercept at 45° to the extrusion direction.

2.9 Testing Procedures

A Floor Model Instron was used for all tensile tests. Both constant and variable crosshead speed tests were used, utilizing speeds from 2×10^{-4} in/min to 2 in/min. During variable crosshead speed tests (used to evaluate strain-rate sensitivity), constant speed was maintained until the specimen had deformed a minimum of 1% at the steady state stress before a strain-rate change was made.

Tensile tests were performed in the following media:

-196°C	liquid nitrogen
-140°C to -100°C	liquid nitrogen cooled petroleum ether
-100°C to +20°C	liquid nitrogen cooled ethyl alcohol
+20°C to +100°C	heated water
+100°C to +250°C	heated cooking oil
+250°C and above	molten salt



Fig. 5 Zn - 0.6 wt.% Ti alloy extruded from -35 + 100 mesh powder at 150°C .
Transmission technique. (x25000)

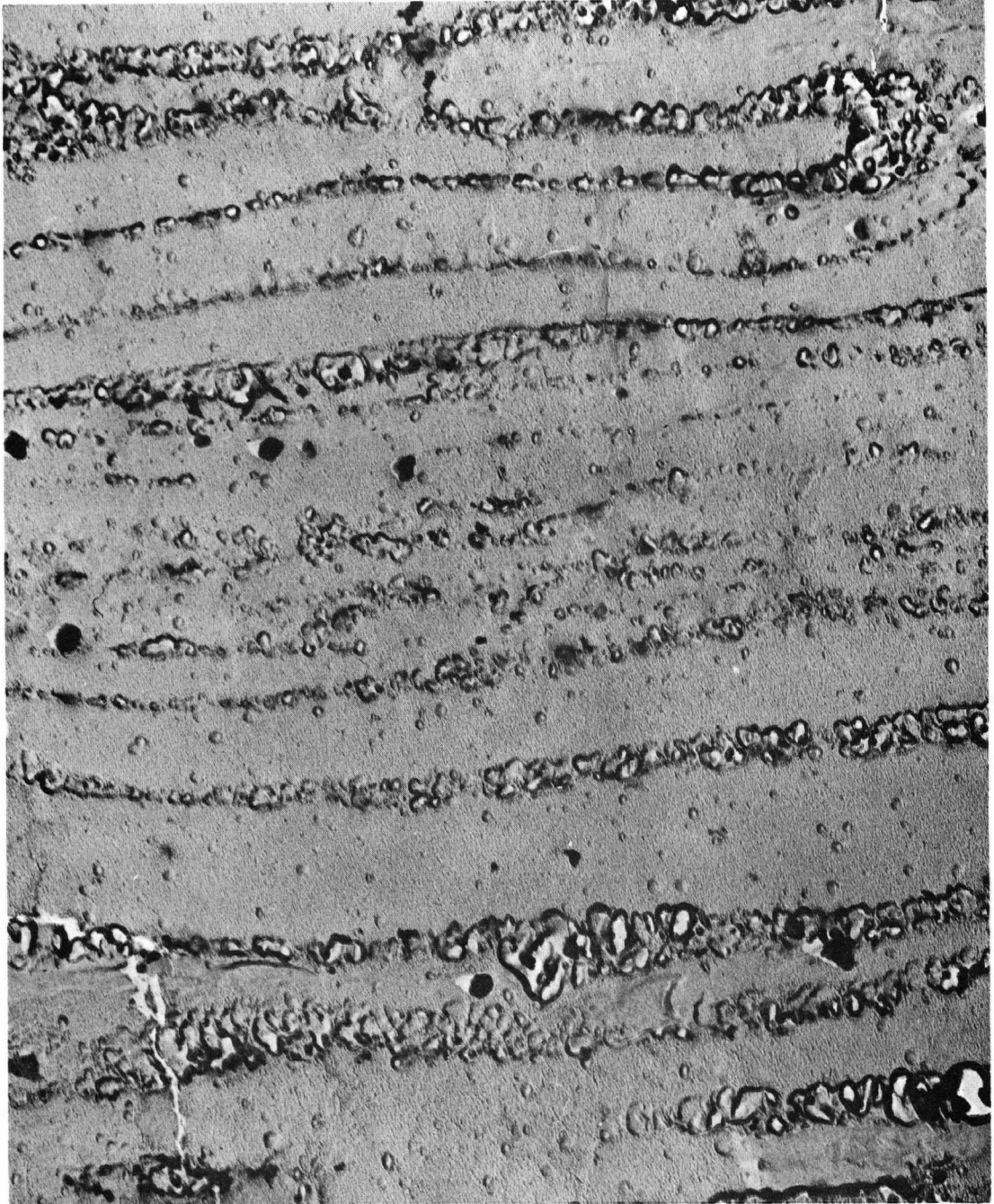


Fig. 6 Zn - 0.6 wt.% Ti alloy extruded from -35 + 100 mesh powder at 150°C.
Replication technique. (x25000)

True stress, strain, and strain-rate were calculated on the assumption that deformation had occurred homogeneously throughout the gauge length. True stress - strain curves presented in this work are valid up to the maximum stress. The apparent decrease in true stress at higher strain values is due to necking of the specimen.

3. ZINC - TITANIUM PHASE DIAGRAM

Several independent investigations have been made on the zinc rich portion of the zinc-titanium phase diagram. There is considerable disagreement as to the composition of the eutectic and the number and nature of peritectic reactions.

The eutectic composition appears to lie in the range 0.10 wt.% Ti to 0.50 wt.% Ti. Table II summarizes the information regarding the eutectic which has been reported to date. A significant feature of this data is that the eutectic evaluations other than those of Gebhardt, Cominco, and to a certain degree Rennhack, have all been based on metallographic examination. It is probable that large variations of the eutectic morphology and composition can occur depending upon the casting history. Thus it would appear that determination of phase relations by means of analysis of microstructures alone may be somewhat unreliable.

It is of interest to note that determinations made by means of differential cooling techniques yield results which are in close agreement. Figures 7 and 8 show the phase diagrams as determined by these investigations.

Some effort has been made to establish the crystal structure of the two zinc rich intermediate phases which are produced.⁽⁹⁾ It is generally agreed that $Zn_{15}Ti$ is the product of peritectic reaction of the remaining liquid with $Zn_{10}Ti$.

The zinc rich compound ($Zn_{15}Ti$) has an orthorhombic structure with the following composition and lattice parameters:

$$\begin{array}{ll}
 4.5 \text{ wt.}\% \text{ Ti} & a = 3.87 \text{ \AA} \\
 & b = 5.69 \text{ \AA} \\
 & c = 11.87 \text{ \AA}
 \end{array}$$

Table II. Summary of the Experimental Investigations of the Zinc Rich End of the Zinc-Titanium Phase Diagram.

Reference	Year	Eutectic Composition (wt.% Ti)	Eutectic Temperature (°C)	Solid Solubility (wt.% Ti)
Anderson ⁽³⁰⁾	1944	0.12	418.5	<.015 (300°C)
Pelzel ⁽³⁴⁾	1961	0.18		
Heine and Zwicker ⁽³²⁾	1962	0.23		<.0004 (400°C)
Rennhack ⁽³³⁾ ³³	1966	0.19	418.6	
Gebhardt ⁽³¹⁾	1941	0.45	418	<.02 (400°C)
Cominco ⁽³⁴⁾	1964	0.46	418	

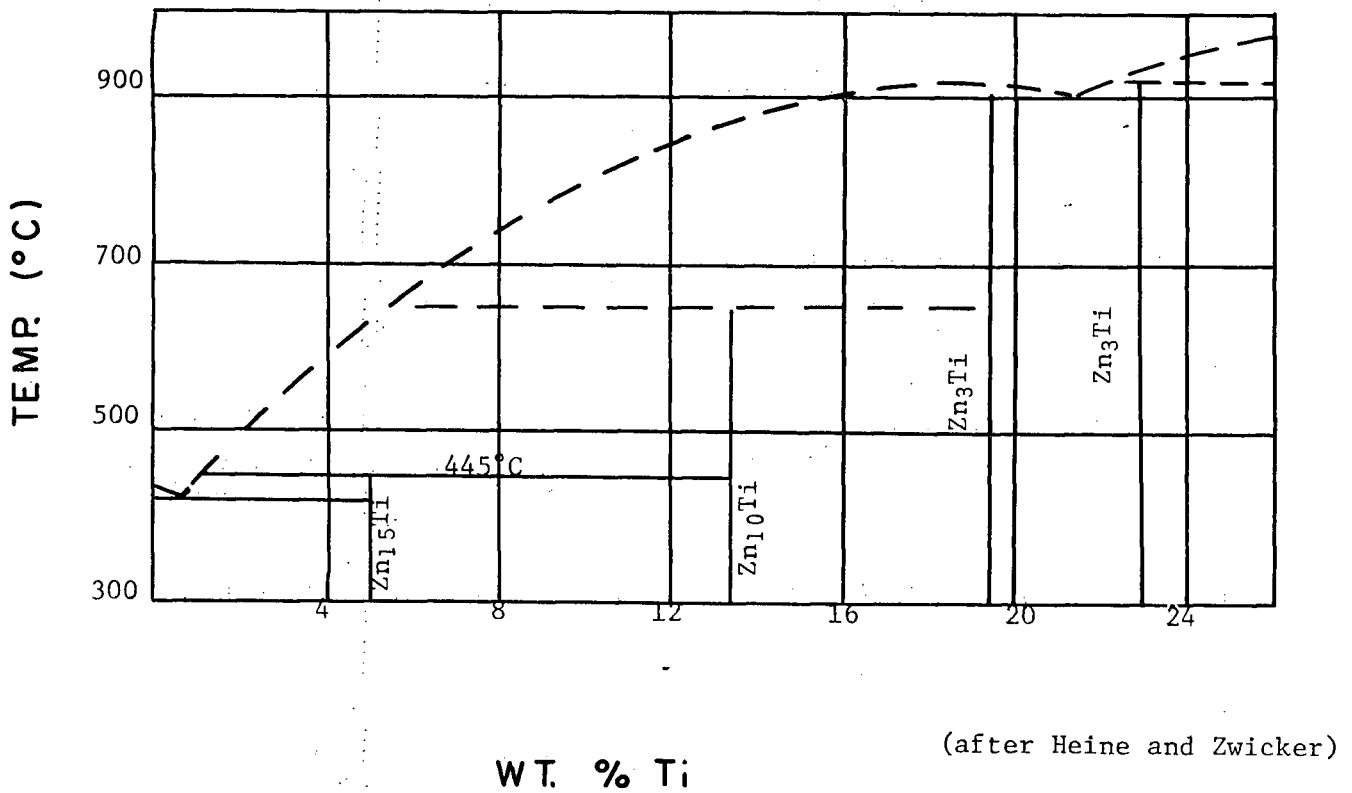
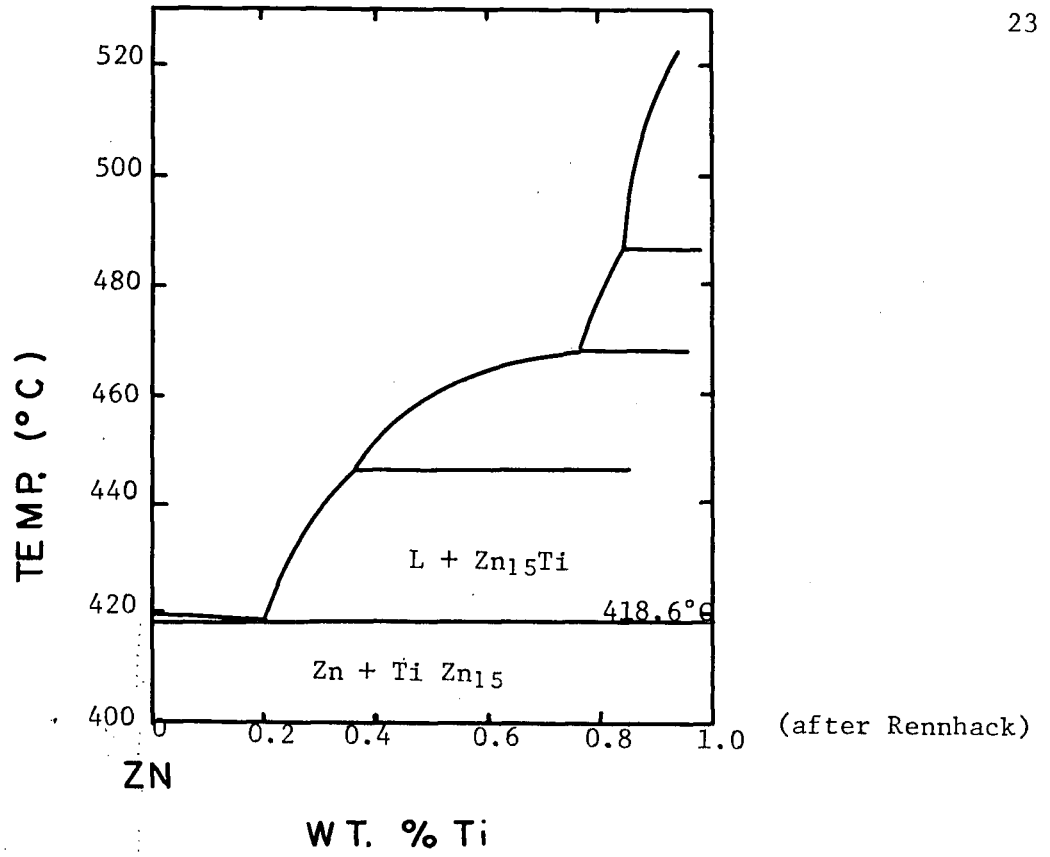


Fig. 7 Zinc - titanium phase diagrams.

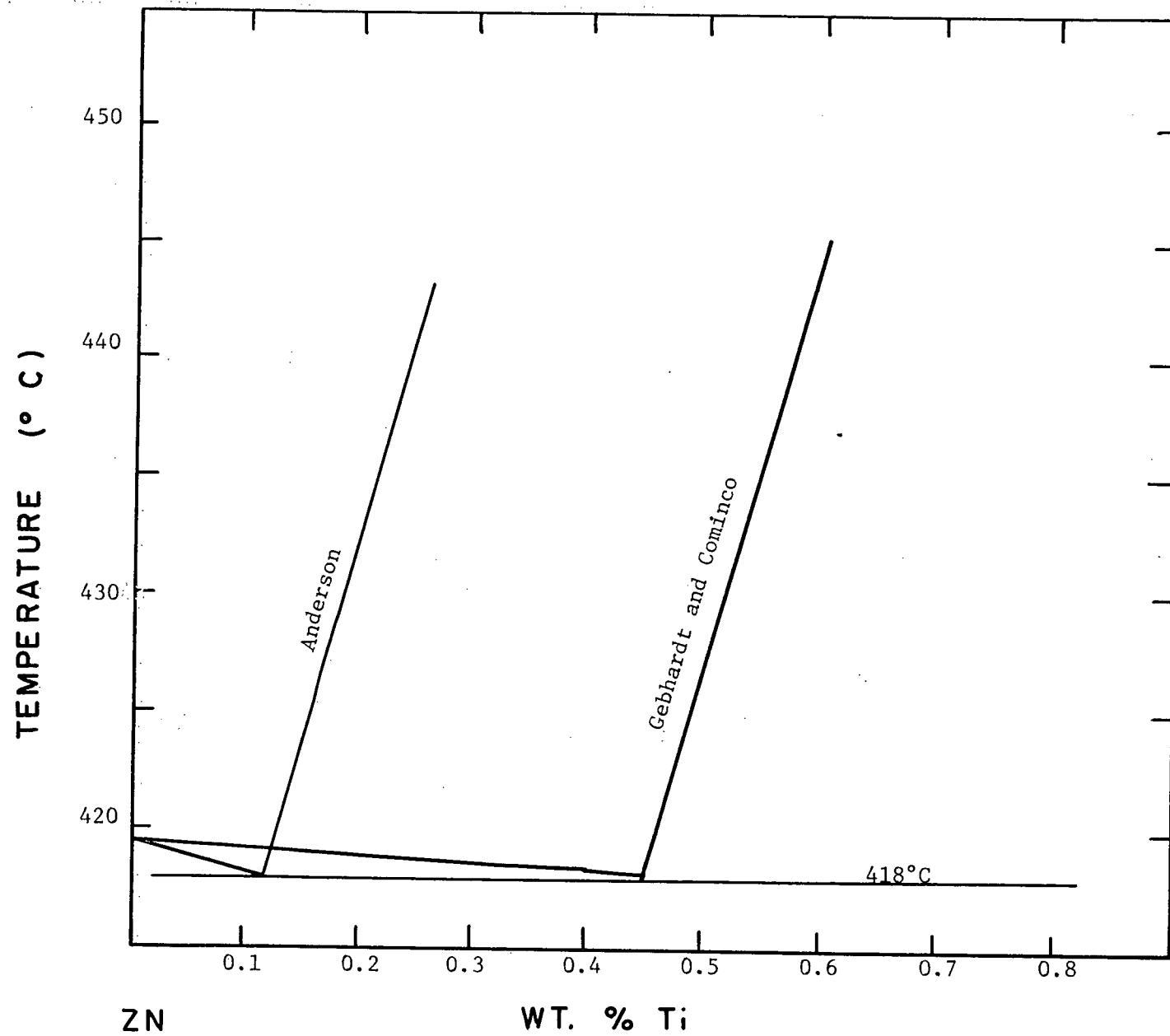


Fig. 8 Zinc rich end of the zinc-titanium phase diagram.

4. RESULTS

Since this work is based on both powder and cast material and since the procedures used in their fabrication have an inherently large number of possible variables, initial investigations were limited to a fixed composition in order that the effect of some of these variables could be established and optimized. The composition chosen was Zn - 0.6 wt.% Ti.

4.1 Reproducibility

Quality control tensile tests were performed on the initial extrusions of both cast and powder materials in order to establish if a gradient in properties existed between the initial and final portions of the extrusion.

The results of these tests are shown in Table III; they indicate that the mechanical properties do not appear to change throughout the length of the extrusion. Therefore for all subsequent extrusions it was assumed that the product was structurally consistent throughout. However as an added precaution, all tensile specimens were labelled according to the section of the extrusion from which they were obtained in the event that some structural or mechanical discontinuity was encountered.

4.2 Effect of Extrusion Temperature

As -100 + 200 mesh powder was a medium size fraction obtained by the atomization process, this size was used to determine the effect of extrusion temperature on the mechanical properties of the material.

Table III. Reproducibility of Mechanical Properties Along Extrusions.

Material	Tx (°C)	Specimen Location	0.2% O.Y.S. (10 ³ psi)	0.5% O.Y.S. (10 ³ psi)	U.T.S. (10 ³ psi)	Total Elongation (%)
cast	150	I	24.4	26.0	27.5	24.8
cast	150	F	24.2	25.8	26.7	22.6
cast	200	I	25.1	26.6	27.7	14.8
cast	200	F	25.4	26.8	27.6	19.7
cast	250	I	30.3	32.2	33.0	14.4
cast	250	F	30.2	31.7	32.3	12.4
cast	300	I	29.7	31.2	31.9	12.8
cast	300	F	29.9	31.7	32.5	14.4
cast	350	I	24.6	26.0	28.8	14.9
cast	350	F	24.5	27.2	29.7	18.0
-100 + 200 mesh	150	I	62.4	63.7	63.7	6.8
-100 + 200 mesh	150	F	60.9	63.4	63.5	6.0
-100 + 200 mesh	250	I	28.7	31.1	32.1	16.3
-100 + 200 mesh	250	F	29.1	31.5	32.6	14.6
-100 + 200 mesh	350	I	28.5	30.3	31.4	18.5
-100 + 200 mesh	350	F	30.1	32.4	33.5	11.0

Tx = Extrusion Temperature

I = Initial specimen from extrusion

F = Final specimen from extrusion

O.Y.S. = Offset Yield Stress

Note: The composition of all extrusions is
0.6 wt.% Ti.

A simultaneous investigation was carried out using cast material. The results of this study are shown in Figs. 9 and 10. There is no significant difference in the strength of specimens manufactured using powder and those extruded from the as-cast billets when an extrusion temperature greater than 250°C is used.

When the starting material is a cast billet there is only a slight change in yield strength as the extrusion temperature is lowered. A maximum in strength occurs at an extrusion temperature of 250°C. This can be attributed to a grain size effect and its relationship to the distribution of the second phase. The significance of this relationship is discussed in detail later.

For extruded powder material, a rapid increase in strength is obtained as the extrusion temperature is lowered below 250°C. The minimum extrusion temperature used was 150°C, and was determined by equipment limitations.

Cast and powder products possess equivalent ductilities when extruded above 250°C. Below this temperature, the ductility of the powder material decreases whereas the ductility of the cast material increases.

Tensile properties of Zn - 0.6 wt.% Ti alloys extruded at 175°C using three different powder sizes are shown in Table IV. These results indicate that no significant increase in strengthening is realized through the use of finer powders.

The most significant feature of Fig. 9 is the strength differential between cast and powder extrusions at low fabrication temperatures. This must arise due to microstructural differences in the original material. The decrease in strength of powder extrusions which

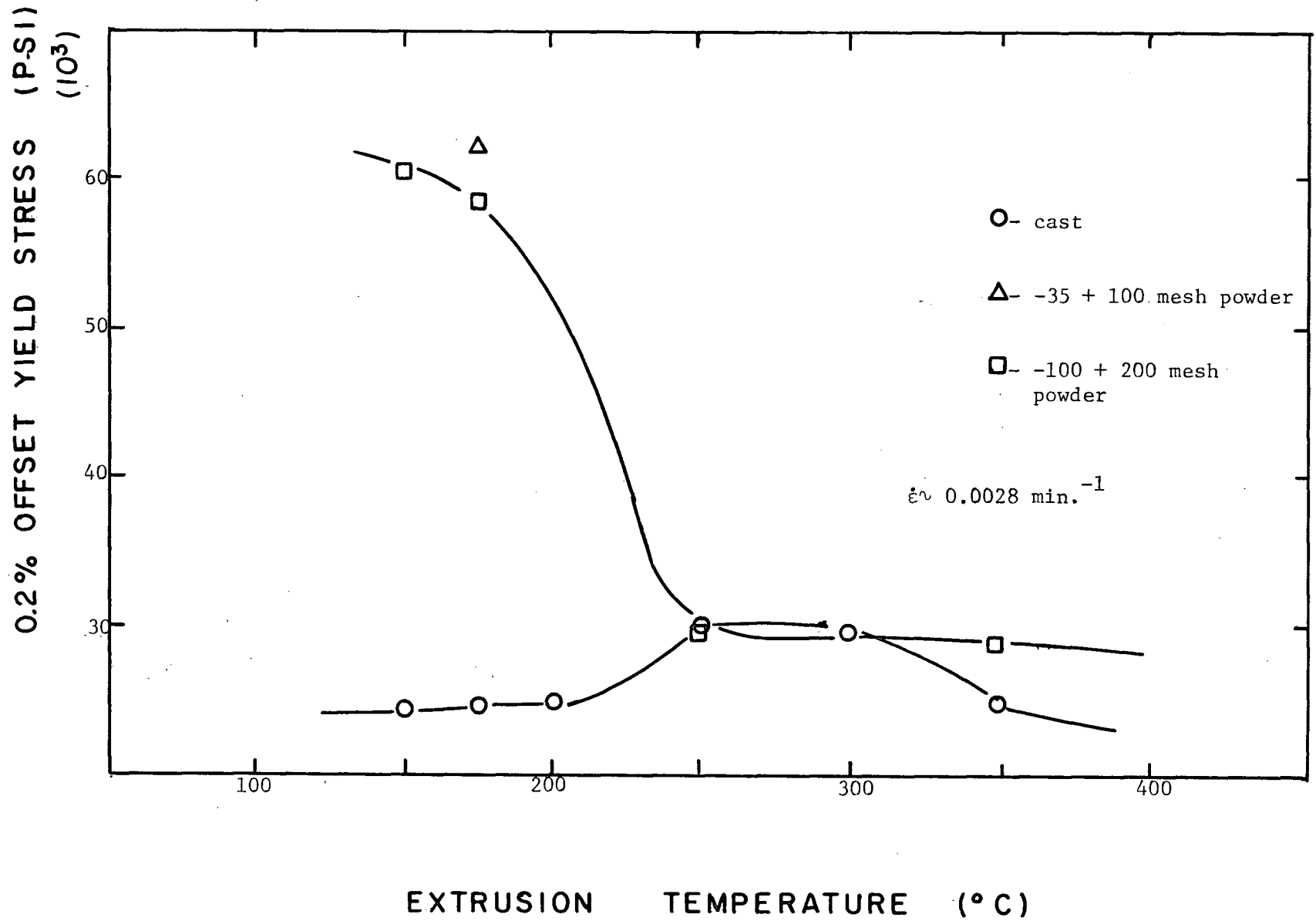


Fig. 9 The effect of extrusion temperature on the yield strength of Zn - 0.6 wt.% Ti alloys.

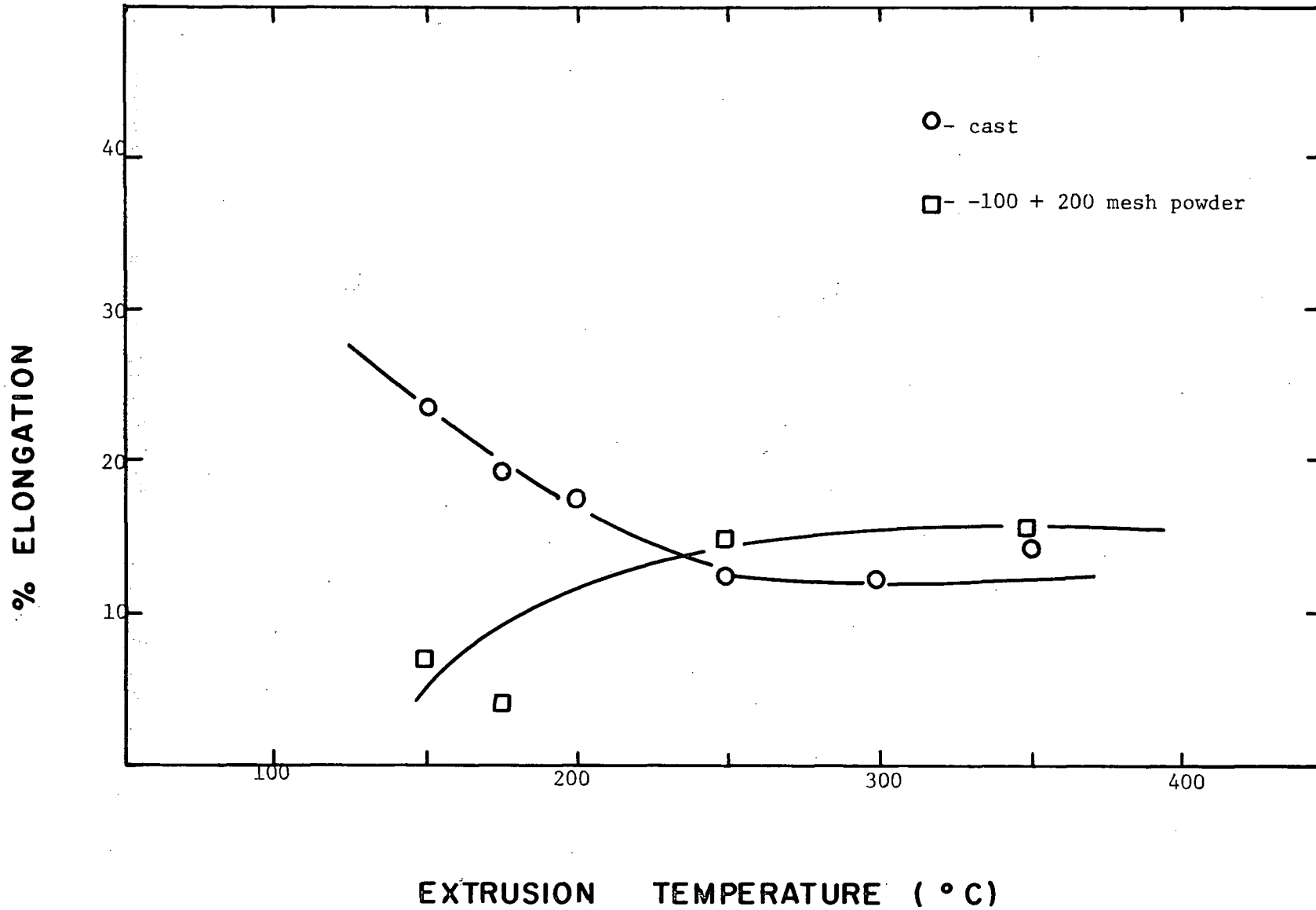


Fig. 10 The effect of extrusion temperature on the ductility of Zn - 0.6 wt.% Ti alloys.

Table IV. The Effect of Powder Size on the Mechanical Properties of Zn - 0.6 wt.% Ti Alloys.

Powder Size	0.2% O.Y.S. (10^3 psi)	0.5% O.Y.S. (10^3 psi)	U.T.S. (10^3 psi)	Total Elongation (%)
-35 + 100 mesh	60.1	64.0	65.0	2
-100 + 200 mesh	60.0	63.7	64.0	4
-325 mesh	60.7	67.0	75.0	2

Note: $\dot{\epsilon} \sim .0028 \text{ min.}^{-1}$

Tx = 175°C

Extrusion Ratio = 25:1

occurs at higher extrusion temperatures must also be associated with microstructural modifications.

4.3 Chill Cast and Powder Microstructures

4.3.1 Microstructure of Cast Billets

Most of the previous investigations of cast zinc-titanium alloys have been carried out at low titanium concentrations (<0.2 wt.%). (28,29,34) This corresponds to a composition which is hypoeutectic according to most of the published phase diagrams.

The microstructure of a chill cast hypereutectic alloy is expected to consist of primary particles of intermetallic ($Zn_{15}Ti$) surrounded by a Zn - $Zn_{15}Ti$ eutectic. Similarly, in a hypoeutectic alloy primary zinc dendrites and eutectic are expected to make up the microstructure.

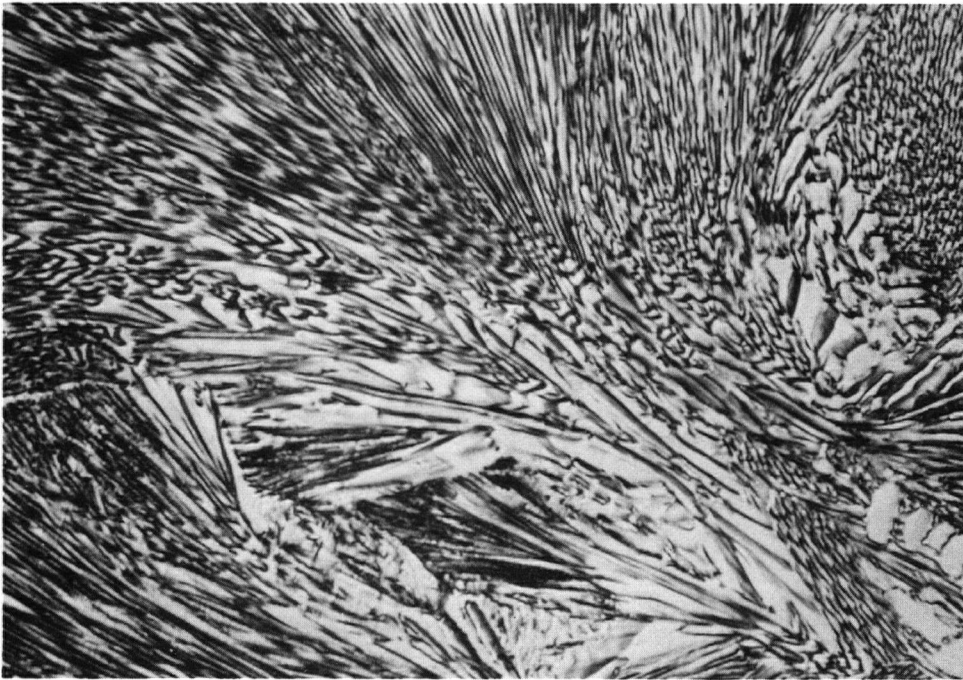
Figures 11(a) and 11(b) indicate the microstructure of a chill cast billet containing 0.36 wt.% Ti. This titanium concentration is considerably higher than most of the published eutectic compositions (~ 0.2 wt.% Ti). The structure consists of a zinc dendritic structure with large areas of eutectic.

Electron microprobe analysis revealed that the primary dendrites were titanium depleted and that the titanium was essentially present only in the eutectic structures. Figures 12(a) and 12(b) show the absorbed electron image of a primary particle along with a corresponding Ti X-ray scan.

Quantitative measurements obtained by scanning both the primary particles and eutectic indicate no detectable titanium in the primary zinc dendrites.



(a)
(x325)



(b)
(x325)

Fig. 11 Zn - 0.36 wt.% Ti alloy chill cast microstructure.

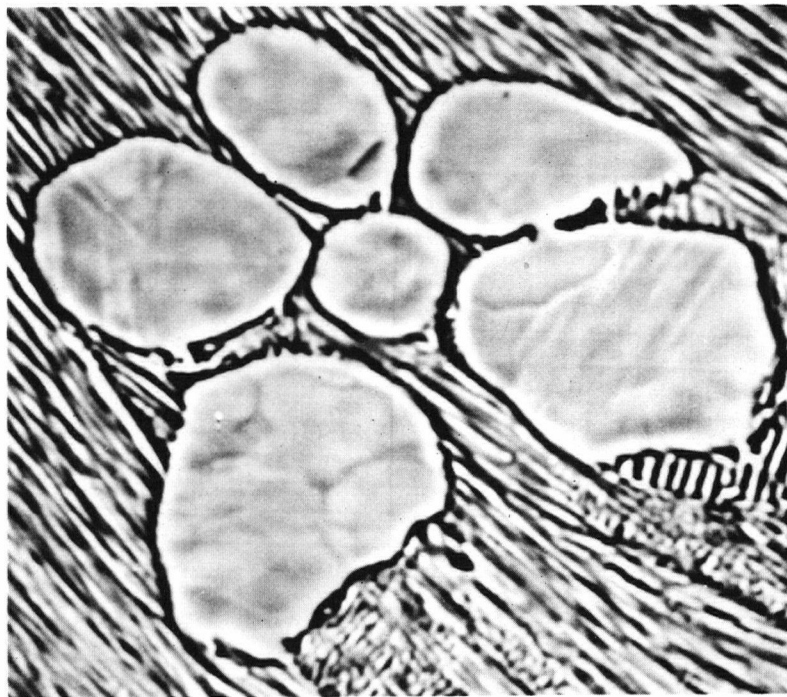


Fig. 12(a) Electron microprobe absorbed electron image of Zn - 0.36 wt.% Ti chill cast microstructure. (x1500)



Fig. 12(b) Ti X-ray scan of Zn - 0.36 wt% Ti chill cast microstructure. (x1500)

The average titanium concentration in the eutectic structure was calculated from uncorrected microprobe data to be 0.45 wt.% Ti. Applying absorption and fluorescence corrections as developed by Birk⁽⁶⁶⁾ increased this value to 0.49 wt.% Ti. Considering the sensitivity of the microprobe analysis, this would suggest that the eutectic composition is in the range 0.4 - 0.6 wt.% Ti. Clearly the solidification rates used in this study are non-equilibrium. Therefore this value should not be related to values obtained from phase diagrams.

Figures 13(a) and 13(b) indicate the morphology of the eutectic observed in a chill cast Zn - 0.36 wt.% Ti alloy.

The microstructure of a chill cast Zn - 0.6 wt.% Ti alloy (Fig. 14) indicates large areas of primary zinc as well as primary particles of $Zn_{15}Ti$. This observation is not consistent with the expected structure. It is possible that with supercooling, the intermetallic particles may act as preferential nucleating centres for zinc. This would lead to the premature solidification of the zinc rich phase and could explain the observed microstructure. Basically these microstructures indicate that at these solidification rates, the apparent eutectic composition is between 0.36 wt.% Ti and 0.6 wt.% Ti.

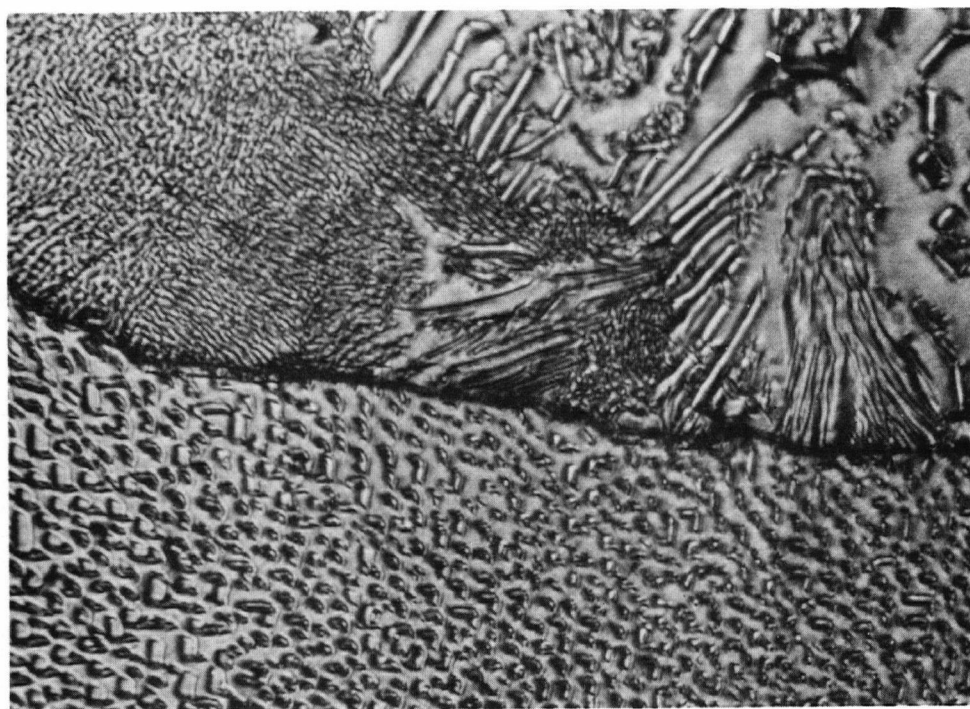
4.3.2 Microstructure of Powder

In order to investigate the structure in the powder particles, metallographic and microprobe studies were made using powder billets compacted at pressures sufficiently high to provide a completely dense specimen. These analyses were carried out using -35+100 mesh powder containing 0.6 wt.% Ti.

Figures 15(a) and 15(b) are electron micrographs of the



(a)
(x925)



(b)
(x925)

Fig. 13 Microstructural characteristics of the eutectic in a chill cast Zn - 0.36 wt.% Ti alloy.

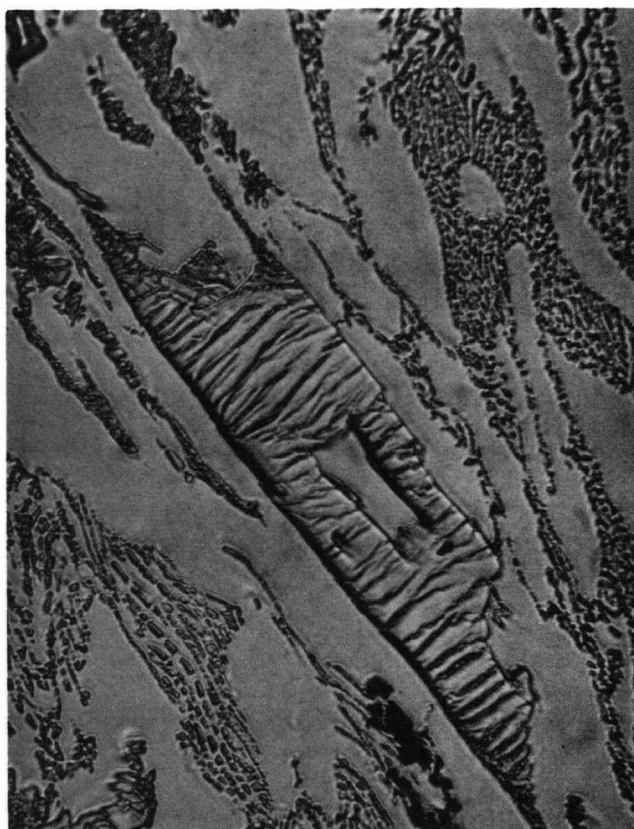
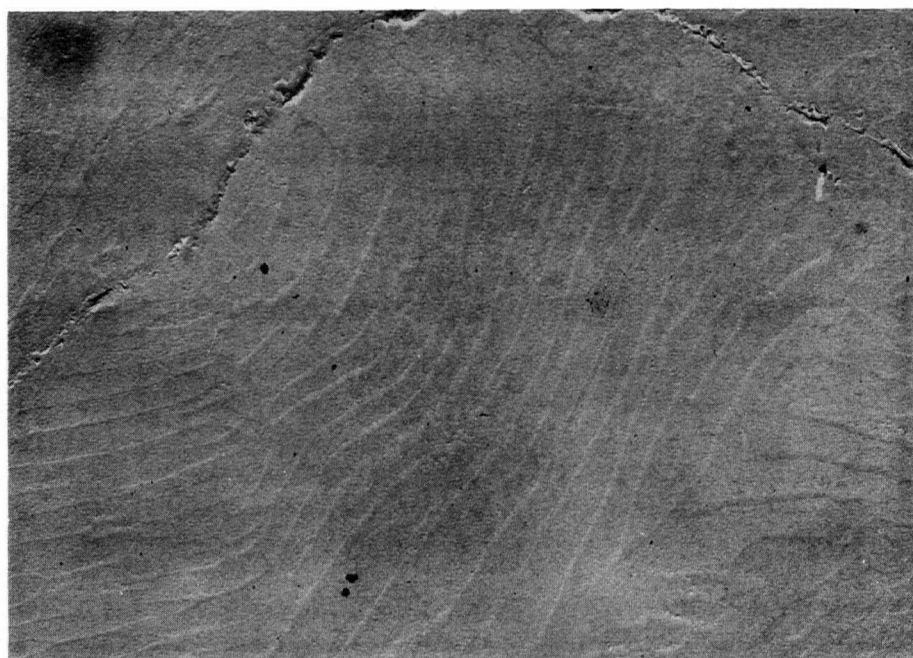
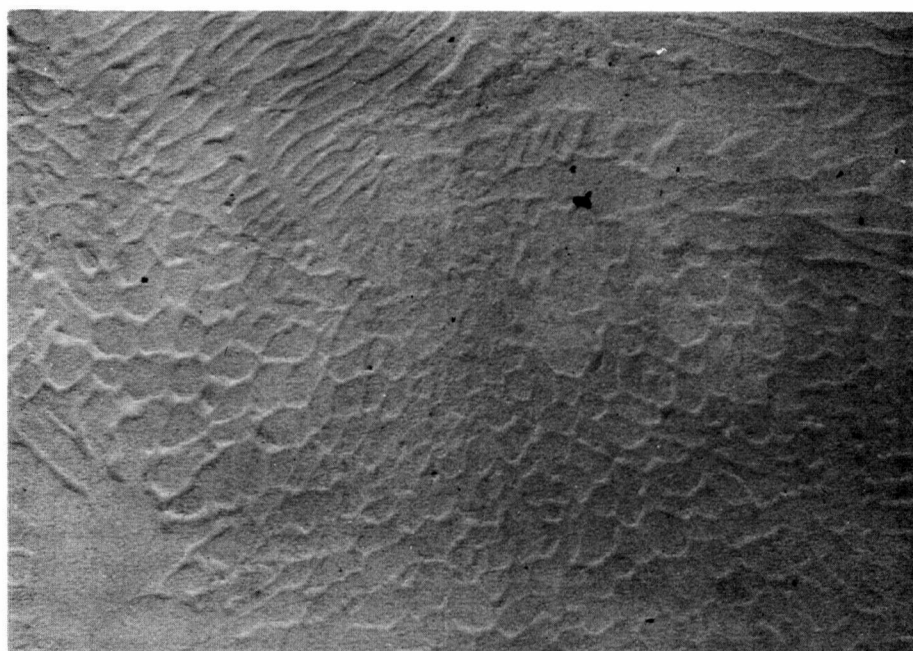


Fig. 14 Chill cast microstructure of Zn - 0.6 wt% Ti alloy.
(x625)



(a)
(x4000)



(b)
(x4000)

Fig. 15 Electron micrograph of the eutectic structure in -35 + 100 mesh Zn - 0.6 wt.% Ti powder.

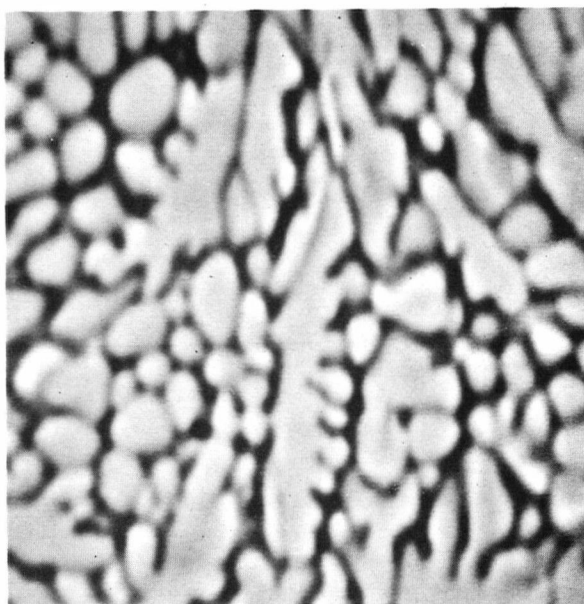
eutectic structure which was present. The morphology of the eutectic was highly variable, a feature also observed in chill cast structures. Although not shown in these electron micrographs, primary intermetallic particles were also present. What appears to be an oxide surface coating on the powder particles remained relatively intact. This suggests that compaction of the powder did not modify the as-solidified microstructure to any significant degree.

Microprobe analysis confirmed that the continuous phase was titanium rich and that the non-continuous phase was titanium depleted (Figs. 16(a) and 16(b)). The eutectic has solidified dendritically and is much finer than that observed in cast billets.

4.3.3 Extent of Oxidation of Atomized Powder

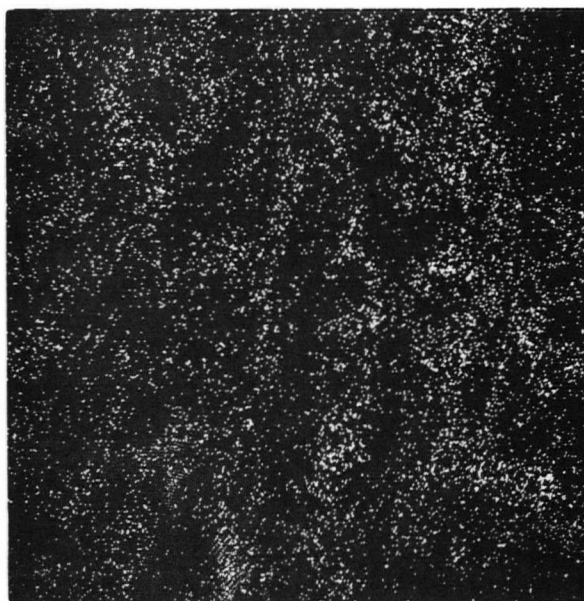
The study of the microstructure of the powder also provided the opportunity to evaluate the extent of surface oxidation which occurred during atomization. There is an apparent surface coating on the powder as is shown in Fig. 15(b). However this could not be confirmed to be oxide as it was too thin to be resolved in the microprobe.

No oxide was found in either powder compacts or extruded product. This suggests that the powder solidified within the argon atmosphere used during atomization. This further indicates that the titanium is present as intermetallic and not as an oxide. In fact the microprobe analysis suggests that the surface of the particles may be oxygen depleted (Figs. 17(a), (b), and (c)). The zinc matrix oxidizes to a limited extent during preparation for metallographic or microprobe analysis. The intermetallic compound is not expected to oxidize. Thus areas rich in intermetallic would tend to exhibit an apparent lower oxygen concentration.



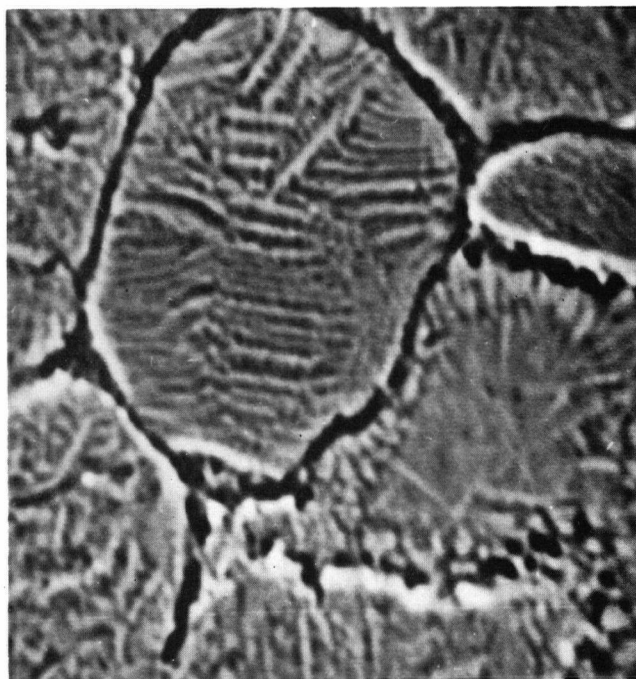
x2000

Fig. 16(a) Absorbed electron image from an electron microprobe analysis of -35 + 100 mesh Zn - 0.6 wt.% Ti powder.



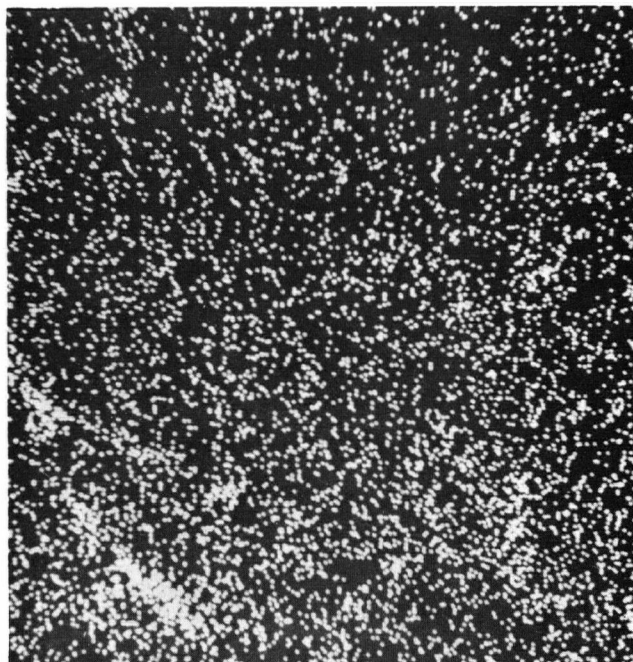
x2000

Fig. 16(b) Ti X-ray scan from an electron microprobe analysis of -35 + 100 mesh Zn - 0.6 wt.% Ti powder.



(a)

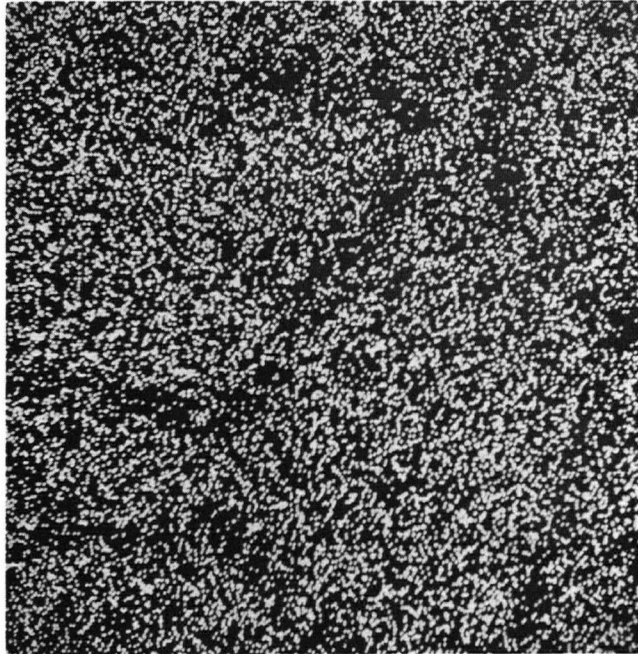
(x1500)



(b)

(x1500)

Fig. 17 Electron microprobe analysis of Zn - 0.6 wt.% Ti -35 + 100 mesh powder compact: (a) Absorbed electron image
(b) Ti X-ray scan
(c) O₂ X-ray scan.



(c)

(x1500)

4.4 Microstructural Characteristics of Extruded Alloys

A basic difference between the microstructures of cast billets and powder is the decrease in dendrite and lamellar spacing which occurs with more rapid solidification rates. The nature of the microstructure formed during extrusion is dependent on the characteristics of the starting material and on the fabrication conditions.

Figures 18, 19 and 20 show the effect of extrusion temperature on the microstructure of extruded powders. At low extrusion temperatures alignment of the intermetallic occurs to give the microstructure a "stringered" appearance in which the grain size is equivalent to the stringer spacing. As the fabrication temperature is increased, intermetallic coarsening and grain growth occur resulting in a loss of this type of structure. There is a corresponding decrease in strength as stringering becomes more poorly defined. During this process the grain size and interparticle spacing remain approximately equivalent.

4.4.1 Stringering During Extrusion of Powders

Since the microstructure of material manufactured utilizing low extrusion temperatures and a high extrusion ratio consists of a well-defined stringered structure, an extrusion was carried out at an extrusion ratio sufficiently low so as to reduce the amount of plastic flow of the matrix to the point at which not all powder particles would deform.

An extrusion ratio of 10:1 was found to be sufficiently low such that some particles were in a "hard" orientation, or in areas of the extrusion in which flow was minimized. As a result, the development of the stringered structure could be followed.

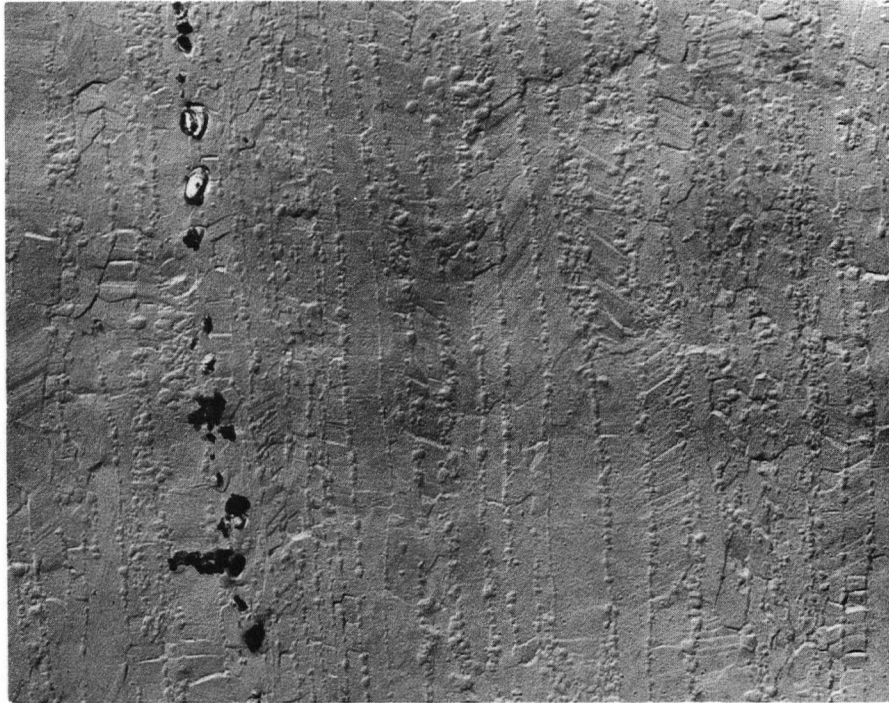


Fig. 18 Microstructure of a Zn - 0.6 wt.% Ti alloy extruded at 150°C using -35 + 100 mesh powder. (x8000)

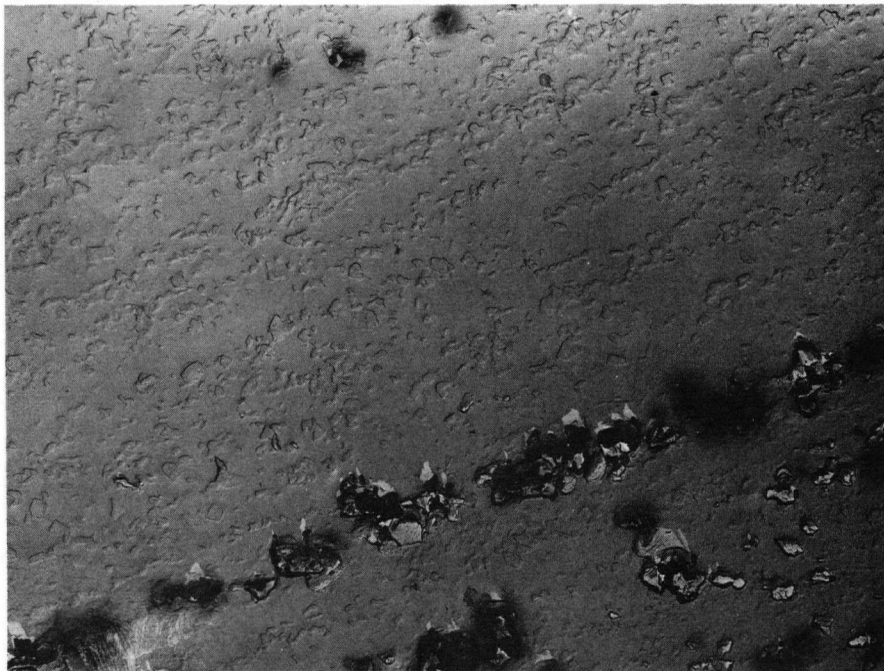


Fig. 19 Microstructure of a Zn - 0.6 wt.% Ti alloy extruded at 250°C using -35 + 100 mesh powder. (x4000)

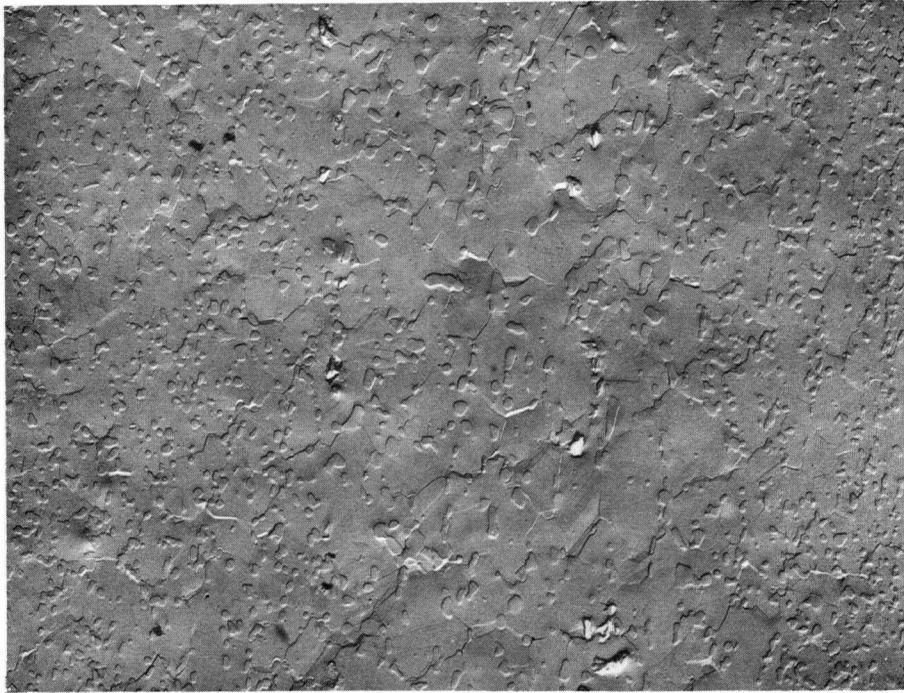


Fig. 20 Microstructure of a Zn - 0.6 wt.% Ti alloy extruded at 350°C using -35 + 100 mesh powder. (x4000)

As can be seen from Figs. 21 and 22, the stringered structure is a direct result of the structure which is produced during solidification of the powder. The continuous network of intermetallic surrounding the zinc phase is directed in the extrusion direction. Any intermetallic which is perpendicular to the extrusion direction is displaced by the plastic flow of the zinc down the "pipes" of intermetallic to give an overall stringered appearance.

The contribution of the oxide to the overall stringering can also be seen in these electron micrographs. It appears reasonable to assume that the amount present has a negligible effect, since only a small percentage of the stringering is due to oxide and the distance between oxide stringers is generally several grain diameters (partially the result of the use of coarse powders).

As a result of the short diffusion paths involved, high temperature soaking prior to extrusion results in a considerable degree of intermetallic coarsening. Because of the ease of flow of the matrix at these temperatures, effective second phase alignment is also minimized. Primary particles formed during solidification appear as coarse stringers in the extruded product (Figs. 23(a), (b) and (c)). High titanium concentrations in such areas may give the impression that other areas of the alloy have intermetallic concentrations somewhat lower than is consistent with the analysis.

4.4.2 Cast Material

The coarse microstructures of chill cast billets result in rather coarse extruded microstructures, as is shown in Figs. 24, 25 and 26. However lower extrusion temperatures promote fragmentation and displacement

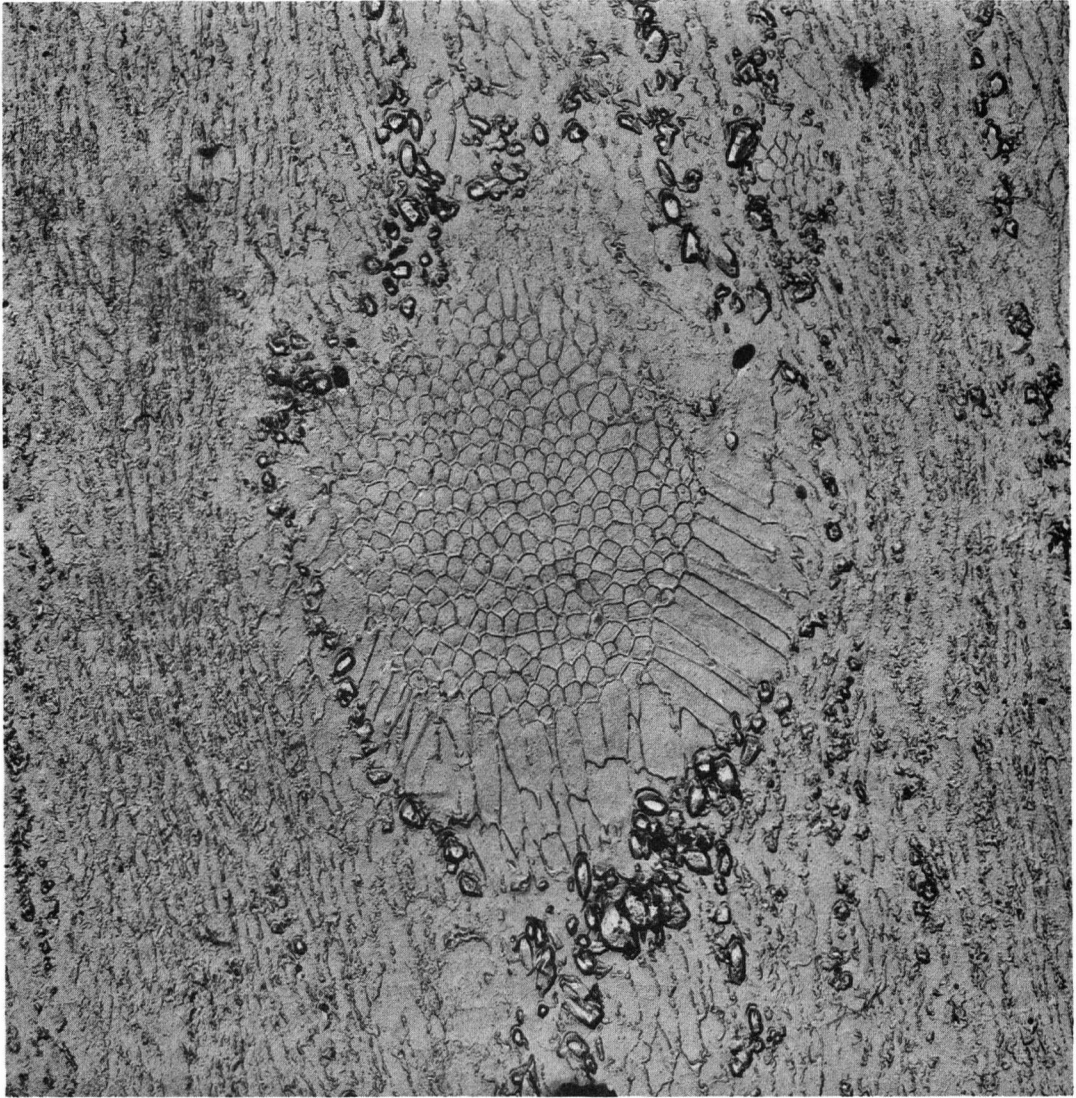


Fig. 21 The origin of the stringered structure in a Zn - 0.6 wt.% Ti alloy fabricated from -35 + 100 mesh powder at 175°C. (x4000)

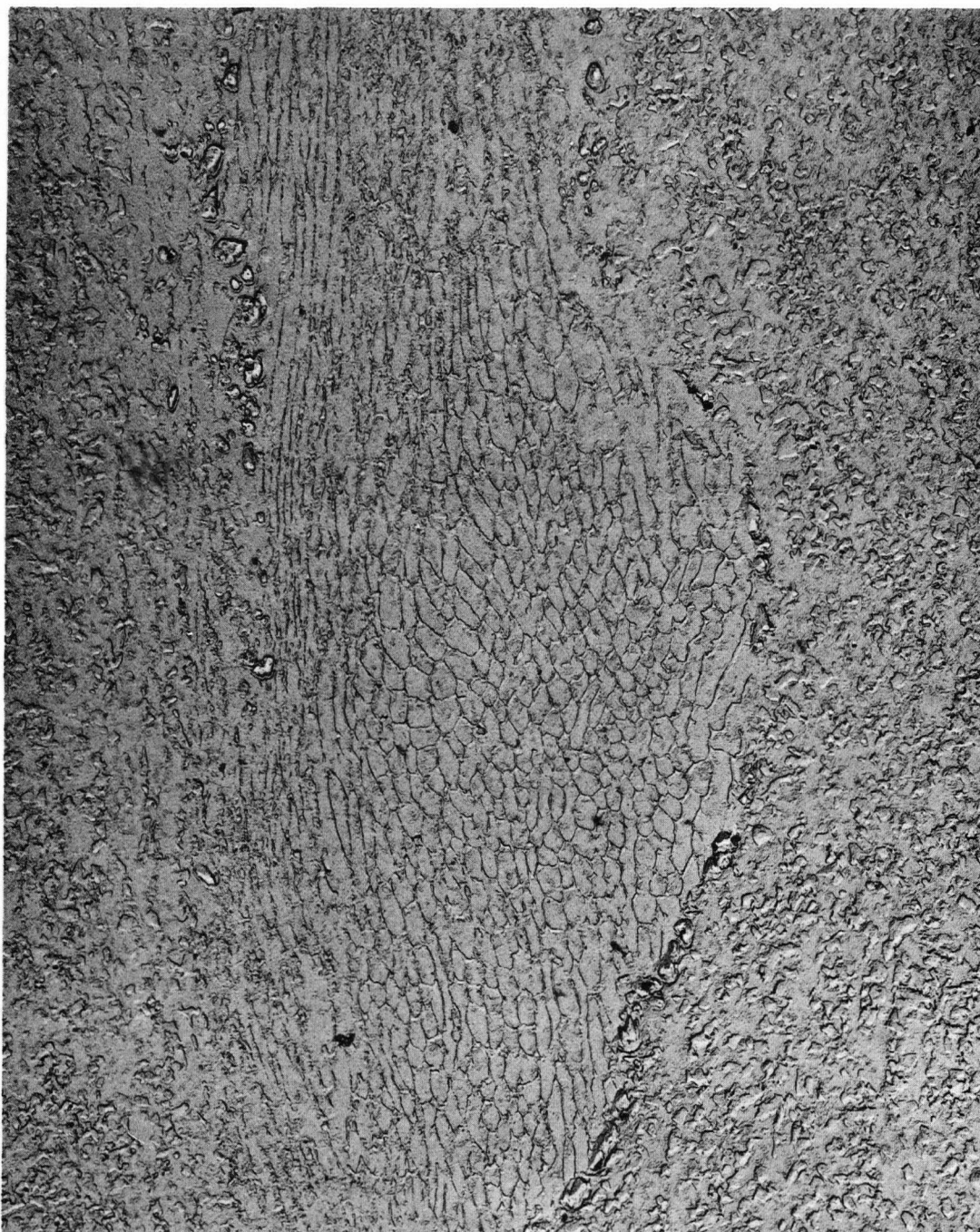
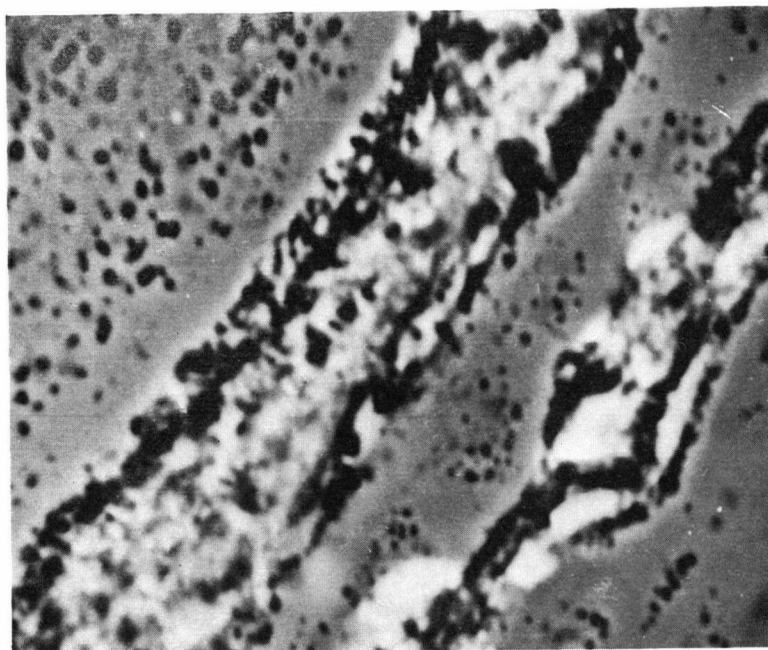
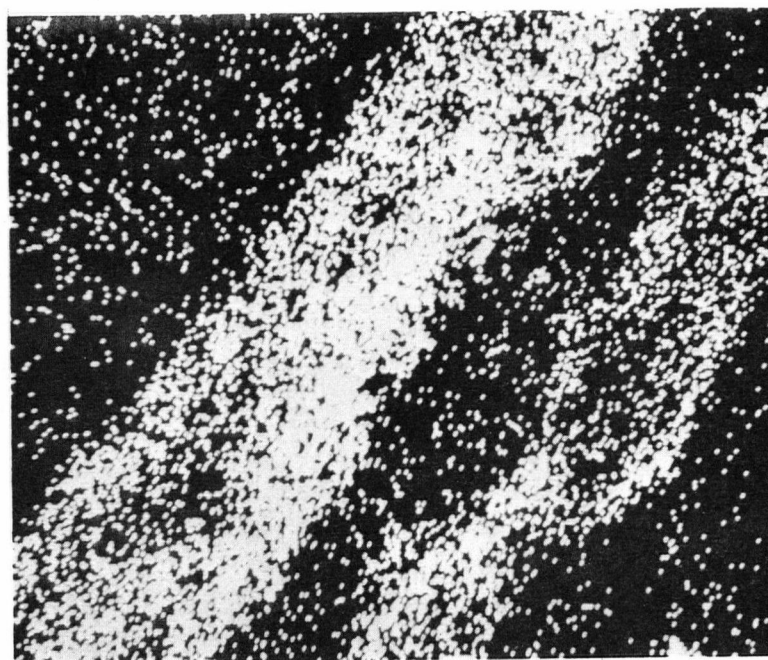


Fig. 22 The origin of the stringered structure in a Zn - 0.6 wt.% Ti alloy fabricated from -35 + 100 powder at 175°C. (x4000)



(a)

(x1500)

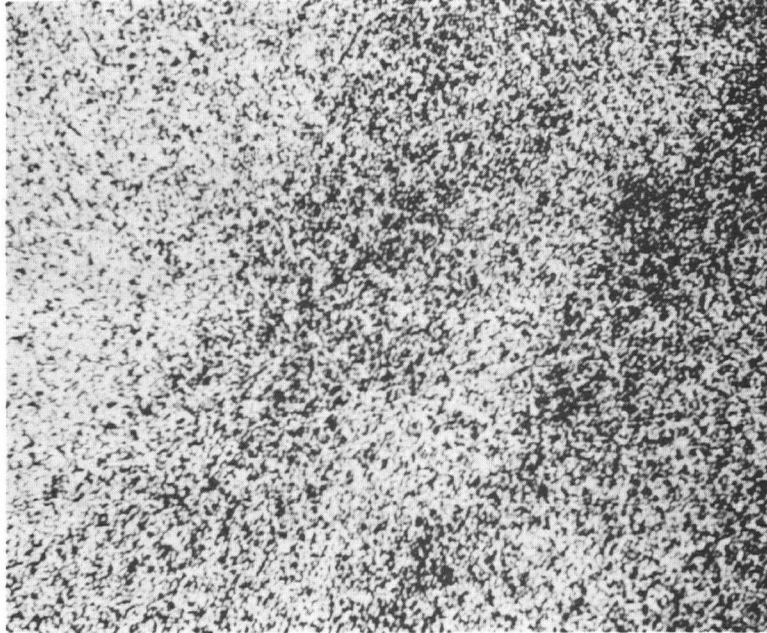


(b)

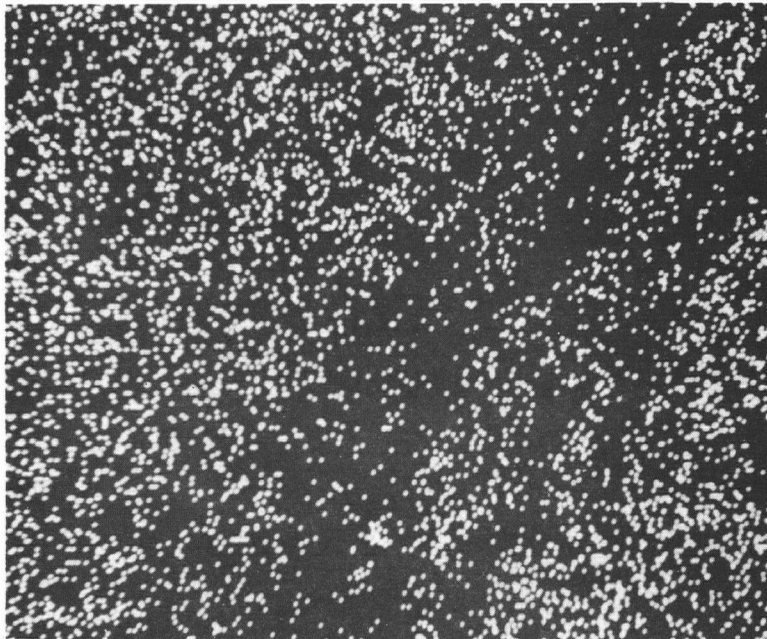
(x1500)

Fig. 23 Electron microprobe analysis of Zn - 0.6 wt.% Ti alloy extruded at 250°C using -35 + 100 mesh powder (specimens annealed 44 hours at 350°C):

- (a) Absorbed electron image
- (b) Ti X-ray scan
- (c) Zn X-ray scan.
- (d) O₂ X-ray scan.



(c)
(x1500)



(d)
(x1500)

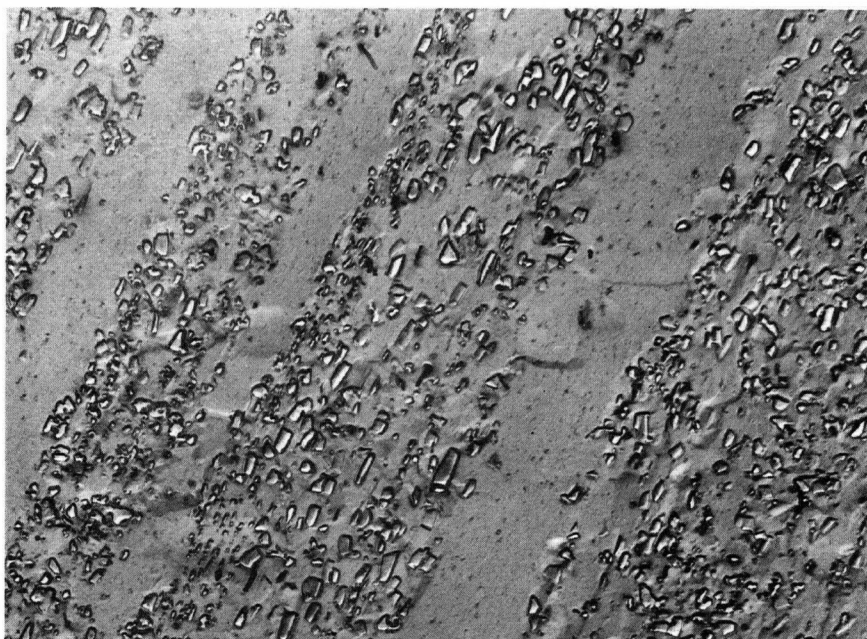


Fig. 24 Microstructure of a chill cast Zn - 0.6 wt.% Ti alloy extruded at 150°C. (x4000)

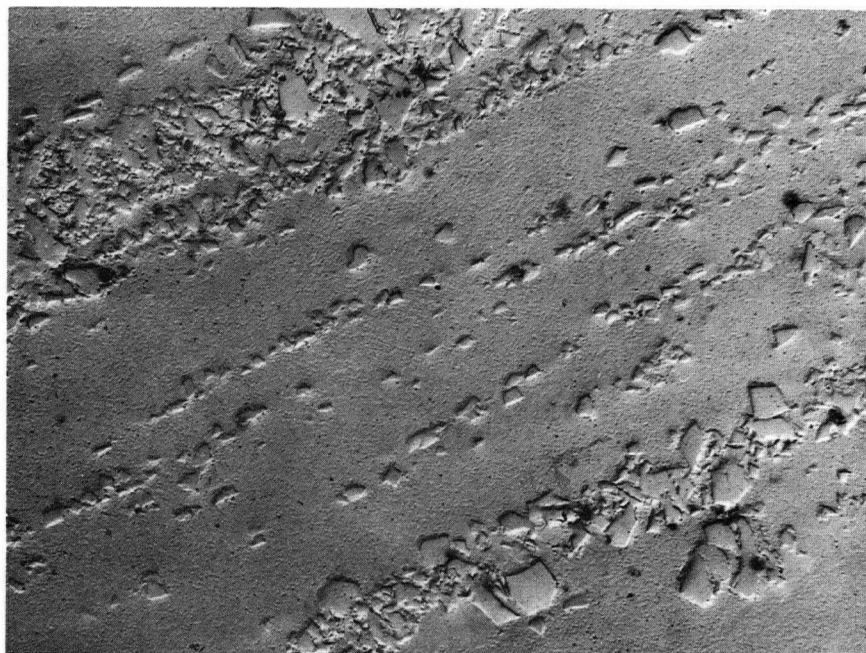


Fig. 25 Microstructure of a chill cast Zn - 0.6 wt.% Ti alloy extruded at 250°C. (x4000)

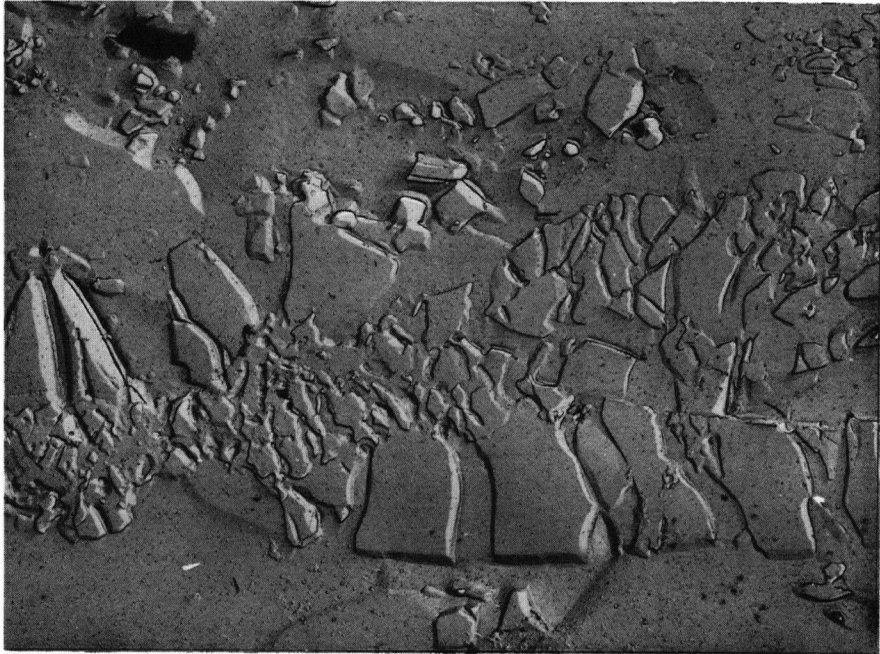


Fig. 26 Microstructure of a chill cast Zn - 0.6 wt.% Ti alloy extruded at 350°C. (x4000)

of the intermetallic particles to give the structure a more directional appearance.

4.5 The Effect of Extrusion Ratio

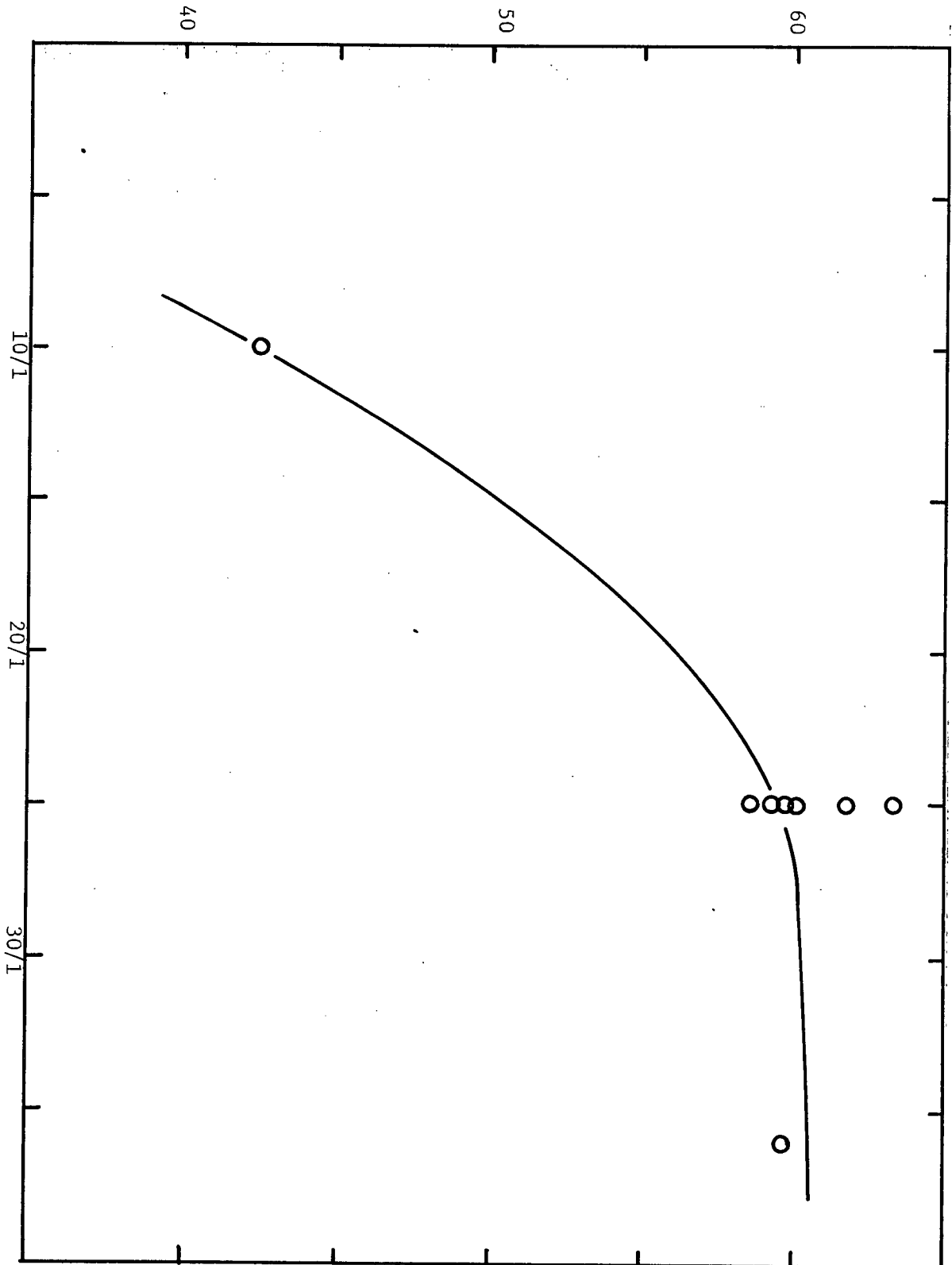
Qualitatively, a reduction in extrusion ratio should decrease the degree of deformation during fabrication and ultimately should result in a coarser, softer microstructure. An indication of the effect of the extrusion ratio is shown in Fig. 27. The data included in this plot were obtained under conditions in which microstructural coarsening due to thermal effects is minimal. Although the data do not allow a definitive statement to be made regarding an optimum extrusion ratio, they indicate qualitatively that the mechanical properties are indeed a function of the extrusion ratio. All subsequent extrusions were carried out with a 25:1 ratio.

4.6 Importance of Preferred Orientation

Investigations of extruded and rolled cast zinc-titanium alloys have shown the tendency for a preferred orientation to develop.^(28,35) These studies were confined to titanium concentrations less than 0.2 wt.%. Cominco carried out an extensive study of textures developed during extrusion of cast Zn - 0.16 wt.% Ti alloys.⁽³⁴⁾ Two distinct textures were observed, one being characteristic of the surface and another characteristic of the bulk material. It was concluded that the hardness did not depend significantly on the development of a texture.

Cast and rolled Zn - 0.16 wt.% Ti alloys also tend to develop a well-defined texture.⁽²⁸⁾ Apparently the formation of dendrites permits an extension of the growth process during which favourably oriented grains absorb those less favourably oriented.⁽³⁶⁾ Continued rolling of cast

0.2% OFFSET YIELD STRESS (10^3 PSI)



EXTRUSION RATIO

Fig. 27 The effect of extrusion ratio on the yield stress of Zn - 0.6 wt.% Ti alloys extruded at 175°C using -35 + 100 mesh powder.

structures tended to produce an increasingly more random structure with only a slight texture being encountered at 50% deformation. The breakdown of the cast texture was promoted by increasing the titanium concentration.

Data suitable for pole figure plots were obtained using a highly stringered material formed by low temperature extrusion of $-35 + 100$ mesh powder containing 0.6 wt.% Ti. No preferred orientation was detected in either the longitudinal or transverse directions. This result suggests that the development of high strength can not be associated with preferred orientation. The lack of texture in extruded rod has been observed in cases in which a reasonably high concentration of undeformable second phase exists in a zinc matrix. It is thought that the second phase tends to cause "turbulent" plastic flow of the matrix, resulting in randomness. (46)

Thus previous work has shown that the existence of a texture has relatively little effect on the creep properties or hardness of zinc-titanium alloys. The properties of the extrusion resulting from the directional nature of the dispersoid would overshadow effects due to the development of a texture. On this basis it was thought that further efforts in this direction would provide little knowledge as to the understanding of the mechanical properties of these alloys.

4.7 Thermal Stability

4.7.1 Introduction

As has been indicated earlier, the major factor limiting the use of zinc or zinc alloys in commercial applications is the poor creep behaviour resulting from the operation of recovery mechanisms and

grain boundary shear at room temperature ($T_H = 0.42$). The development of a commercially useful zinc alloy depends upon the development of a microstructure which inherently retards the operation of these processes and thus preserves reasonable creep properties up to at least 75°C. Therefore if this type of microstructure is contingent on a particular dispersion of a second phase such as is present in extruded zinc-titanium alloys, then creep and tensile properties at elevated temperatures will be determined by the thermal stability of the intermetallic compound $Zn_{15}Ti$.

4.7.2 Effect of Extrusion Temperature

Consideration of the effect of extrusion temperature shown in Figs. 9 and 10 suggests that coarsening of the intermetallic occurs at temperatures above 200°C. This results in essentially equivalent mechanical properties for extruded castings and extruded powders. Therefore to develop the potential strength obtainable through the use of powder metallurgical techniques, fabrication should be carried out at temperatures less than 200°C. In all instances, high temperature extrusion of powders results in the production of an equiaxed grain structure and a spheroidized second phase. Quoted extrusion temperatures are somewhat misleading in as much as the actual temperature at the die - billet interface can be expected to be considerably higher. For this reason it is difficult to define the thermal stability of a structure in terms of fabrication temperature.

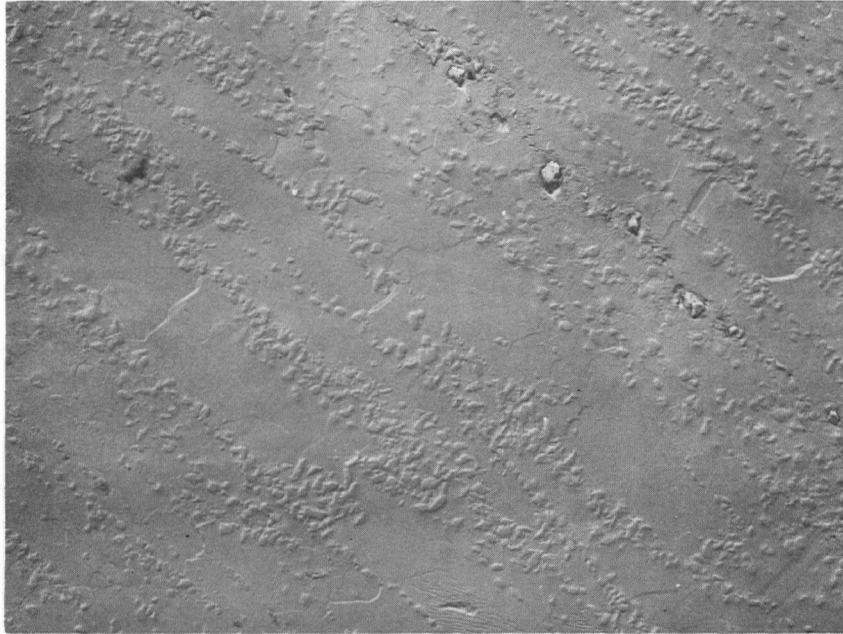
From these results it is apparent that a fine second phase dispersion in the fabricated product is contingent on retaining the fine intermetallic structure formed during atomization. It has been seen that low temperature fabrication is not an effective method of fragmenting

and dispersing larger primary intermetallic particles to the extent that substantial enhancement of the mechanical properties is realized. This has already been demonstrated in Figs. 24, 25 and 26, which indicate the degree to which fracture and dispersion of large second phase particles occurs as the extrusion temperature is lowered.

From the previous discussion, it is apparent that prior thermal treatment of the powder should have an intermetallic agglomeration effect similar to that obtained by extruding at elevated temperatures. This was substantiated by annealing a billet of -35 + 100 mesh 0.6 wt.% Ti powder at 300°C for 1/2 hour prior to extrusion at 175°C. The mechanical properties which result are substantially the same as those of cast and extruded material or powders fabricated at higher temperatures. As can be seen from Fig. 28, no evidence of intermetallic fragmentation was observed after low temperature extrusion, further demonstrating that the second phase remains hard relative to the matrix. Thus thermal treatment prior to or during deformation must be avoided in order to ensure development of the potential strength of the alloys.

The role of extrusion temperature and its effect on the dispersion of spheroidized or thermally treated powder billets was investigated by varying the extrusion temperature of -100 + 200 billets containing 0.6 wt.% Ti which had undergone a one hour anneal at 350°C. Thermal treatment under these conditions results in a reasonably coarse, spheroidized intermetallic structure. Figure 29 indicates the mechanical properties of the alloy produced under these conditions.

Higher extrusion temperatures tend to coarsen the intermetallic slightly. This is thought to be a function of the availability of thermal energy for diffusion during the pre-extrusion soak. As is



(x4000)

$\dot{\epsilon}$ (min. ⁻¹)	.2% O.Y.S. (10 ³ psi)	U.T.S. (10 ³ psi)	Total Elongation (%)
0.0028	25.0	27.2	8.2
0.028	26.3	28.7	7.1
0.28	29.7	33.6	9.0
2.8	37.2	42.3	7.5

Fig. 28 The structure and mechanical properties of a Zn - 0.6 wt.% Ti alloy extruded at 175°C using -35 + 100 mesh powder. (The billet was annealed for 1/2 hour at 300°C prior to extrusion.)

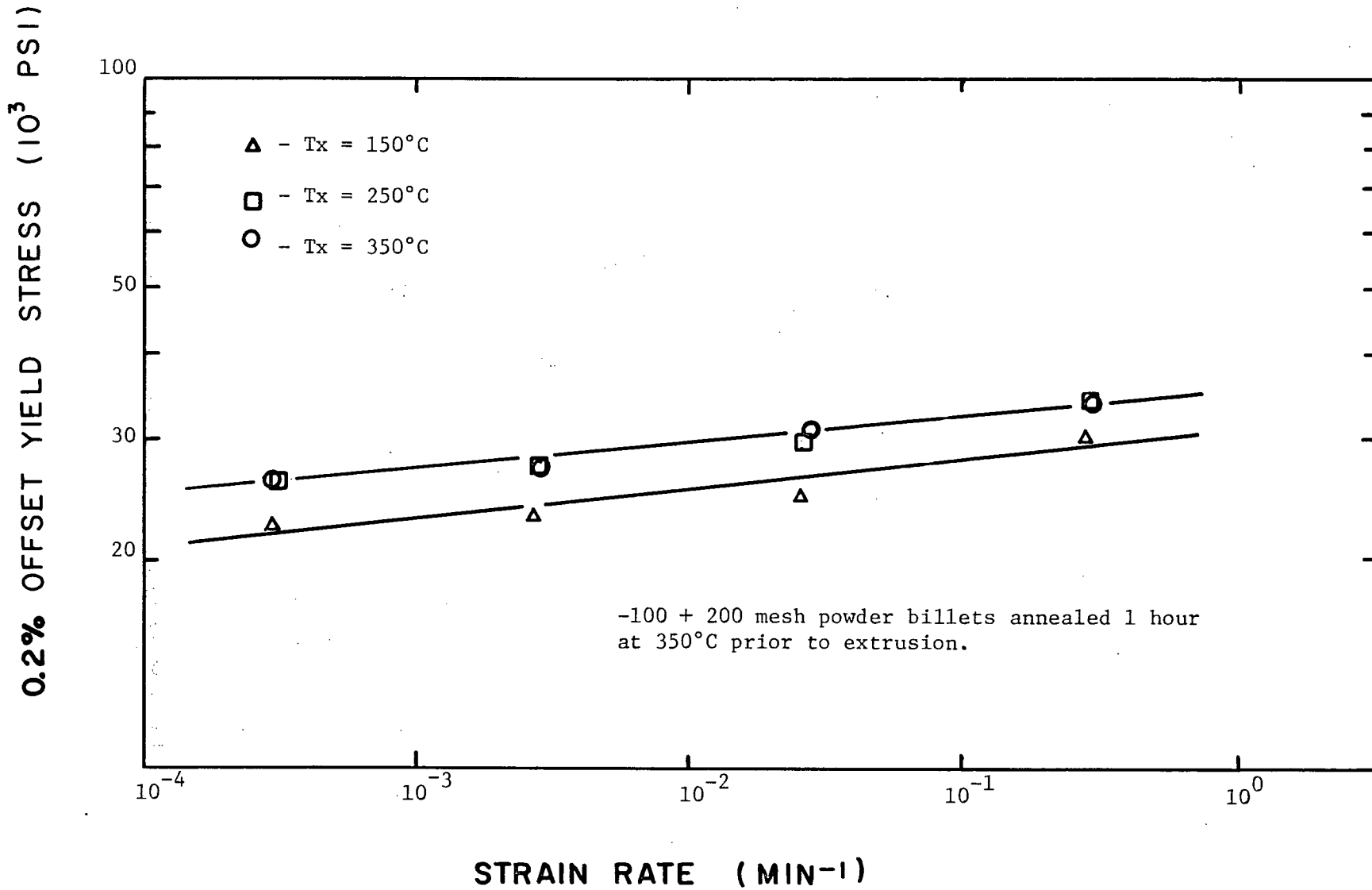


Fig. 29 The effect of extrusion temperature on the yield stress of a thermally stabilized Zn - 0.6 wt.% Ti alloy.

to be expected, the coarsening of the second phase also results in a slight increase in grain size. The overall result is a slight loss in strength. However it should not be assumed that the observed strengthening effect at the lower fabrication temperatures is the result of a change in grain size alone. As has been discussed briefly, grain boundary effects are important at 20°C. Therefore the role and properties of a dispersed second phase and its relation to grain boundaries are important factors which must be considered in a discussion of mechanical properties at this temperature.

Figs. 30(a) and (b) show the structures which typically result from changes in extrusion temperature. From these micrographs it can be seen that only a slight amount of coarsening of the intermetallic and grain size has resulted from extrusion at 350°C. However some alignment of the second phase in the extrusion direction has occurred at 250°C., giving rise to microstructures which are somewhat different in appearance. The degree of directionality of the microstructure is related to the relative ease of flow of the matrix at the temperature under consideration. The development of such a microstructure is significant when considering the effect of the dispersion of the operation of grain boundary shear as an important deformation mechanism.

4.7.3 Effect of Annealing Temperature

4.7.3.1 Powder Material

The use of powder metallurgical techniques to obtain enhanced mechanical properties is especially attractive from a commercial point of view if the desired properties can be developed through the use of relatively

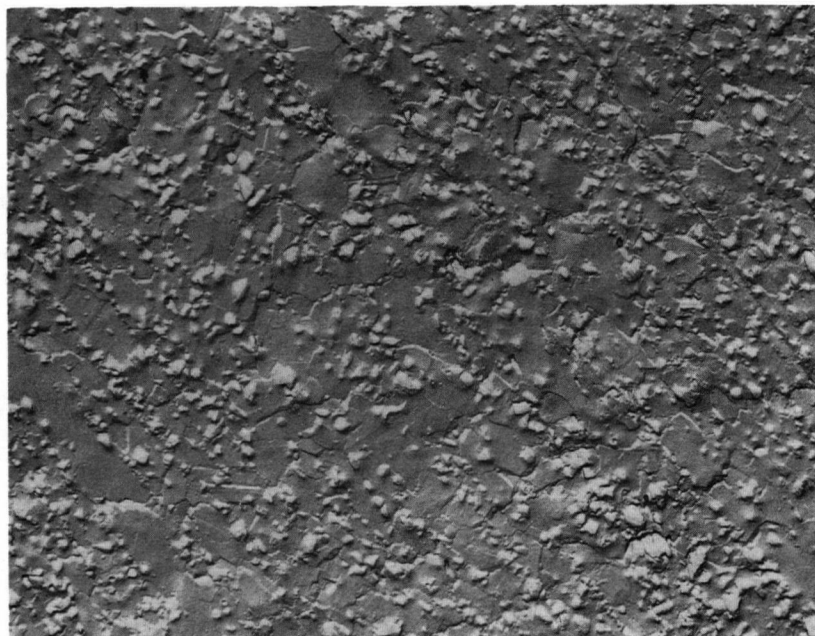


Fig. 30(a) The microstructure resulting from extrusion of a -100 + 200 mesh powder billet annealed for 1 hour prior to extrusion at 250°C.
(x4000)

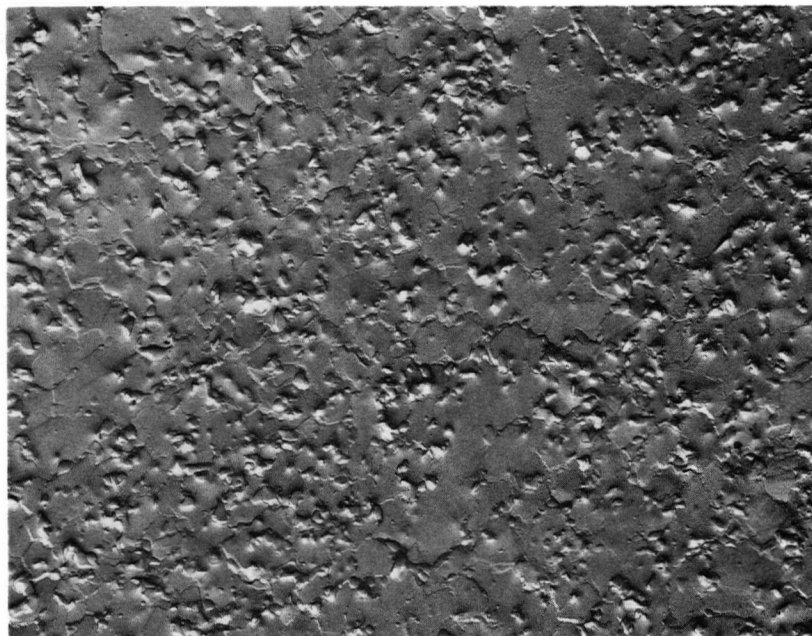


Fig. 30(b) The microstructure resulting from extrusion of a -100 + 200 mesh powder billet annealed for 1 hour prior to extrusion at 350°C.
(x4000)

coarse powders. This is due to the high cost of production of fine powders in large volumes. Thus the high strength levels achieved using -35 + 100 mesh zinc-titanium powder may be of some commercial interest, providing thermal stability can be achieved.

A simple and meaningful method of establishing the stability of as-extruded microstructures is a simple annealing study. The results of such a study on extruded -35 + 100 mesh powder are shown in Figs. 31 and 32. It can be seen that for relatively short times, the intermetallic appears to remain stable up to approximately 160°C. At annealing temperatures above 200°C, the strength is reduced to the same level as that obtained by extruding powders at high temperatures or by extrusion of cast billets. A narrow range exists (175° - 200°C) in which the microstructure is very temperature sensitive.

Thus the initial structure which consists of well developed intermetallic stringers and an associated columnar-grained zinc matrix is stable to reasonably high temperatures. At slightly more elevated temperatures, some agglomeration of the intermetallic occurs. This coarsening of the second phase does not appear to take place generally throughout the material but rather occurs preferentially in isolated colonies. Changes in grain shape and some minor grain growth accompany this coarsening. The result is that a transition structure is formed consisting of colonies of equiaxed grains and spheroidized intermetallic. An example of this type of structure is shown in Fig. 33.

Above 200°C, the stringered structure has been completely lost, with extensive modifications of the grain shape and second phase distribution. Higher annealing temperatures result in a slight increase in the amount of second phase coarsening and an increase in grain size.

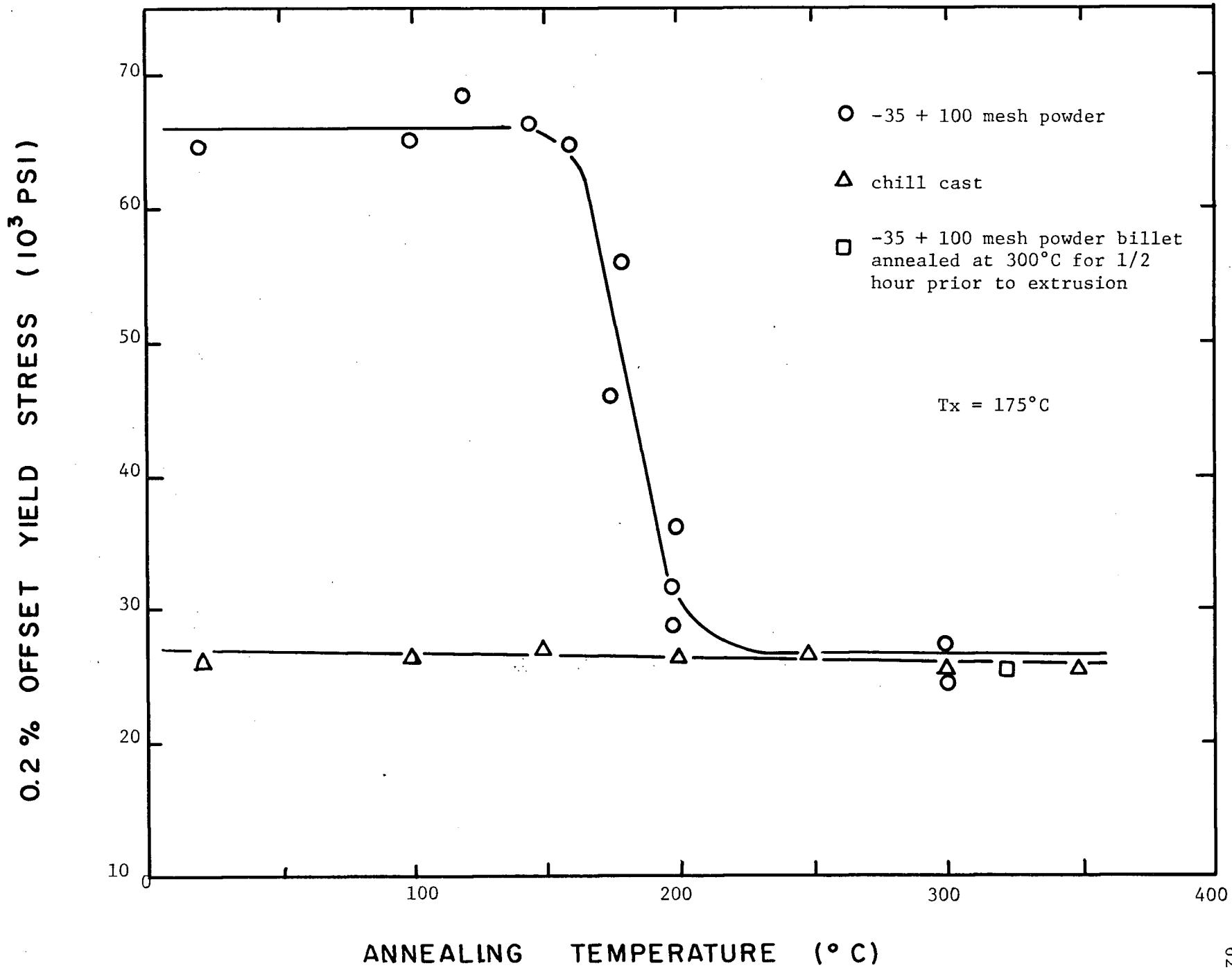


Fig. 31 The effect of annealing temperature on the yield strength of Zn - 0.6 wt.% Ti alloy at 20°C.

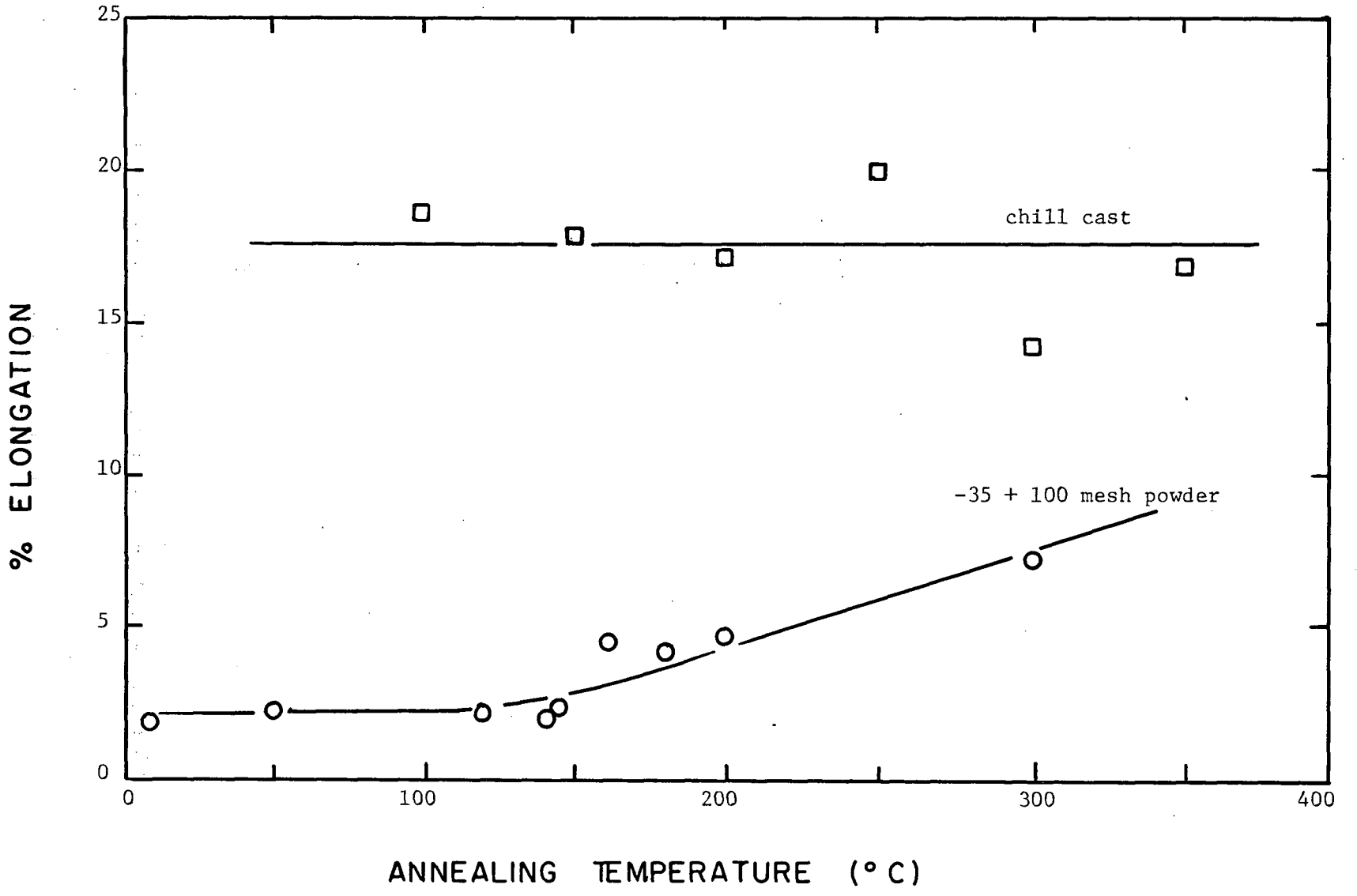


Fig. 32 The effect of annealing temperature on the ductility of Zn - 0.6 wt.% Ti alloy at 20°C.

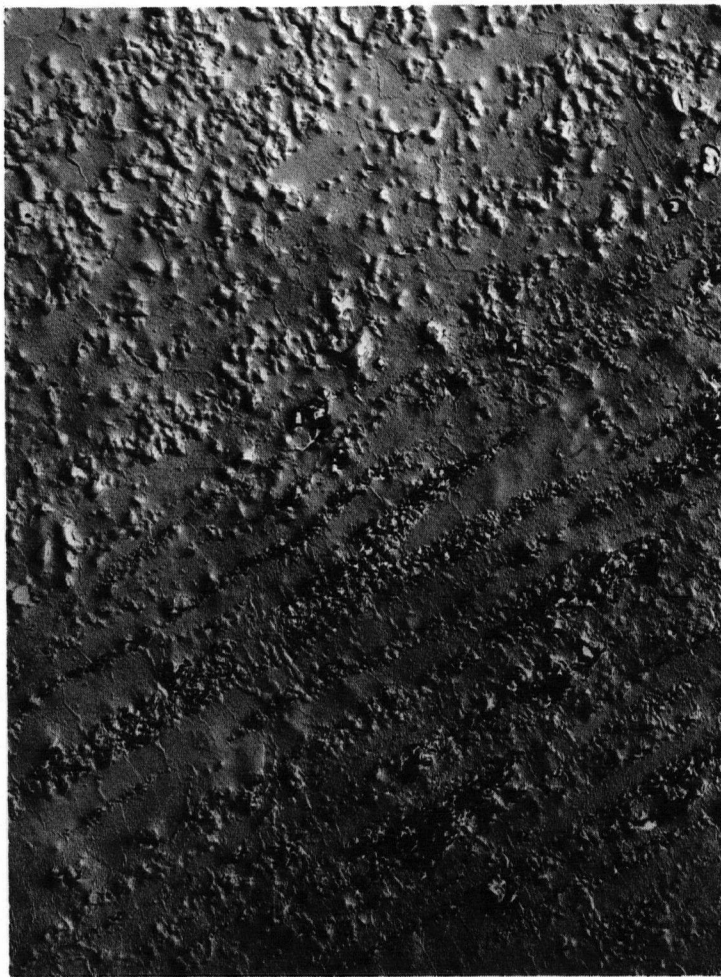


Fig. 33 The microstructure resulting from a short term anneal at 180°C of a Zn - 0.6 wt.% Ti alloy fabricated at 175°C using -35 + 100 mesh powder. (x4000)

The overall effect on the mechanical properties is small, and the microstructure can be considered to be "thermally stable".

Long term - high temperature anneals simply allow an extension of the coarsening process with a slow decrease in strength accompanying increased agglomeration. The structure and properties which result after such thermal treatments are shown in Figs. 34 and 35.

4.7.3.2 True Stress-Strain Curves

Figure 36 shows true stress-strain curves for material annealed at various temperatures. It can be seen that the work hardening characteristics change from parabolic hardening for as-extruded material and extrusions annealed at low and high temperatures to a high degree of linear hardening if the material is thermally treated at intermediate temperatures. Fibre strengthened materials often show analogous behaviour. However the microstructures involved here do not lend themselves to interpretation in terms of fibre composite theories since no strength can be attributed to the discontinuous intermetallic stringers.

Table V tabulates the tensile properties and work hardening rates obtained from these curves (Fig. 36) and other curves which have not been presented. From these results it is apparent that though the nature of the hardening is modified as the annealing temperature is increased, the work hardening rate at 0.5% strain is constant up to annealing temperatures of approximately 200°C. At higher temperatures, the hardening rate decreases. It is also interesting to note that the amount of work hardening is maximized when linear hardening occurs.

From analysis of the true stress-strain curves, it appears that material thermally treated at intermediate temperatures (160°C and

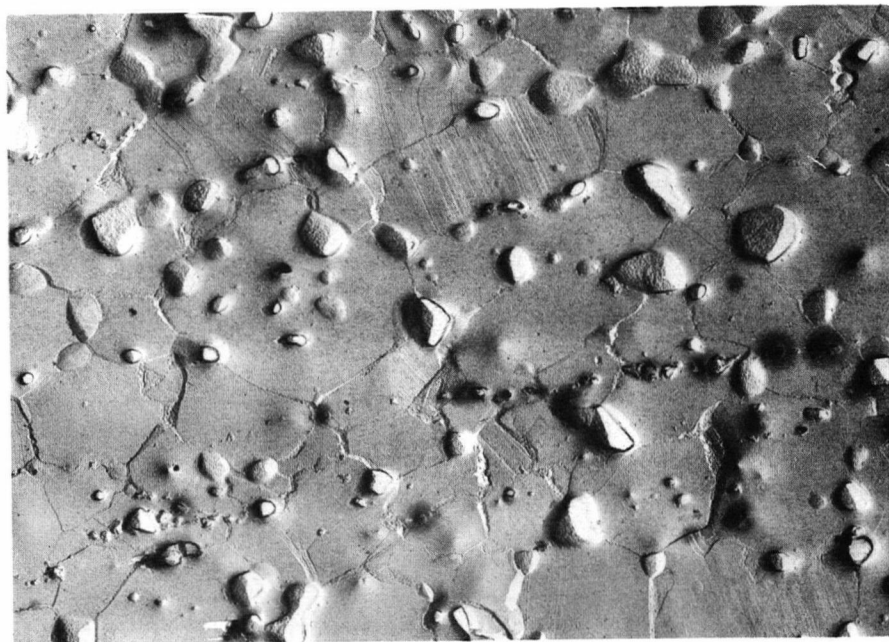


Fig. 34 The microstructure of a Zn - 0.6 wt.% Ti alloy fabricated at 175°C from -35 + 100 mesh powder and annealed for 44 hours at 350°C. (x4000)

O.Y.S. ($\dot{\epsilon} \sim 0.0028 \text{ min.}^{-1}$) = 22,500 p.s.i.
 Total elongation = 12%

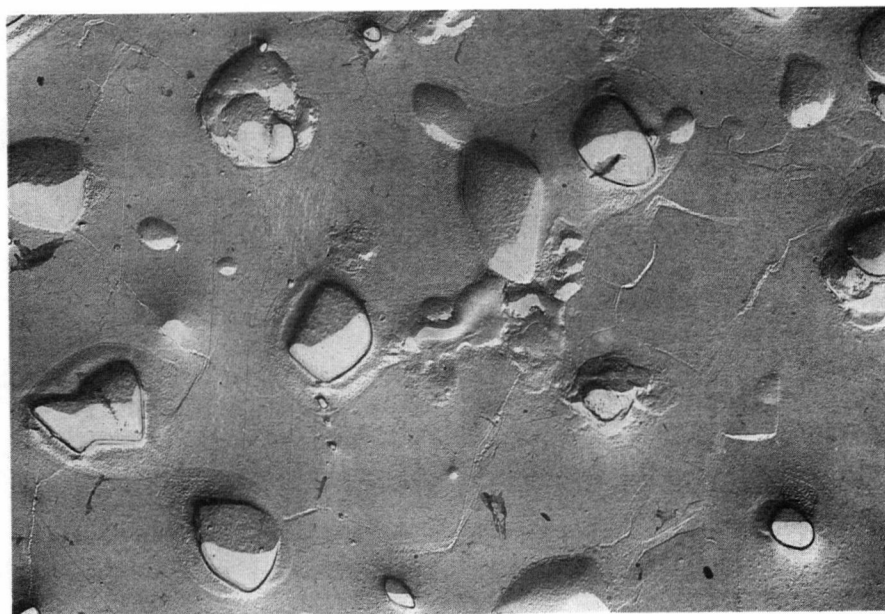


Fig. 35 The microstructure of a Zn - 0.6 wt.% Ti alloy fabricated at 175°C from -35 + 100 mesh powder and annealed for 94 hours at 400°C. (x4000)

O.Y.S. ($\dot{\epsilon} \sim 0.0028 \text{ min.}^{-1}$) = 17,800
 Total elongation = 14%

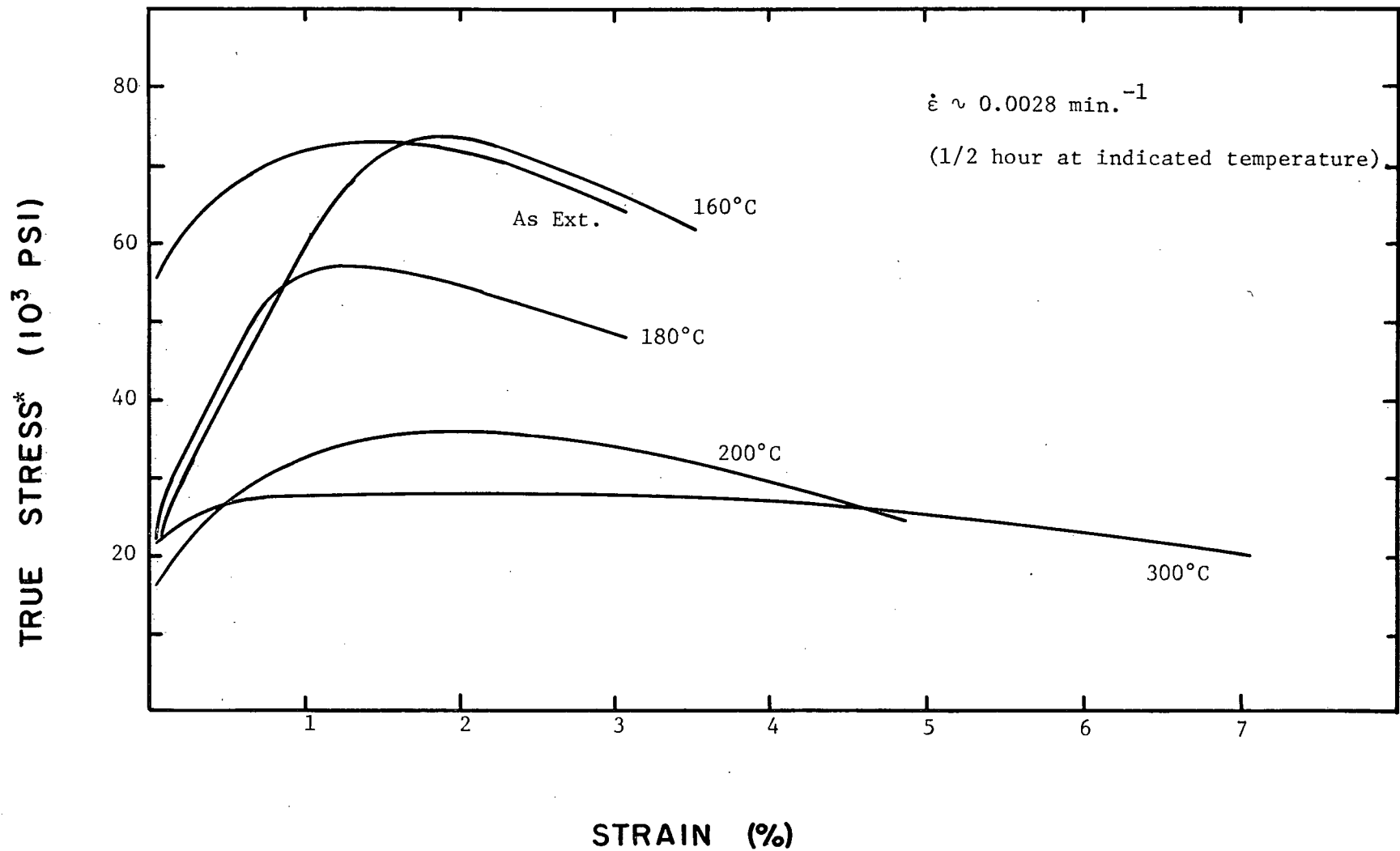


Fig. 36 The effect of annealing temperature on the true stress - strain relationship at 20°C for Zn - 0.6 wt.% Ti alloys extruded at 175°C using -35 + 100 mesh powder.
 *(See page 20).

Table V. Mechanical Properties of -35 + 100 Mesh Zn - 0.6 wt.% Ti
Powder Extruded at 175°C and Annealed at Various Temperatures.

Annealing Conditions (1/2 hr at temperature)	Work Hardening Rate at 0.5% Strain (10 ⁶ psi)	0.2% O.Y.S. (10 ³ psi)	U.T.S. (10 ³ psi)
as-extruded	2.0	60.2	64.5
100°C	2.7	61.9	67.7
120°C	4.2	59.6	69.3
140°C	4.2	59.9	66.5
160°C	4.1	29.0	73.5
180°C	4.2	31.7	57.1
200°C	2.9	21.4	35.7
300°C	0.45	24.6	27.4

Note: The high observed hardening rates are not true rates as such.
The values are indicative of a pseudo-elastic effect.

180°C) undergoes "quasi-yielding" at very low stress levels and low strains. The stress at which this type of yielding occurs corresponds closely to yielding in softer extrusions, i.e. extruded material heat-treated at higher temperatures.

As has already been indicated, the zinc-titanium intermetallic appears to be thermally stable up to approximately 160°C when held for 30 minutes at temperature. The transition structure which is the result of intermediate thermal treatments can be thought of as consisting of both hard and soft regions, the hard regions being areas in which the microstructure remains stringered. Deformation within the soft region gives rise to an apparent low yield stress ("quasi-yield"). For general deformation to occur, some stringered areas must also deform. This gives rise to a high ultimate tensile strength.

If the material is annealed at a sufficiently high temperature, coarsening of the complete microstructure will take place, resulting in both low yield and low ultimate tensile stresses.

4.7.3.3 Annealed Cast-Extruded Zn-Ti Alloys

Short period thermal treatment has virtually no effect on the mechanical properties of cast and extruded material. If any significant effect were possible it was thought it would occur in low temperature extrusions in which the microstructure is somewhat finer.

The experimental results obtained by thermal treatment of a cast 0.6 wt.% Ti alloy extruded at 150°C shown in Figs. 31 and 32 indicate that microstructural modifications are minor.

4.8 The Effect of Titanium Concentration

The mechanical properties of zinc-titanium alloys are determined by the nature of the microstructure, which in turn is determined by the fabrication processes used. It has been shown that the extrusion temperature has a significant influence on the mechanical properties of material fabricated from powder and a minor effect on the properties of cast material. Thus it is useful to discuss the effects of the second phase content in conjunction with both high and low fabrication temperatures.

Table VI indicates the effect of titanium concentration on the mechanical properties of alloys investigated in this study. These data show that the concentration effect is significant when extrusion is carried out at a low temperature. This effect is marginal when an extrusion temperature of 350°C is used. Figures 37 through 40 illustrate the true stress-strain curves obtained for these materials.

4.8.1 Powder Material

Extrusion of powder at low temperatures results in the formation of a stringered structure in which the stringer spacing and thus the grain size are reduced as the titanium concentration is increased. Thus significant increases in strength are observed in alloys of higher titanium content.

At 350°C, short diffusion paths give rise to coarsening of the fine as-solidified intermetallic structure, thereby leading to the development of rather coarse extruded microstructures with no stringered appearance. Low strengths are associated with such microstructures.

Ti Concentration (wt.%)	Billet	Tx (°C)	0.2% O.Y.S. (10 ³ psi)	U.T.S. (10 ³ psi)	Elongation to Maximum Stress (%)	Reduction in Cross-sectional Area (%)	Total Elongation (%)
0.07	-35 + 100 mesh powder	175	37.2	40.8	1.2	15	4.5
0.16	"	175	44.9	49.8	1.4	—	3.1
0.32	"	175	45.7	49.2	1.0	10	2.8
0.60	"	175	60.1	64.4	0.8	—	3.5
0.07	cast	175	17.0	19.5	10.0	>90	30.0
0.16	cast	175	18.9	22.1	7.0	—	21.0
0.32	cast	175	23.9	26.2	3.0	>90	16.0
0.60	cast	175	23.1	25.7	6.5	—	26.0
0.07	-35 + 100	350	22.7	24.3	6.0	75	20.3
0.16	-35 + 100	350	21.3	23.4	2.0	—	17.5
0.32	-35 + 100	350	23.7	25.7	2.0	65	11.7
0.60	-100 + 200	350	28.1	29.5	1.8	—	8.8
0.07	cast	350	18.2	22.8	9.0	>90	21.0
0.16	cast	350	23.4	26.4	8.0	—	20.5
0.32	cast	350	24.6	27.8	8.0	>90	19.0
0.60	cast	350	21.1	25.7	9.0	—	16.3

Table VI. The Effect of Titanium Concentration on Mechanical Properties.

($\dot{\epsilon} \sim 0.0028 \text{ min.}^{-1}$)

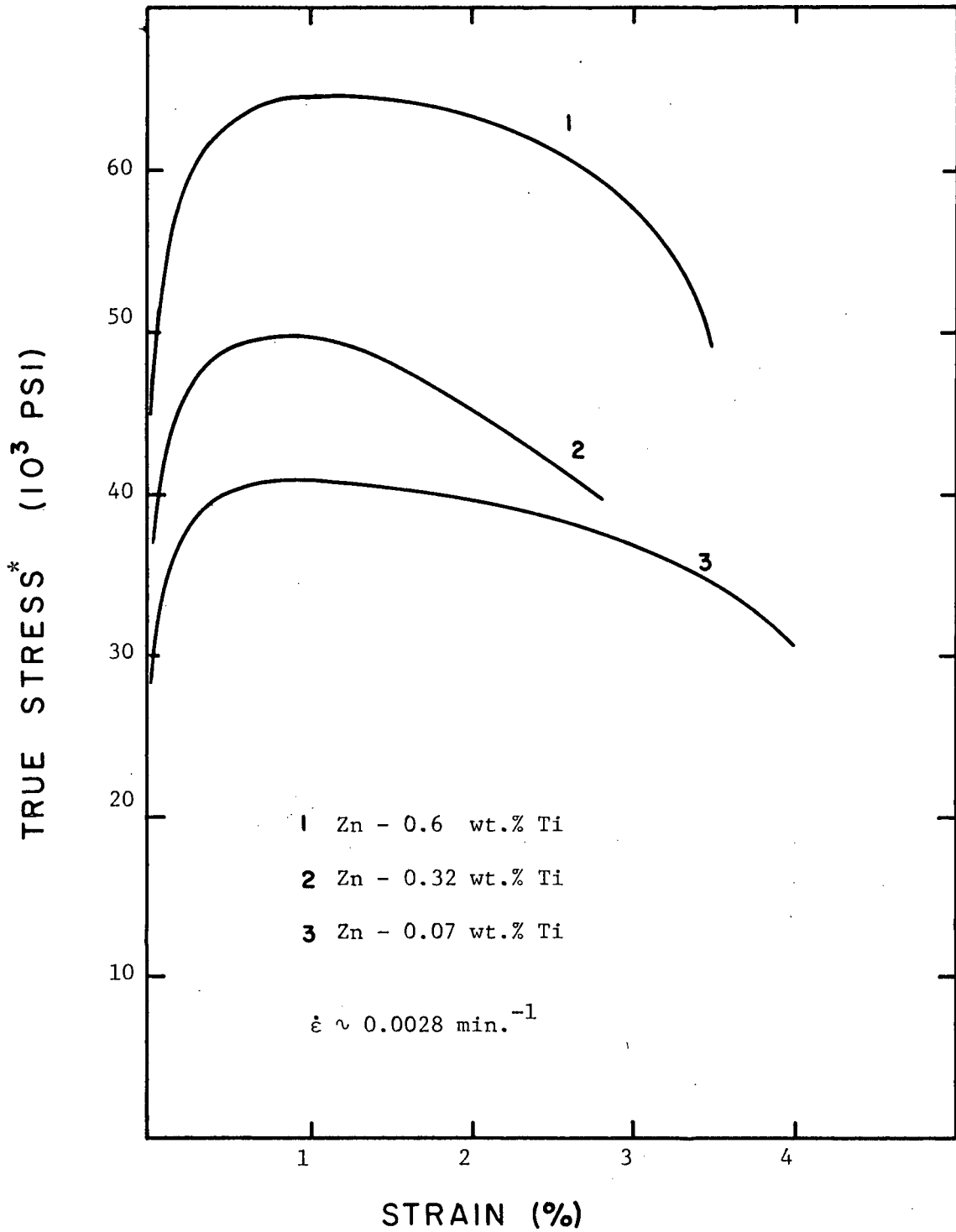


Fig. 37 True stress - strain curves for zinc - titanium extrusions of -35 + 100 mesh powder at 175°C.

* (See page 20).

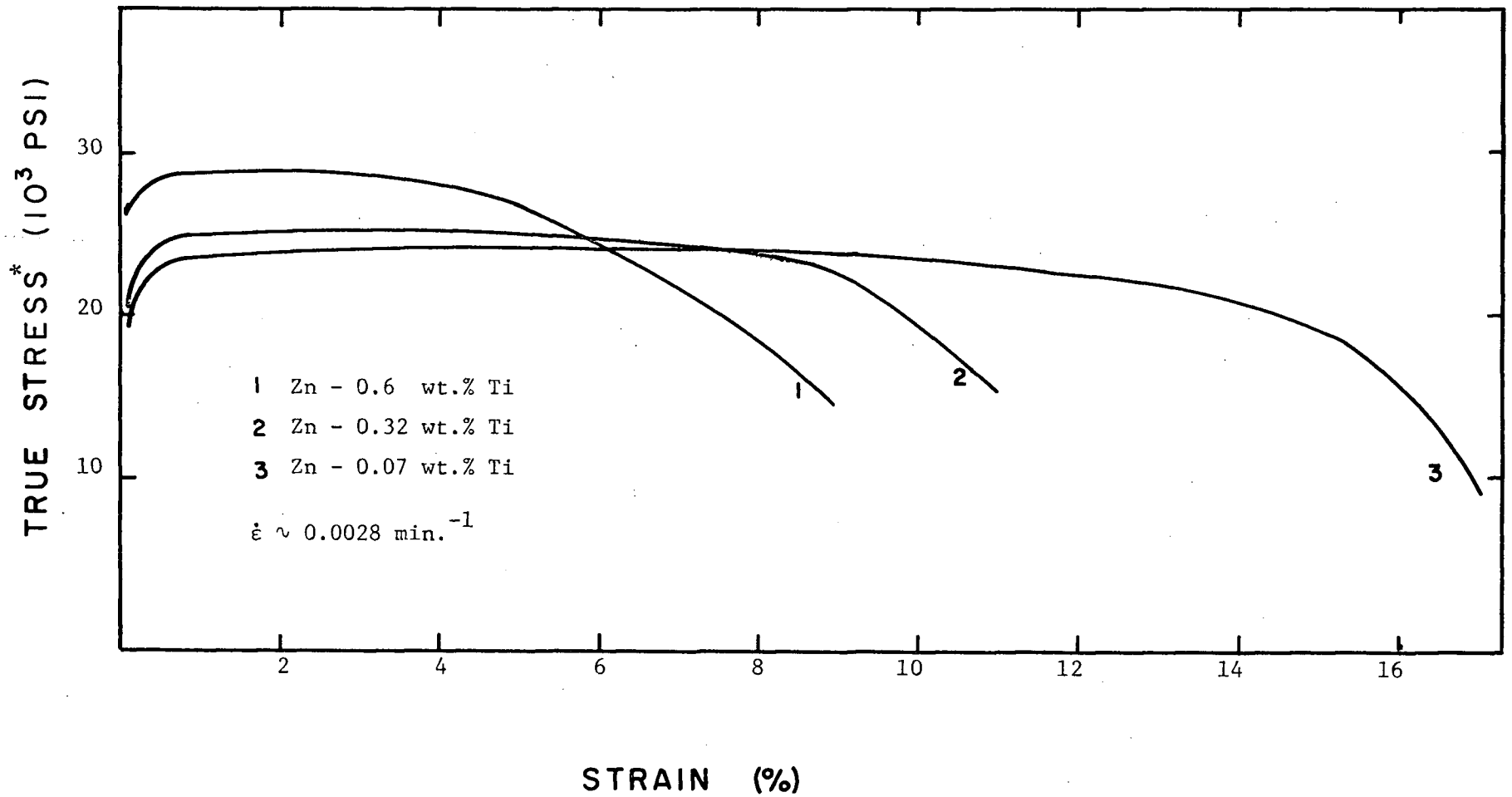


Fig. 38 True stress - strain curves for zinc - titanium extrusions of -35 + 100 mesh powder at 350°C.

* (See page 20).

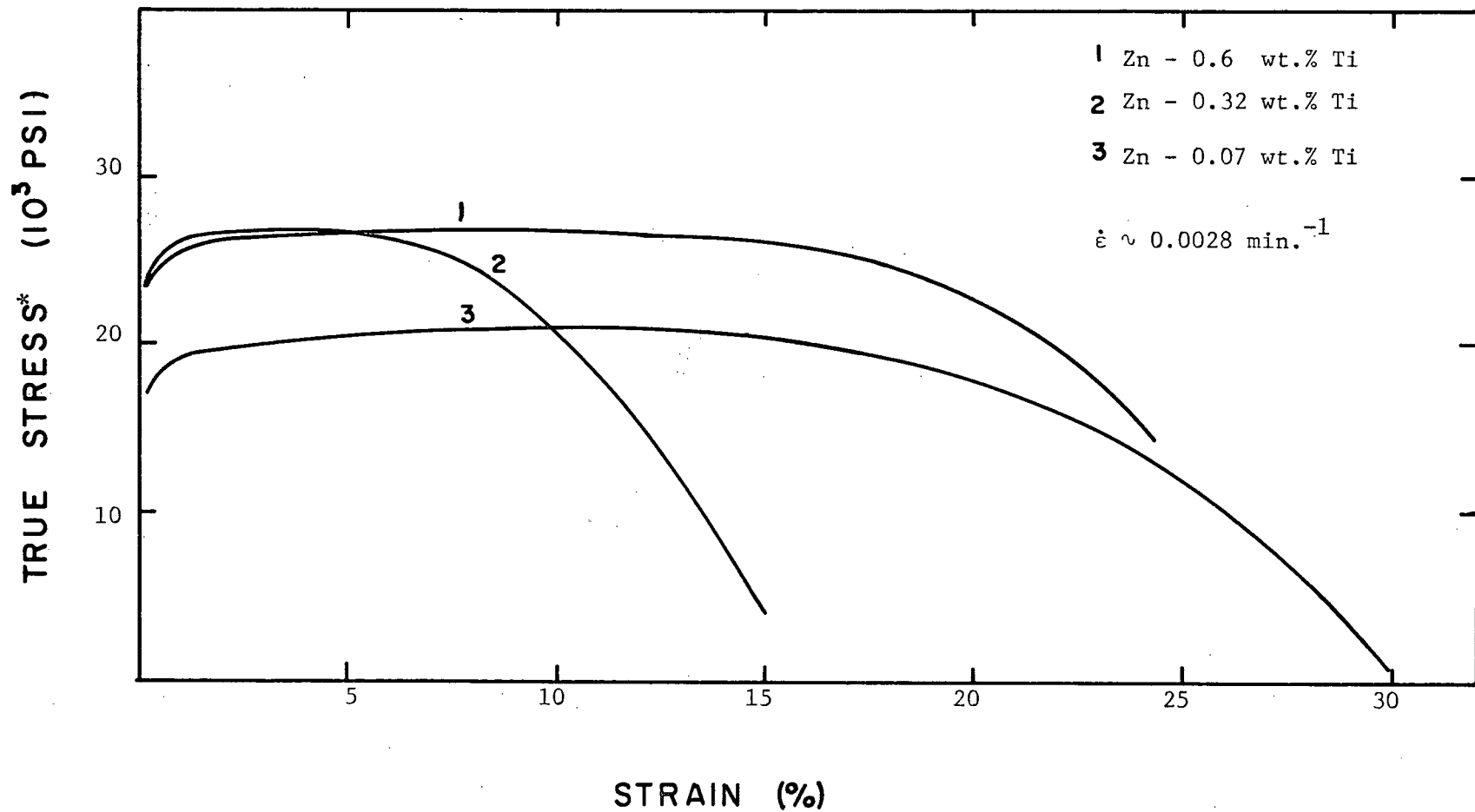


Fig. 39 True stress - strain curves for zinc - titanium extrusions of chill castings at 175°C.

* (See page 20).

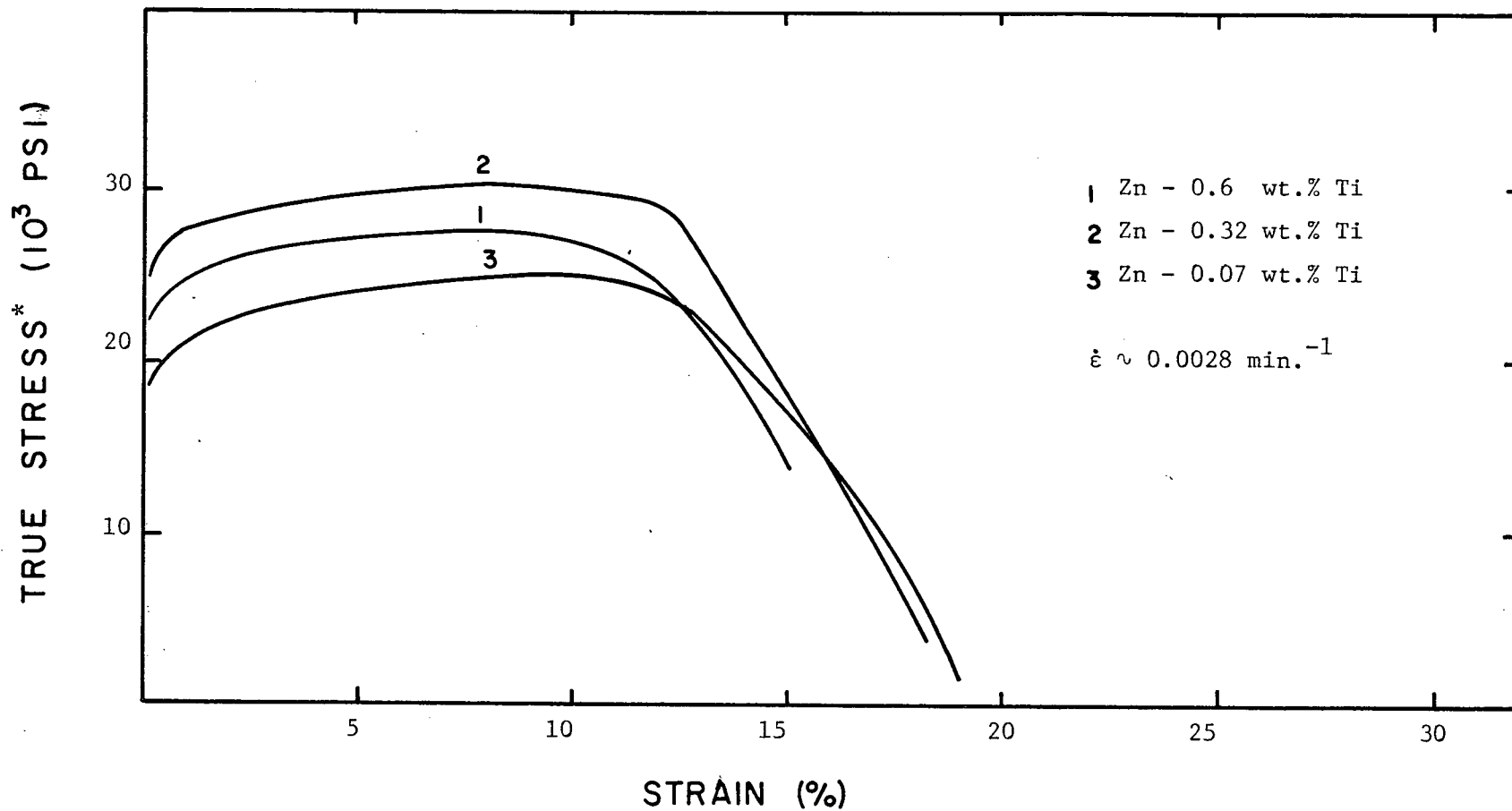


Fig. 40 True stress - strain curves for zinc - titanium extrusions of chill castings at 350°C.
* (See page 20).

4.8.2 Cast Material

Some grain refinement and rather coarse intermetallic stringering are characteristic of low temperature cast extrusions. Increasing titanium concentrations give rise to more extensive stringering and slightly greater strength. The mechanical properties are insensitive to concentration when extrusion is carried out at 350°C. These properties must be discussed in terms of the second phase distribution and size, the grain size, and grain shape. This discussion appears in a later section.

4.8.3 Ductility

As can be seen from Table VI, fabrication history is the major factor controlling ductility, with second phase content playing a minor role. In the absence of a stringered structure, reduction in area values are consistently above 50% with the highest values being obtained for cast and extruded material. Total elongation varies between 20% and 30% for cast and extruded material. The elongation values are slightly lower for powders extruded at 350°C. As expected, the lowest total elongation values were observed with low temperature powder extrusions. Similar trends were exhibited in elongation to maximum stress values.

Any analysis of mechanical properties at constant strain-rate as a function of titanium concentration is not complete since it must be assumed that the strain-rate sensitivity is the same for all compositions. Therefore to rigorously analyze trends in the mechanical properties, the strain-rate sensitivity must be established and related to the operative deformation mechanisms.

4.9 Deformation Characteristics

4.9.1 Introduction

It is generally thought that five independent deformation modes must be operative before a polycrystalline metal can exhibit any significant ductility. Slip, twinning, and grain boundary shear may fulfill or partially fulfill these requirements. The yield stress is determined by the number of deformation modes available and by the ease of activation of these mechanisms.

4.9.2 Deformation Mechanisms

4.9.2.1 Slip

The predominant slip system in zinc is the basal system $\{0001\} \langle 11\bar{2}0 \rangle$. Two independent modes can be attributed to slip on these systems. The only non-basal slip system observed to be operative in zinc is the second order pyramidal system $\{11\bar{2}2\} \langle 11\bar{2}3 \rangle$. The operation of non-basal slip itself is sufficient for homogeneous deformation in as much as it provides five independent slip systems. The stress levels associated with the activation of non-basal slip are significantly higher than those required for basal slip. ⁽⁶⁾

In zinc-titanium alloys, both basal and non-basal slip (Fig. 41) were observed. Basal slip traces were generally well-defined, straight and continuous, while non-basal traces were often wavy and discontinuous.

4.9.2.2 Twinning

Deformation twinning is a common occurrence in large-grained

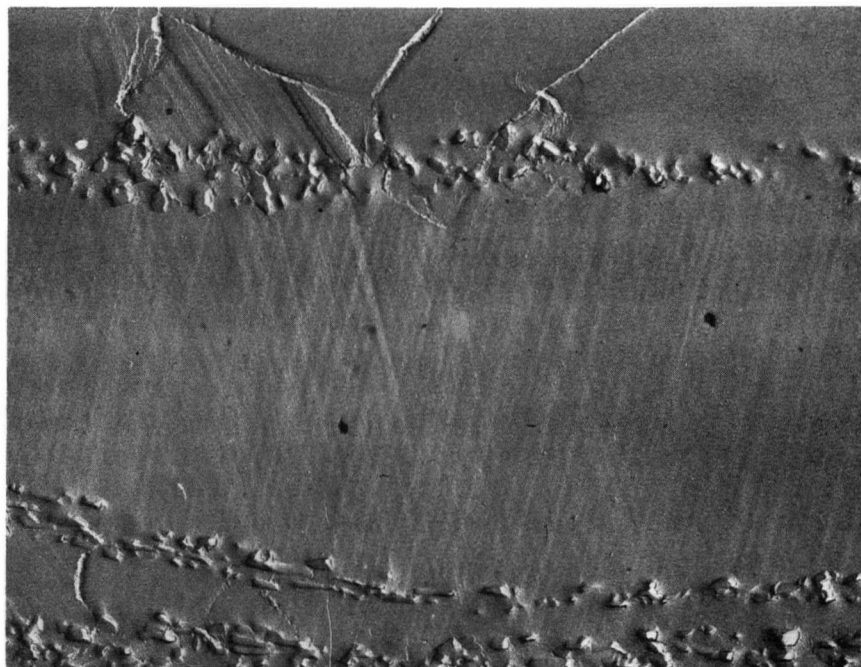


Fig. 41 Metallographic evidence of non-basal slip in a chill cast Zn - 0.32 wt.% Ti alloy extruded at 175°C. (x6000)

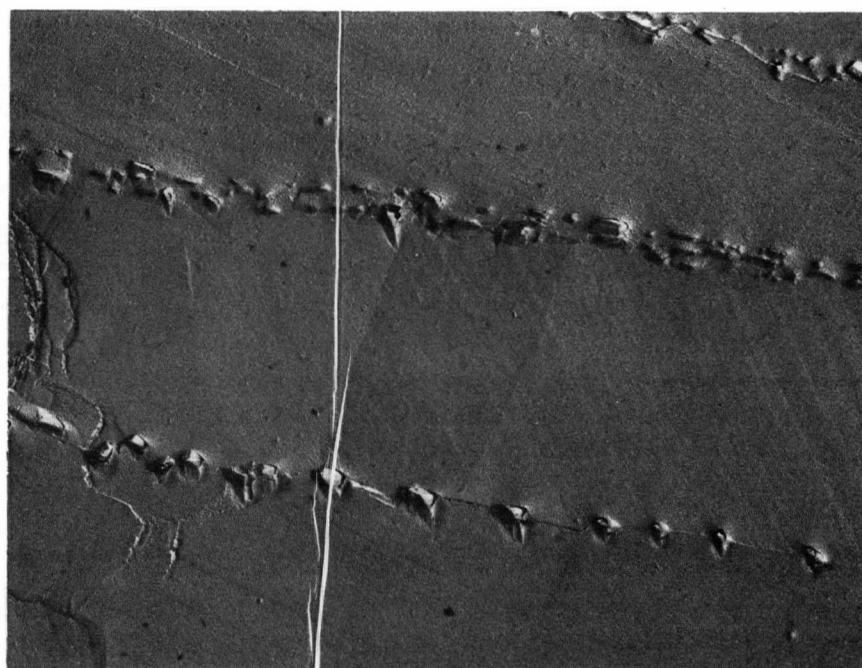


Fig. 42 Metallographic evidence of twinning in a chill cast Zn - 0.16 wt.% Ti alloy extruded at 175°C. (x6000)

hexagonal metals. The importance of this mechanism is a function of temperature, grain size, and the presence and nature of a dispersed second phase. Twinning rarely occurs in fine-grained zinc alloys produced by powder metallurgical techniques. The literature contains no information regarding the effect of a fine grain size on twinning. However the lack of its presence suggests that the critical stress required for nucleation may be related to a critical dislocation pile-up length, the size of which may not be present in fine-grained material. Because of the limited occurrence of twinning, it is not considered to affect significantly the mechanical properties of alloys investigated in this study. Figure 42 shows an example of a twin in a Zn - 0.16 wt.% Ti alloy.

4.9.2.3 Grain Boundary Shear

A deformation process which is of particular importance when considering fine-grained materials at high effective temperatures is grain boundary shear. Numerous theories as to the actual mechanisms involved in this process have been proposed,⁽¹⁴⁾ but as yet the mechanism is not completely understood. However the effect of temperature, strain-rate and presence of a second phase are areas in which extensive investigations are being carried out, particularly in the area of superplasticity.

The number of independent modes which can be attributed to shear is a matter of controversy. It is generally agreed, however, that this process may occur at very low stress levels.

A large percentage of metallographical information is based on surface observations. It is possible that the nature and degree of grain boundary shear within the material might differ significantly from that suggested by observations of the surface. Thus accurate estimates

of the contribution of shear to the overall deformation of a material are difficult to make and involve sophisticated experimental procedures.

It is important to realize that a grain boundary deformation mechanism must operate in conjunction with a diffusion mechanism or with a mechanism whereby intragranular deformation occurs in order to fulfill accommodation requirements. Figure 43 shows grain boundary shear operating in conjunction with grain boundary migration.

4.9.3 Recovery Mechanisms

4.9.3.1 Introduction

In view of the high effective temperature of zinc at room temperature, dynamic recovery effects may have a substantial influence on the observed mechanical properties. In the broad sense, dynamic recovery may be defined as the continuous loss of dislocations through diffusion controlled processes.

Cross slip is not considered an important recovery mechanism in zinc due to the lack of a cross slip system.

4.9.3.2 Grain Boundary Migration

An important function of grain boundary migration is the partial fulfillment of accommodation requirements at phase boundaries and triple points. This process is considered a dynamic recovery mechanism if migration results in a net decrease in dislocation density at or near the boundary.

Grain boundary shear results in the formation of a shear zone during sliding. The generation of dislocations within this zone acts

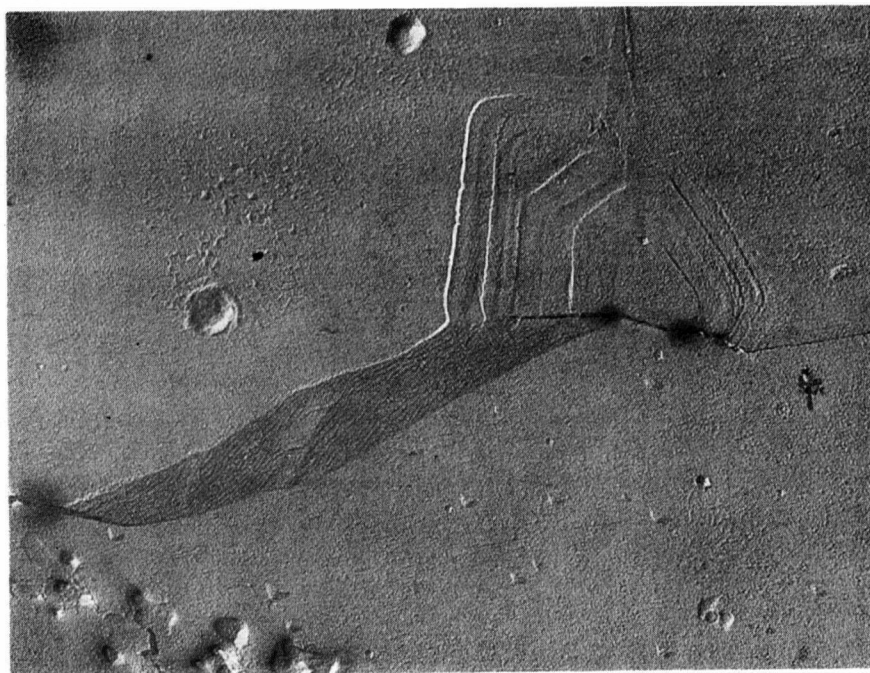


Fig. 43 Metallographic evidence of grain boundary shear and migration in a chill cast Zn - 0.32 wt.% Ti alloy extruded at 350°C. (x6000)

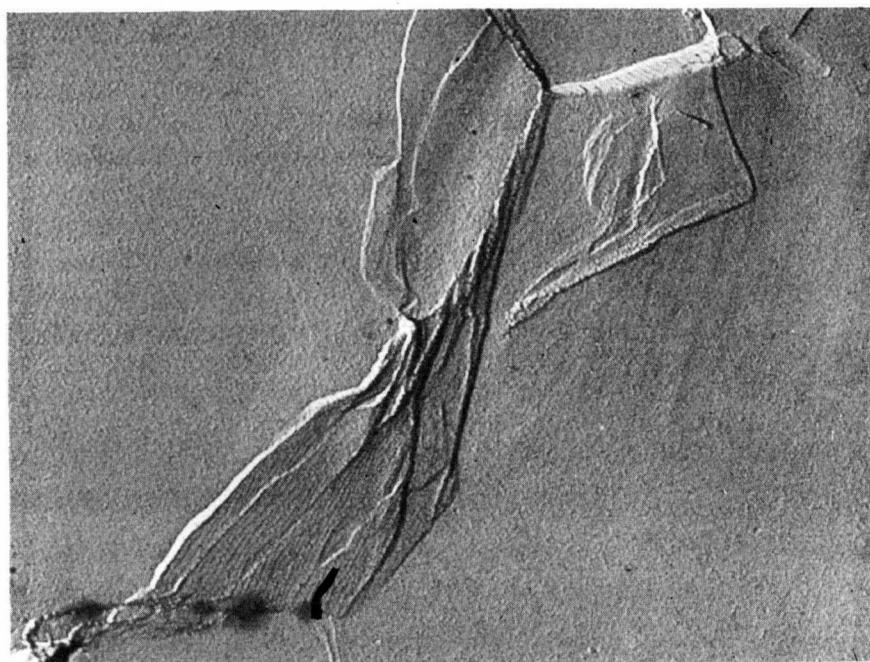


Fig. 44 Metallographic evidence of grain boundary shear and migration in a chill cast Zn - 0.32 wt.% Ti alloy extruded at 350°C. (x6000)

as the driving force for local migration.^(42,43,50) Further dislocation loss may occur through the annihilation of pile-ups by a migrating boundary. Figure 44 shows an example of grain boundary migration.

The presence of a second phase on a boundary may retard migration. The dispersoid spacing will determine the degree to which migration occurs.

4.9.3.3 Dislocation Climb

The climb of dislocations around obstacles or out of dislocation pile-ups at grain boundaries is thought to be the most important recovery mechanism at $T_H = .4$ or higher. This mechanism has received much attention in the general theories of recovery creep where the rate of recovery is thought to be controlled by the rate and distance of dislocation climb.^(44,45) Recovery by climb may be discussed quantitatively when considering steady state creep conditions, but only qualitative observations may be made when dealing with tensile data. It is expected that recovery by climb will show a temperature dependence related to bulk self-diffusion of the material.

4.9.4 The Occurrence and Importance of Substructure in Zinc

Complete recrystallization of the zinc matrix occurs during the extrusion of dilute zinc-titanium alloys. This is confirmed by the low dislocation density observed through transmission microscopy (Fig. 5). Thus no significant substructure should be present in the as-extruded condition. In view of this, the effect of substructure on the yield strength will be negligible since the formation of a substructure will

be the result of deformation; in other words any substructure which is produced will be formed after the fact.

Some glide polygonization can be expected to occur (not a thermally activated process). Dislocation glide in zinc occurs primarily on a single plane i.e. basal plane and thus glide polygonization will result in the formation of low angle boundaries perpendicular to the basal plane. This process can not be considered as a hardening mechanism but rather should be thought of as a softening mechanism, in as much as it tends to accommodate strain in a direction perpendicular to the basal plane.

A sub-boundary generally extends completely across a grain and can move under the influence of a stress.⁽⁶⁾ (Fig. 45)

4.10 Strain-Rate Sensitivity

4.10.1 Introduction

A deformation characteristic which is excluded from many studies but which must be considered in any investigation of zinc or zinc alloy is the strain-rate sensitivity of the flow stress. Studies of this nature must be made before any qualitative appraisal of the potential creep properties can be given. Low rate sensitivity is generally associated with superior creep behavior.

For high temperature deformation ($T_H > 0.4$), the flow stress and strain-rate are usually related by the equation:^(19,20,22,47,48)

$$\tau = Ke^m \quad \text{or} \quad m = \frac{\partial \ln \tau}{\partial \ln \dot{\epsilon}}$$

The rate sensitivity parameter "m" commonly has values between 0.15 and 0.2 for high temperature deformation (recovery creep) where



Fig. 45 Metallographic evidence of substructure in a chill cast Zn - 0.16 wt.% Ti alloy extruded at 175°C. (x6000)

deformation may be associated with some grain boundary shear but is nevertheless thought to be controlled by slip. At very fine grain sizes or much lower strain-rates m may increase to approximately 0.5 and under such conditions the material may be superplastic. Increasing m values are thought to be associated with an increasing degree to which grain boundary shear contributes to the overall deformation of the material.

4.10.2 Deformation of Pure Zinc

Turner⁽⁴⁹⁾ employed powder metallurgical techniques identical to those used in this work to obtain zinc extrusions with a grain size of 2μ . A subsequent deformation study indicated that the flow or yield stress versus strain-rate plot was "S"-shaped in nature as is shown in Fig. 46. The variation of m with strain-rate is shown in Fig.47; it can be noted that m varies between 0.1 and 0.2 as expected for a "hot" deformation process.⁽⁶⁴⁾ However it must be appreciated that a significant amount of zinc oxide was present as a result of the formation of an oxide layer during powder production. This inert second phase can be expected to have a stabilizing effect on the grain boundaries, limiting both shear and migration somewhat, thus preventing the material from exhibiting superplastic behavior. The results of the work by Tromans and Lund⁽²⁵⁾ have demonstrated the effect of oxide on the boundaries on the mechanical properties of zinc.

It is probably accurate to assume that the changes in the range of $m = 0.1$ to 0.2 were related to the degree of grain boundary shear even though the deformation was always slip controlled.

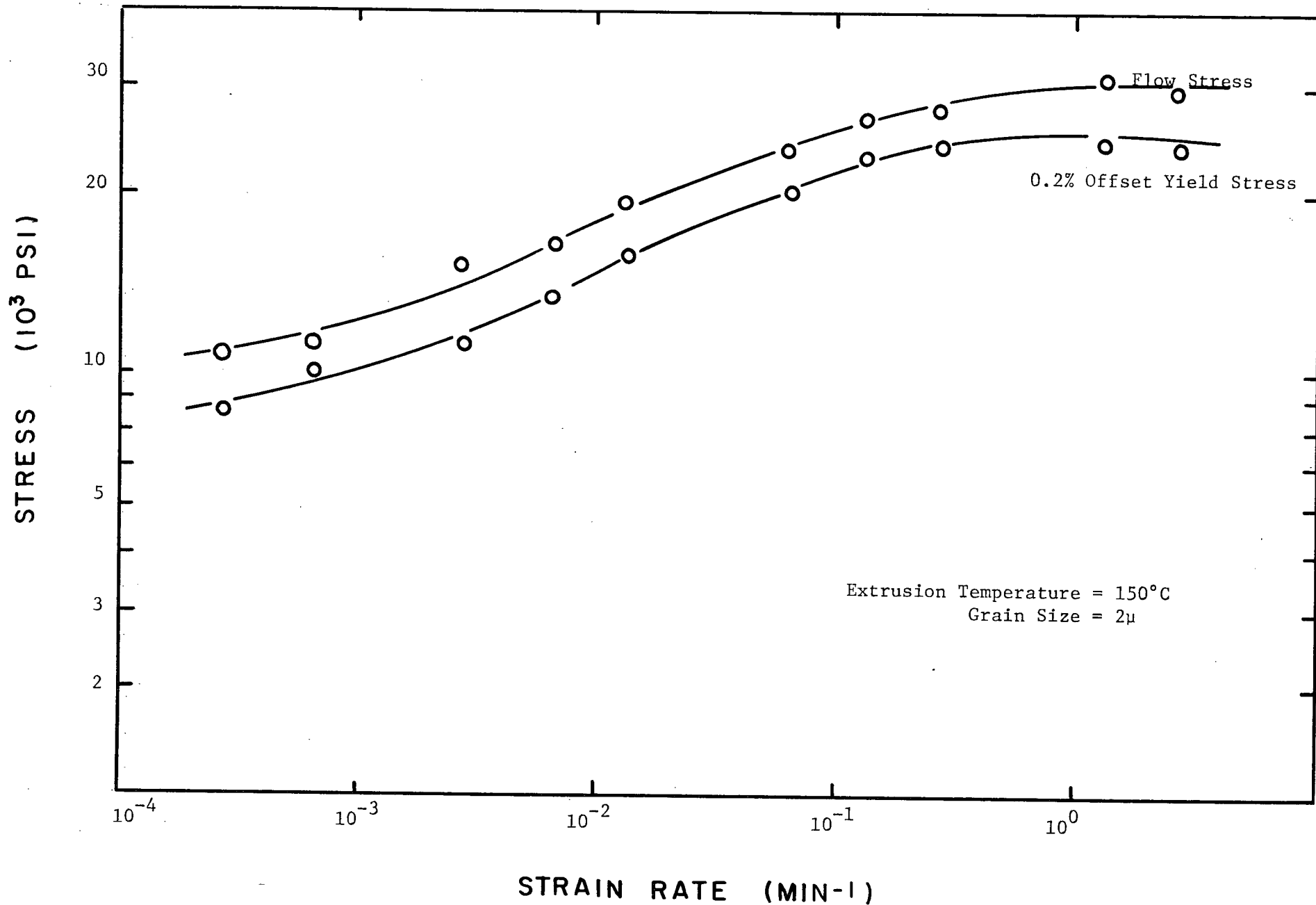


Fig. 46 The flow stress - yield stress dependence on strain-rate of zinc fabricated from -325 mesh powder at room temperature. (after Turner⁽⁴⁹⁾)

RATE SENSITIVITY PARAMETER "m"

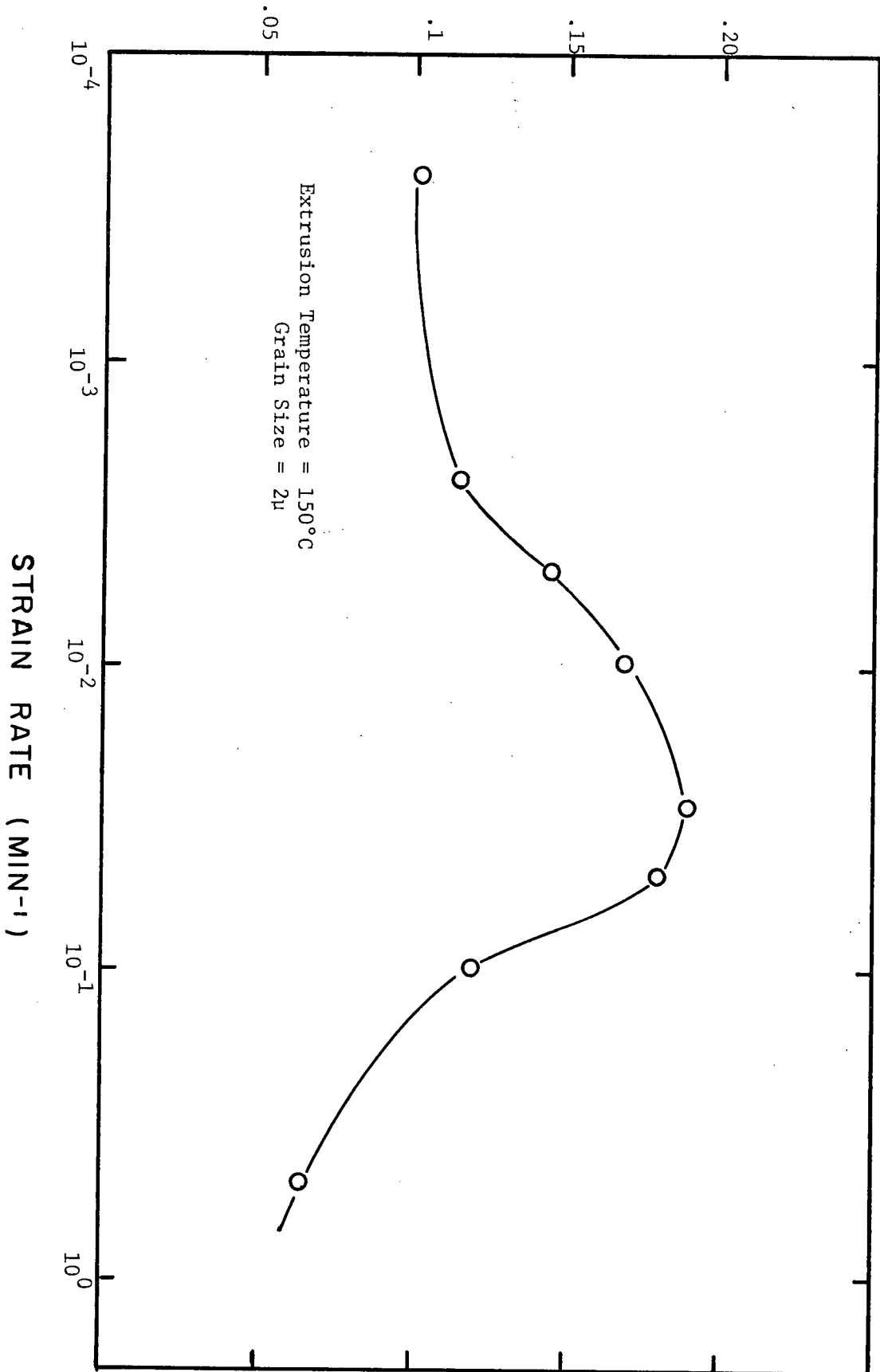


Fig. 47 The variation of "m" with strain-rate for pure zinc fabricated from -325 mesh powder. (after Turner (49))

4.10.3 Deformation of Zinc-Titanium Alloys

4.10.3.1 Strain-Rate Sensitivity

The strain-rate sensitivity of dilute zinc-titanium alloys at 20°C is shown in Figs. 48 through 51. These data indicate that the titanium concentration has virtually no effect on the strain-rate sensitivity. The nature of the second phase distribution as determined by the fabrication conditions is the important parameter. In view of this, Table VII summarizes the strain-rate sensitivity parameters and grain sizes resulting from the fabrication conditions used with a single composition (Zn - 0.16 wt.% Ti).

The rate sensitivity for pure zinc was variable ($m = 0.1 - 0.2$) over the experimental strain-rate range. However for zinc-titanium alloys, the m values are constant over the same range. Thus the presence of the intermetallic effectively extends the low sensitivity region of the $\log \tau - \log \dot{\epsilon}$ curve to much lower strain-rates, resulting in a linear relationship.

The observed m values are very low, indicating the $Zn_{15}Ti$ distribution is effective in stopping grain boundary shear and migration. Although the deformation is slip controlled, some grain boundary deformation will occur and will be reflected by small increases in the value of m . In the case of zinc-titanium alloys the increase in m is small (0.02 to 0.07), but the corresponding decrease in strength is considerable.

The ease with which a boundary may shear or migrate will be determined by the grain size, grain boundary orientation, and distribution of the second phase along the boundary.

The lowest m value was observed for material fabricated from

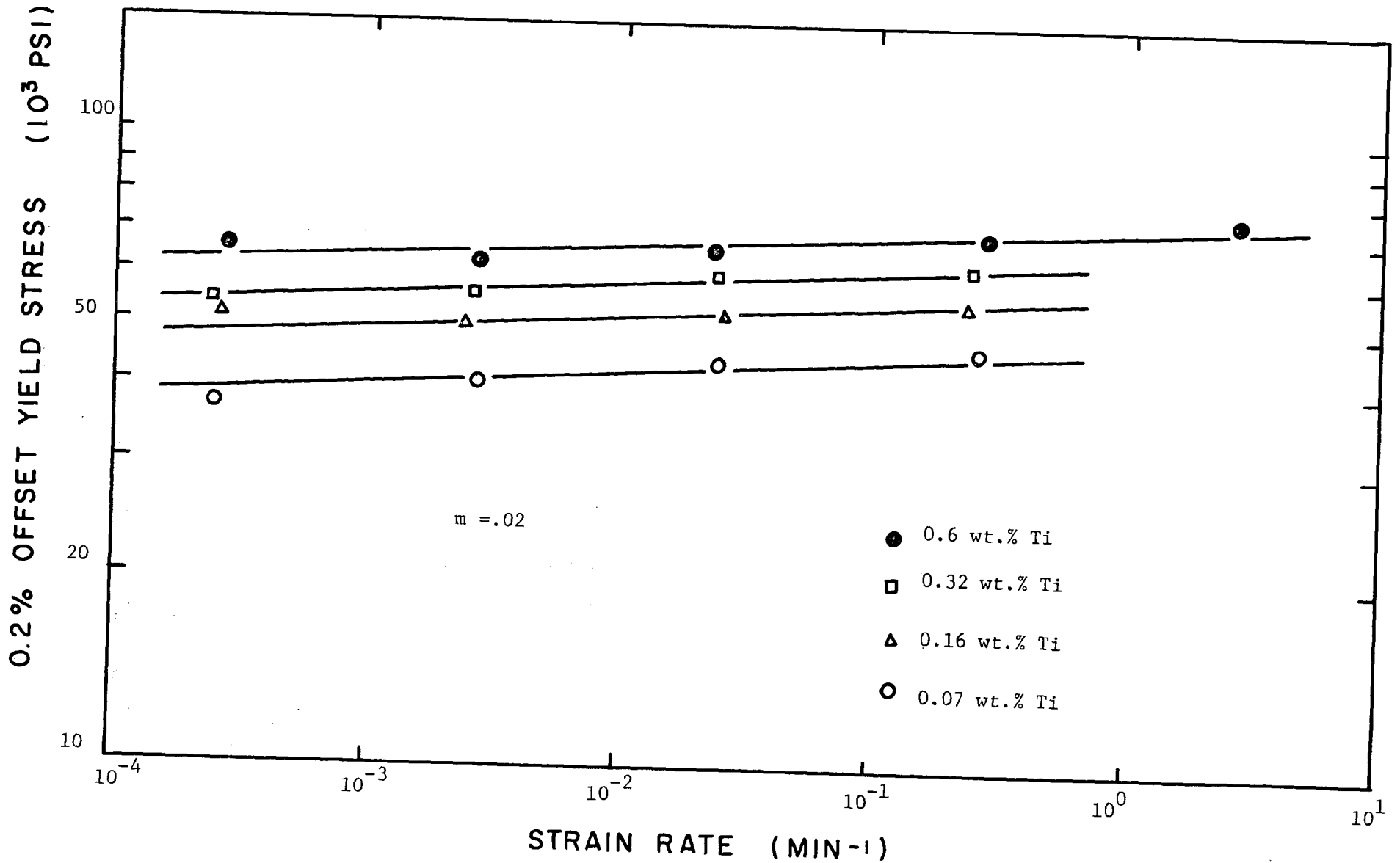


Fig. 48 The strain-rate sensitivity of zinc - titanium alloys fabricated from -35 + 100 mesh powder at 175°C.

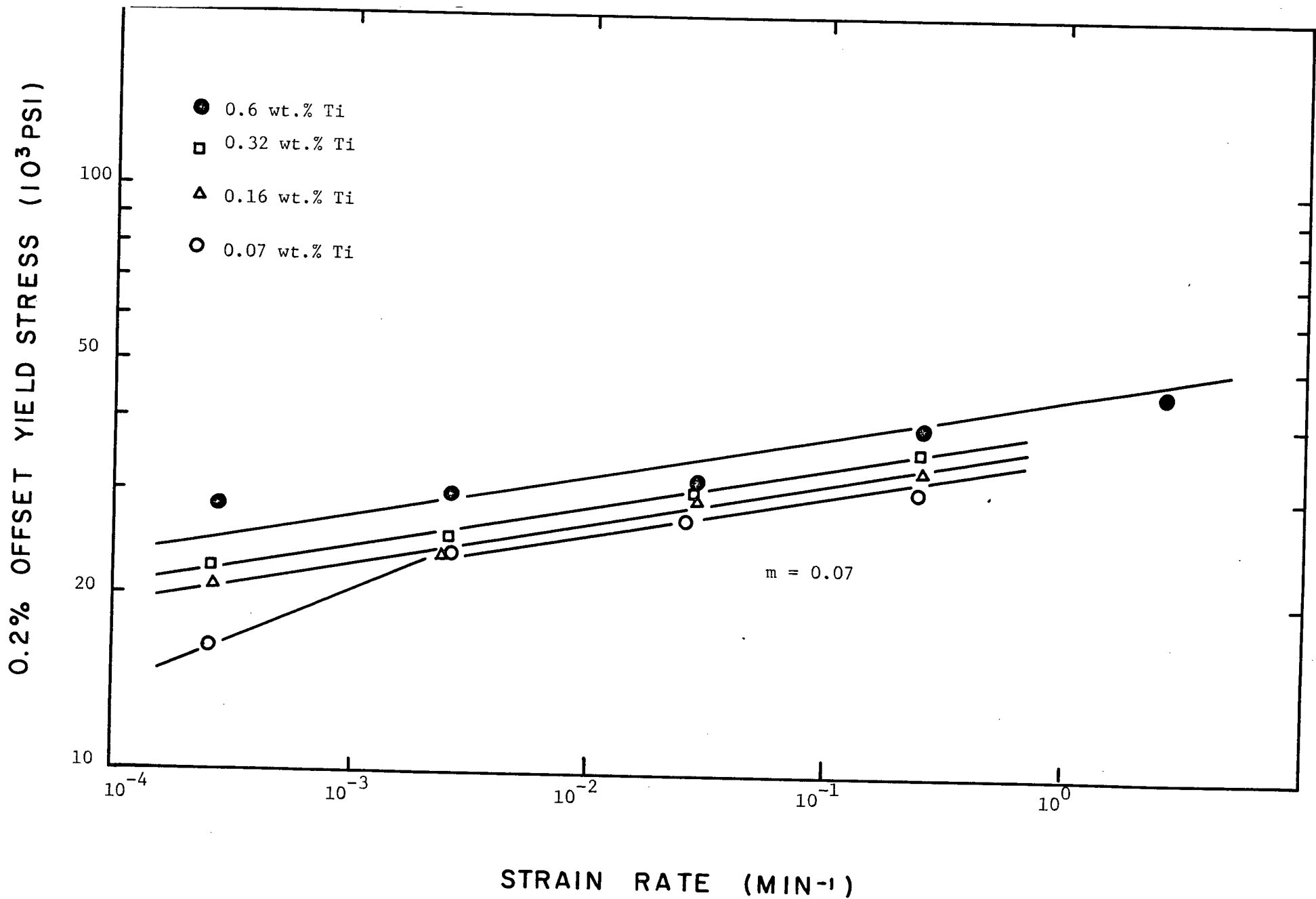


Fig. 49 The strain-rate sensitivity of zinc - titanium alloys fabricated from -35 + 100 mesh powder at 350°C.

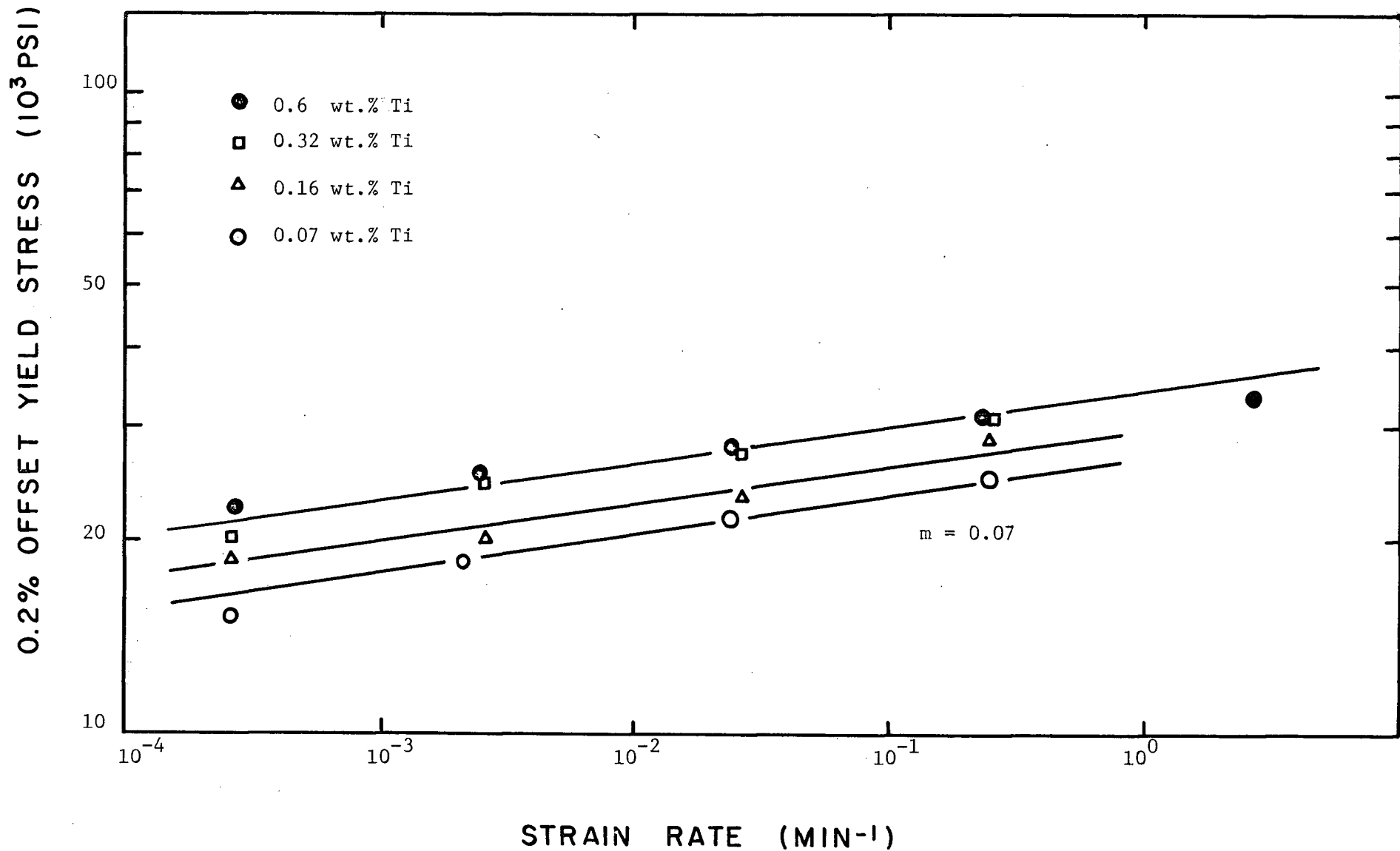


Fig. 50 The strain-rate sensitivity of zinc - titanium alloys fabricated from chill castings at 175°C.

0.2% OFFSET YIELD STRESS (10^3 PSI)

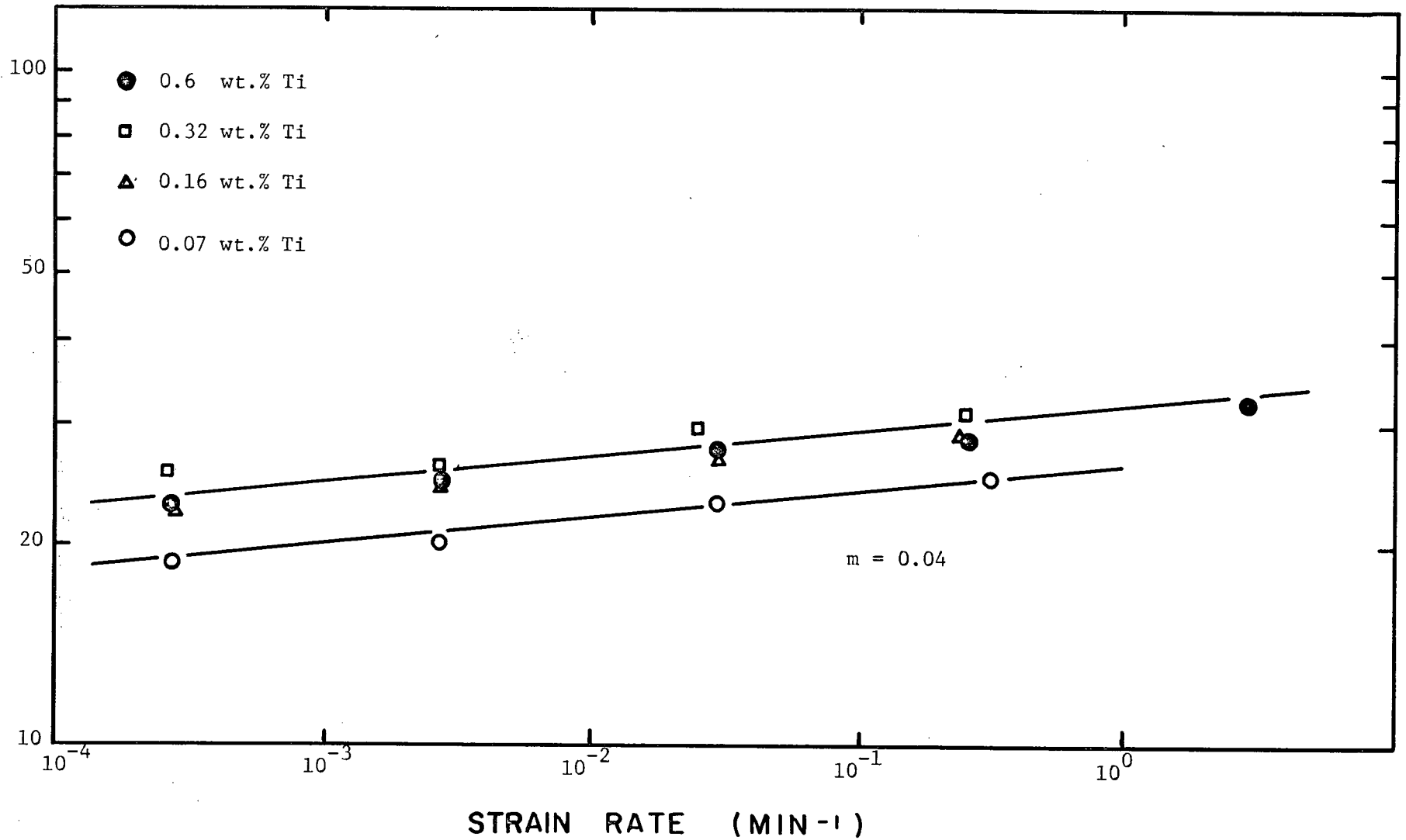


Fig. 51 The strain-rate sensitivity of zinc - titanium alloys fabricated from chill castings at 350°C .

Table VII. Summary of Strain-Rate Sensitivity Parameters and the Variables Affecting these Parameters for Zn - 0.16 wt.% Ti alloys.

Material	Fabrication Temperature	m	Grain Size
-35 + 100 powder	175°C	0.02	1.0 μ
-35 + 100 powder	350°C	0.07	2.1 μ
cast	175°C	0.07	4.1 μ
cast	350°C	0.04	8.1 μ

powder at 175°C ($m = 0.02$). The fine grain size is conducive to shear. However most boundaries are oriented such that there is no resolved shear stress along them. The fine intermetallic stringers also provide a high degree of stabilization. More equiaxed grain structures have a higher percentage of boundaries oriented favourably for shear. The fine grain sizes and coarsened intermetallic present in powders extruded at 350°C lead to higher m values ($m = 0.07$).

The coarse intermetallic distributions in material fabricated from cast billets provided the lowest degree of boundary stabilization. However somewhat larger grain sizes are formed. Material extruded at 175°C has a smaller grain size thus increasing the degree to which shear and migration may occur; such material has higher m values than material fabricated at 350°C.

Qualitatively, good creep properties are related to high stress levels and low m values. The strain-rate data obtained in this study suggest that the properties of these alloys should be excellent. However it is difficult to predict whether the rate sensitivity will remain this low at very low (creep) strain-rates.

4.10.3.2 Ductility

As expected, higher strength materials in general show lower % elongation and % reduction in area values. This is probably due to a condition of instability resulting from stress levels higher than the work hardening rate. Thus high strength extrusions begin to neck immediately following yielding. In this case, % elongation values are actually a reflection of the degree to which necking occurs. These values will be governed by the nature of microstructural modification (probably grain boundary migration) which occurs within the necked region.

The stress levels reached in cast and extruded material are much lower. As a result, necking is initiated at higher strains. Grain boundary migration occurs more readily in these materials and ultimately results in higher reductions of cross-sectional area. Boundary migration is probably retarded by fine intermetallic distribution and by oxide distribution present in extrusions fabricated from powders. These effects are indicated by the data shown in Table VI. (See p. 71)

4.11 High Temperature Deformation Characteristics

4.11.1 Deformation of Zinc-Titanium and Zinc-Aluminum Alloys

4.11.1.1 Introduction

The extent and nature of the distribution of the second phase will determine the amount of grain boundary deformation which will occur in zinc-titanium alloys. Therefore a maximum degree of shear and migration and consequently the higher strain-rate sensitivity will be observed under conditions in which the minimum amount of second phase (required for grain refinement) is present.

Superplasticity has been observed in dilute zinc-aluminum alloys with grain sizes comparable to those of the zinc-titanium alloys used in this study. The important difference is that the properties of the second phases on these alloys are different at 20°C. The intermetallic formed in zinc-titanium alloys is "hard" relative to the zinc matrix but the second phase formed in zinc-aluminum alloys is "soft".

Using Zn - 0.2 wt.% Al alloys, Cook⁽⁵⁵⁾ obtained m values of approximately 0.5 and elongations of over 500% at 20°C. The low m values and ductilities associated with zinc-titanium alloys are attributed to

the mechanical properties of the intermetallic compound. Higher m values and extended ductility can be expected if the mechanical properties of the intermetallic become comparable to the matrix at elevated temperatures.

4.11.1.2 Effect of Temperature on the Flow Stress - Strain-Rate Relationship

The microstructure of Zn - 0.07 wt.% Ti alloys fabricated from -35 + 100 mesh powder at 350°C closely resembles that of the superplastic Zn - 0.2 wt.% Al alloys used by Cook (Figs. 52 and 53). The grain sizes of both alloys are fine and equiaxed, with a large percentage of the grain boundary area apparently free of second phase. The effect of temperature on the flow stress - strain-rate curves of the Zn - 0.07 wt.% Ti alloy is shown in Fig. 54. The rate sensitivity is a function of temperature and varies between 0.07 and 0.35. These values reflect the ease at which grain boundary deformation occurs at elevated temperatures. However the strain-rate sensitivity parameter remains below that required for superplastic behaviour. In the region of higher rate sensitivity there was a tendency for the material to resist necking and spread deformation more uniformly, but extended ductility was not obtained.

Metallography indicated that a slight degree of grain growth and intermetallic coarsening did occur during high temperature deformation. Agglomeration of the second phase is effectively the same as reducing the concentration present. For unstringered alloys such as this, the flow stress dependence on grain size is reasonably small, thus the slight degree of coarsening which resulted will have a minor effect on the observed flow stress. The grain size - flow stress relationship is discussed later.

In Zn - 0.2 wt.% Al alloys, grain boundary shear is thought to be the dominant mechanism under conditions in which higher m values and superplastic behavior are observed. Metallographic evidence indicates

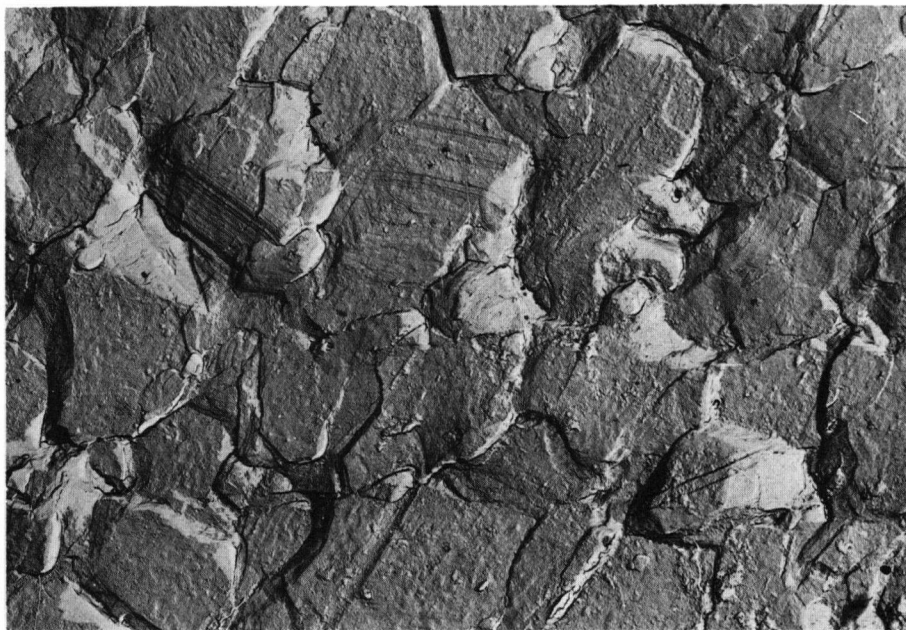


Fig. 52 The microstructure of a Zn - 0.2 wt.% Al alloy, cast and extruded at 150°C. Grain size = 3μ at 43% strain. (x 4000)

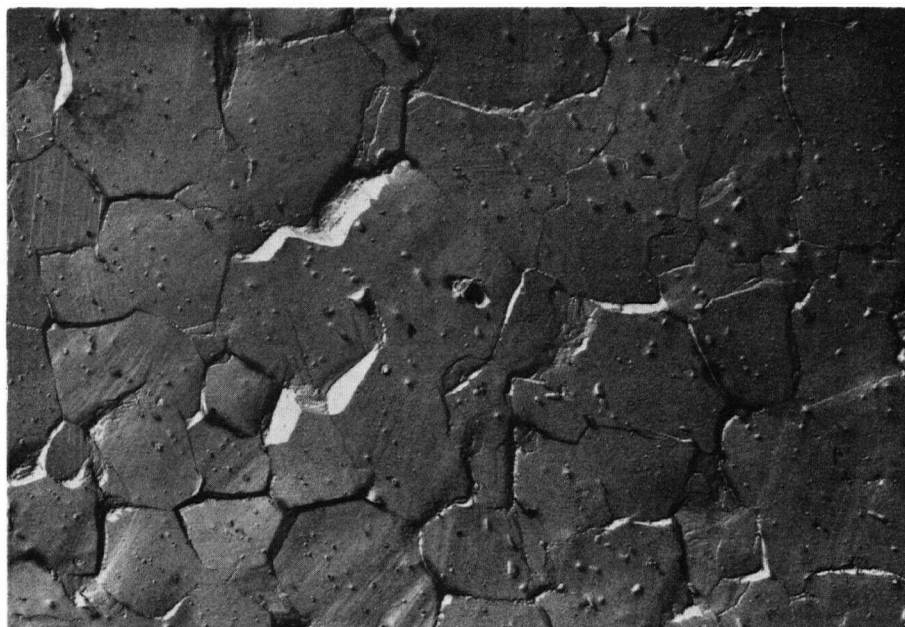


Fig. 53 The microstructure of a Zn - 0.07 wt.% Ti alloy extruded at 350°C using -35 + 100 mesh powder. (x4000)

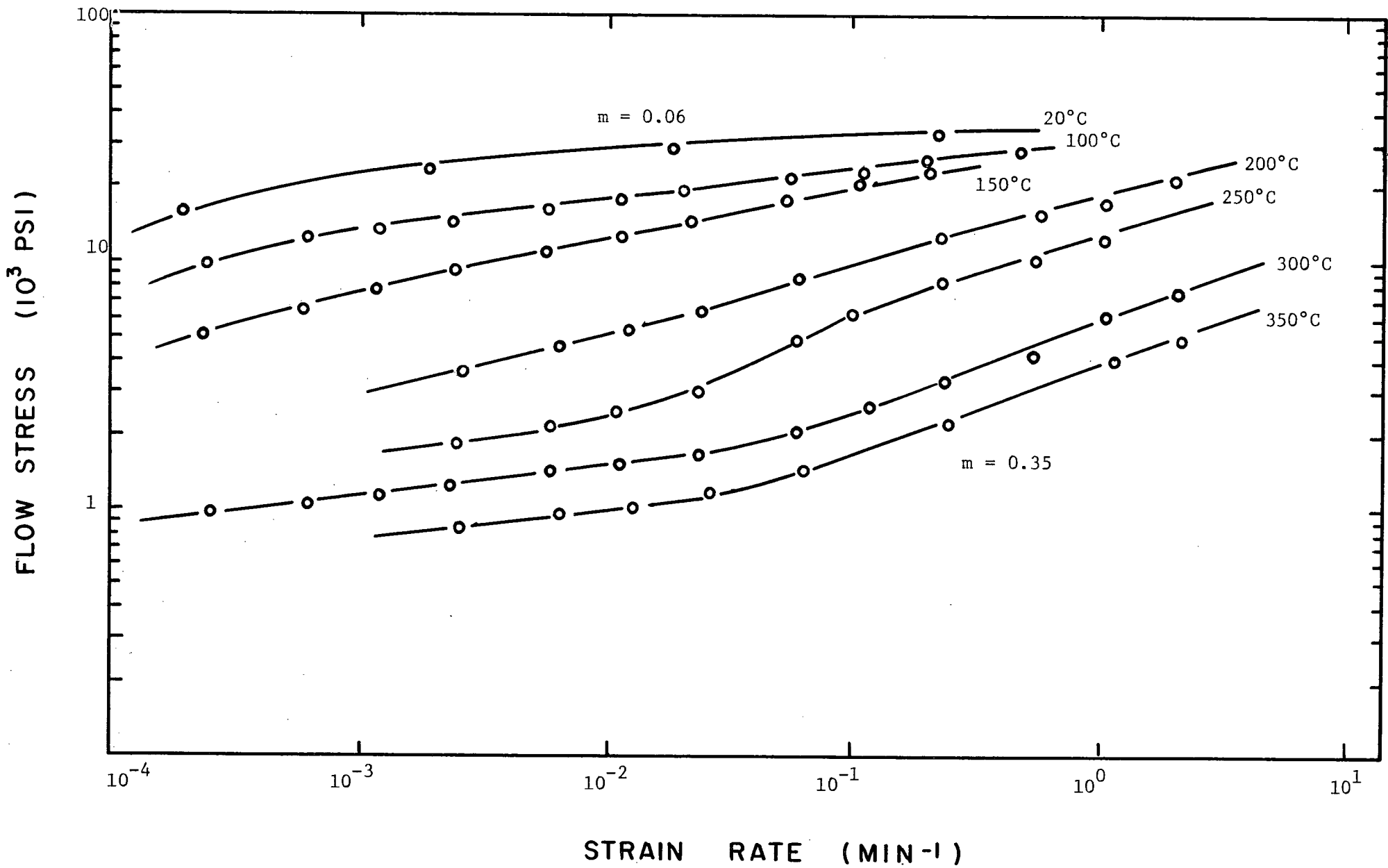


Fig. 54 The effect of temperature on the flow stress - strain-rate relationship for Zn - 0.07 wt% Ti alloys extruded at 350°C, using -35 + 100 mesh powder.

that sliding occurs both at phase boundaries and at grain boundaries of similar phases. The operation of a grain boundary sliding mechanism in a two phase system must be accompanied either by deformation of both phases or by diffusional mechanisms which lead to fulfillment of accommodation requirements; otherwise extended ductility is not observed.

Even though grain boundary shear occurs more readily at elevated temperatures in zinc-titanium alloys, it does not appear to become rate controlling.

4.11.1.3 Ductility and Fracture Mechanisms

The explanation for the rather low amount of ductility observed is found in an analysis of the mode of fracture of this material.

As indicated previously, little tendency toward necking was observed on specimens exhibiting larger m values. The fracture itself from a macroscopic point of view appeared quite brittle in nature. A large number of crack systems in various stages of development were apparent on the surface of the tensile specimens. The occurrence of these cracks increased significantly as the testing temperature was increased. These observations were made on specimens tested in two separate chemically inert testing media. Independent and isolated crack systems were also observed within the interior of the tensile specimen. On this basis, it is assumed that the origin of these cracks is not due to the operation of a corrosion or stress corrosion mechanism.

Since testing was carried out in liquid media, prior metallographical preparation of the surface of the tensile specimen could not be made. Excessive mechanical and/or electrochemical polishing subsequent to testing tended to either smear or enlarge the microcracks. Thus metallography

was restricted to the interior of the specimen with preparation consisting of light mechanical polishing followed by light electrochemical polishing.

A well-developed crack network is shown in Fig. 55. Figure 56 indicates that the origin of the cracks is at the intermetallic-zinc phase boundary. These cracks or voids gradually grow until they combine with other cracks propagating along the same or another grain boundary. This process is extended until a continuous network is formed and failure of the specimen occurs.

When precipitates exist along a grain boundary, triple points are formed on each side of the second phase particle. If grain boundary or interphase boundary shear does occur, then in order to fulfil accommodation constraints, deformation of the two phases by slip or grain boundary migration must take place. If accommodation conditions are not fulfilled at the triple points, the result is the formation of a void or microcrack and consequent premature failure due to cavitation. (62,63) A schematic representation of this type of mechanism is shown in Fig.57 (after McLean⁽¹⁶⁾).

Since for the alloy under consideration variable n values are observed, more than one deformation process is suggested. The relative contribution of these processes is variable and is dependent on the strain-rate and temperature.

Grain boundary shear may result in high elongations and low strength in cases in which both phases of a two phase alloy are "soft". In the instance in which one phase is "hard" relative to the other, the mechanism of grain boundary shear can be the mechanism which leads to cavitation and premature failure.



Fig. 55 Cavitation failure at 300°C in a Zn - 0.07 wt.% Ti alloy extruded at 350°C using -35 + 100 mesh powder. (x950)



(a)
(x3800)



(b)
(x3800)

Fig. 56 Scanning electron micrograph of cavitation failure at 300°C in a Zn - 0.07 wt.% Ti alloy extruded at 350 °C using -35 + 100 mesh powder: (a) Reflected electrons
(b) Secondary electrons.

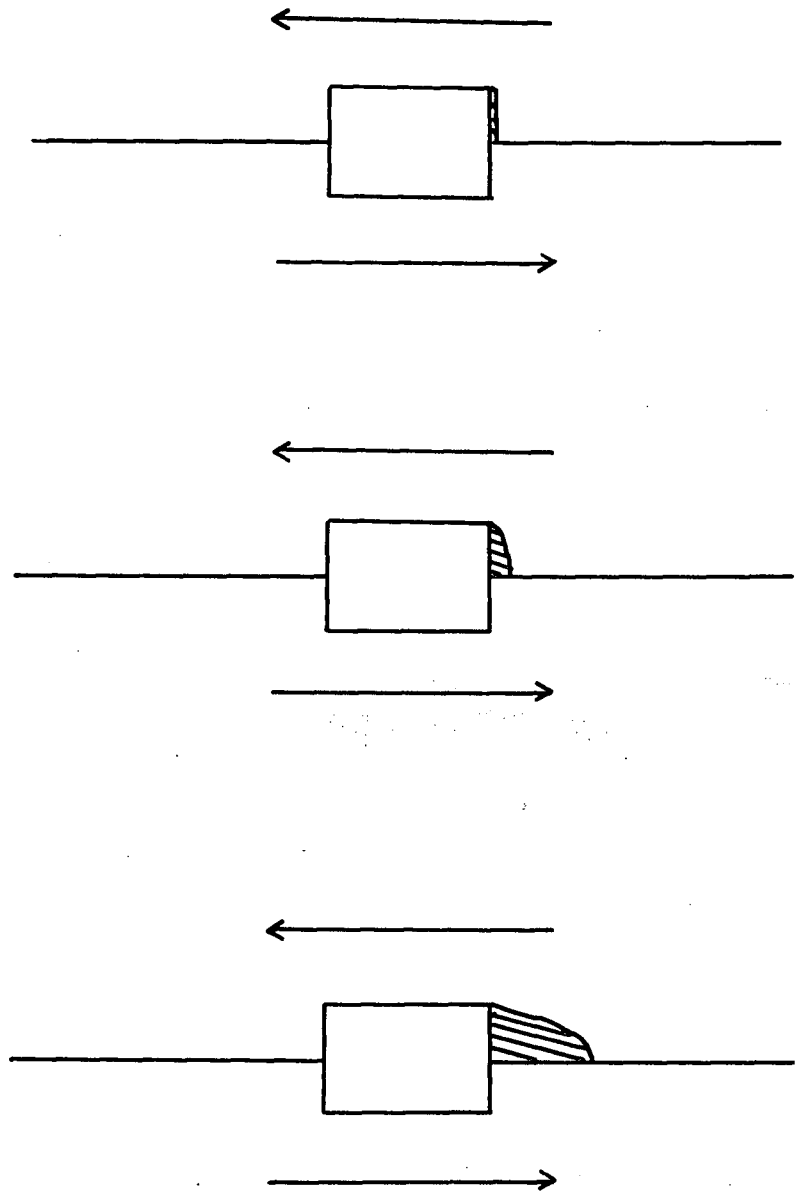


Fig. 57 Schematic representation of cavitation due to the presence of second phase particles on a grain boundary.
(after McLean⁽¹⁶⁾)

4.11.1.4 Activation Energy Analysis

A deformation study establishing the effect of temperature on the yield or flow stress of the alloy under certain conditions may yield data suitable for an activation energy analysis.

Generally speaking, when a wide range of temperatures and stress levels are involved, more than one process may be thermally activated. That is, when considering log stress - log strain-rate curves in which the strain-rate sensitivity parameter is not constant, a number of thermally activated processes may be involved. The rate controlling process may not be the same throughout the complete strain-rate range. Processes may be considered to be acting in either series or parallel. The suggestion that processes act in parallel implies that the mechanisms are interrelated and that their operation has a mutual dependence. Processes are considered to act in series if in fact they operate independently of one another. Arrhenius plots of series processes generally have distinct regions and thus are not linear. However, if limited temperature ranges are considered or if one mechanism is much more dominant then a linear plot could result.

The utilization of tensile data in which the strain-rate is fixed is based upon the assumption that the magnitude of the yield stress and/or flow stress is a direct result of the rate controlling process or processes involved. In other words, at a constant stress level, the strain-rate is a direct measure of the rate of deformation.

If deformation is assumed to be controlled by a single rate controlling process (i.e. parallel model) then the strain-rate is related to the Gibb's Free Energy by the following: (6,50)

$$\dot{\epsilon} = A e^{-\Delta G/RT}$$

Similarly, if two processes are considered to be acting in series:

$$\dot{\epsilon} = B e^{-\Delta G_1/RT} + C e^{-\Delta G_2/RT}$$

However, if one process predominates in the series model, then the expressions for the strain-rate relationship are similar; that is, one term becomes negligible.

If it is further assumed that the entropy change is not significant with respect to the overall free energy change, then the equation may be modified to:

$$\dot{\epsilon} = A' e^{-\Delta H/RT}$$

where ΔH is referred to as the activation energy of the rate controlling process.

Thus an analysis of this nature must be carried out in the region of the flow stress - strain-rate curve in which the strain-rate sensitivity parameter is constant at all temperatures. Under these conditions the relative contributions attributed to differing mechanisms should remain relatively constant.

For an accurate determination of the apparent activation energy it is a necessary condition that the microstructure remain constant. Slight coarsening of the grain size and intermetallic did occur during this study, however for a microstructure of this nature it will be shown that the mechanical properties are rather structure insensitive, and therefore the minor microstructural changes which did take place will not have a great effect on the activation energy analysis.

Data for this type of analysis is conveniently obtained using instantaneous strain-rate change tests previously described. Such procedures

were employed using a Zn - 0.07 wt.% Ti alloy fabricated from -35 + 100 mesh powder at 350°C. The data obtained has already been shown as Fig. 54.

Using a constant stress level of 6000 psi, the Arrhenius plot shown as Fig. 58 was made. The apparent activation energy of the rate controlling process was calculated to be 24.5 ± 3 kcal/mole. This value corresponds closely to published results for the bulk self diffusion of zinc.⁽⁶⁵⁾ Thus the controlling process is diffusion controlled and is probably that of dislocation climb.

4.11.2 Yield Stress Dependence on Temperature

Determination of the yield stress dependence on temperature for fine stringered microstructures is prevented by the thermal instability of the intermetallic compound. It has been seen that a thermally stable material can be produced by annealing these structures at a sufficiently high temperature. (See Fig. 31) Thus such a determination can be made if a stabilized structure is employed. Few microstructural modifications will occur if testing is completed in a relatively short time and if the test temperature does not exceed that which was used during the thermal treatment. Such an investigation was carried out using a 0.6 wt.% Ti alloy produced by extrusion at 175°C of -35 + 100 mesh powder. The stabilizing thermal treatment involved annealing the specimens at 250°C for 1/2 hour prior to testing. The results of this study are shown in Figs. 59 and 60.

The yield stress - temperature plot indicates that a discontinuity occurs at approximately 100°C. The existence of this discontinuity was verified by duplicate tests.

Figure 60 indicates that above 100°C a significant increase in the strain-rate sensitivity from 0.06 to 0.18 is observed. Thus it is

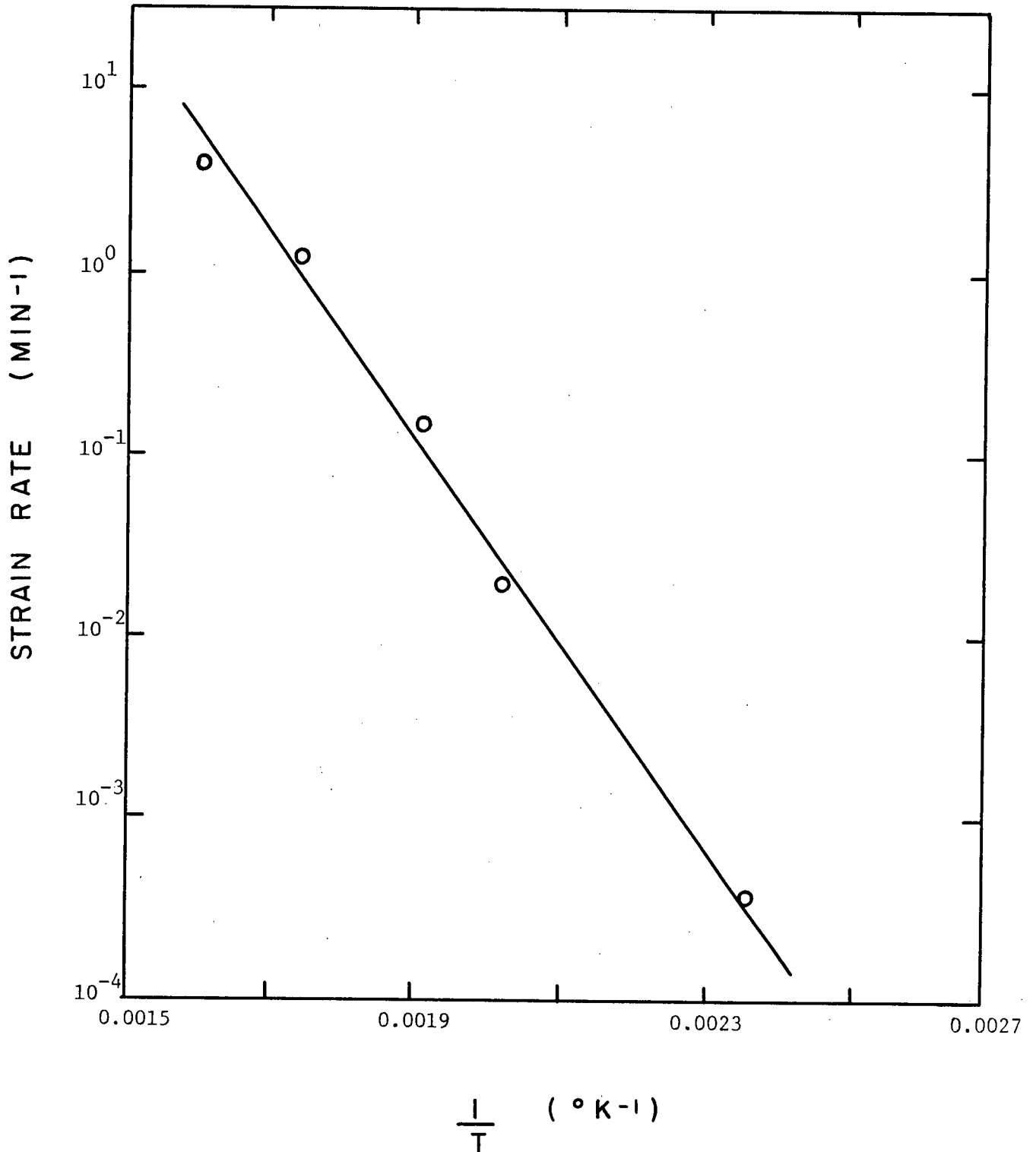


Fig. 58 Arrhenius plot for Zn - 0.07 wt.% Ti alloy extruded at 350°C using -35 + 100 mesh powder.

0.2% OFFSET YIELD STRESS (10^3 PSI)

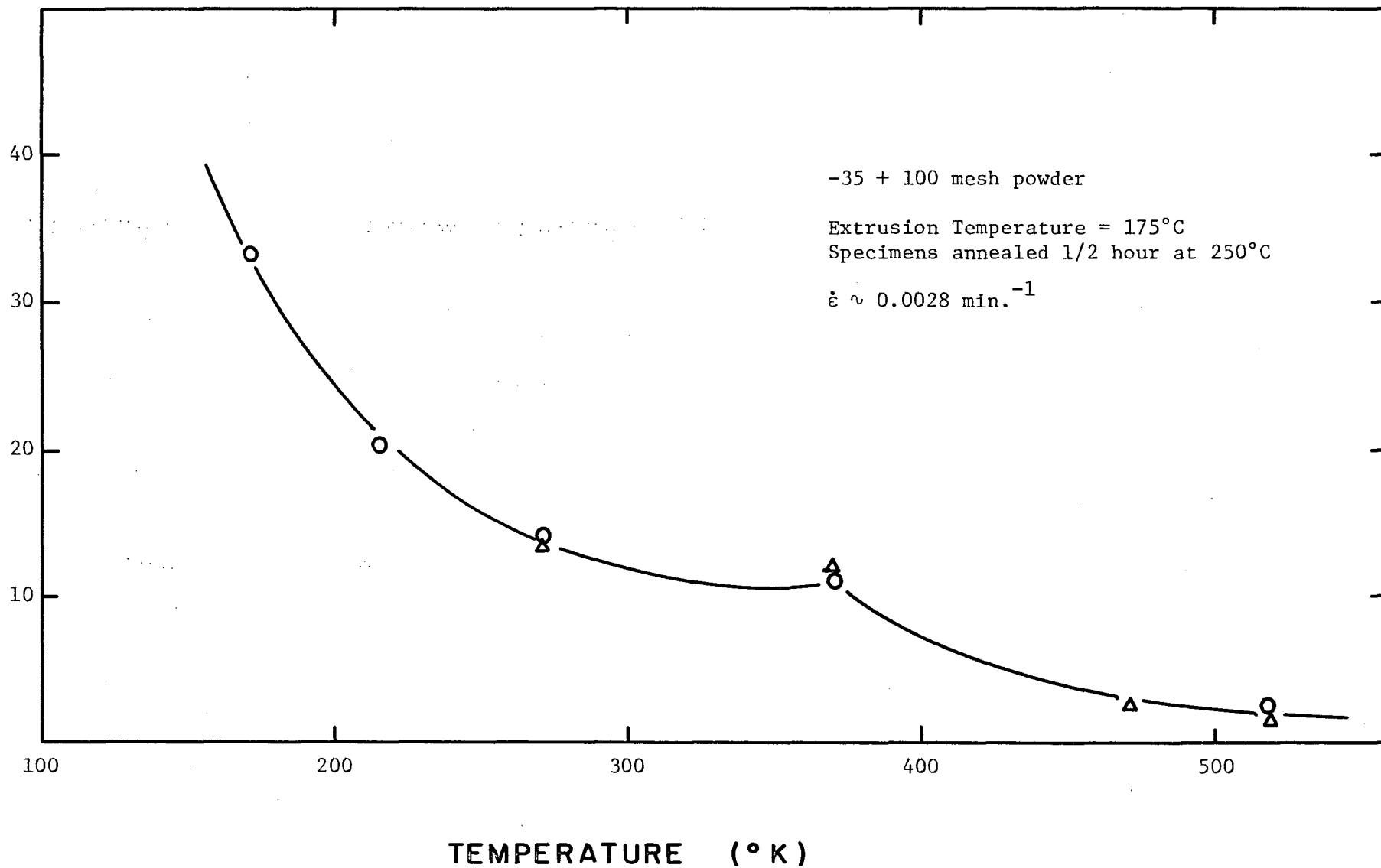


Fig. 59 The dependence of yield stress on temperature of a thermally stabilized Zn - 0.6 wt.% Ti alloy.

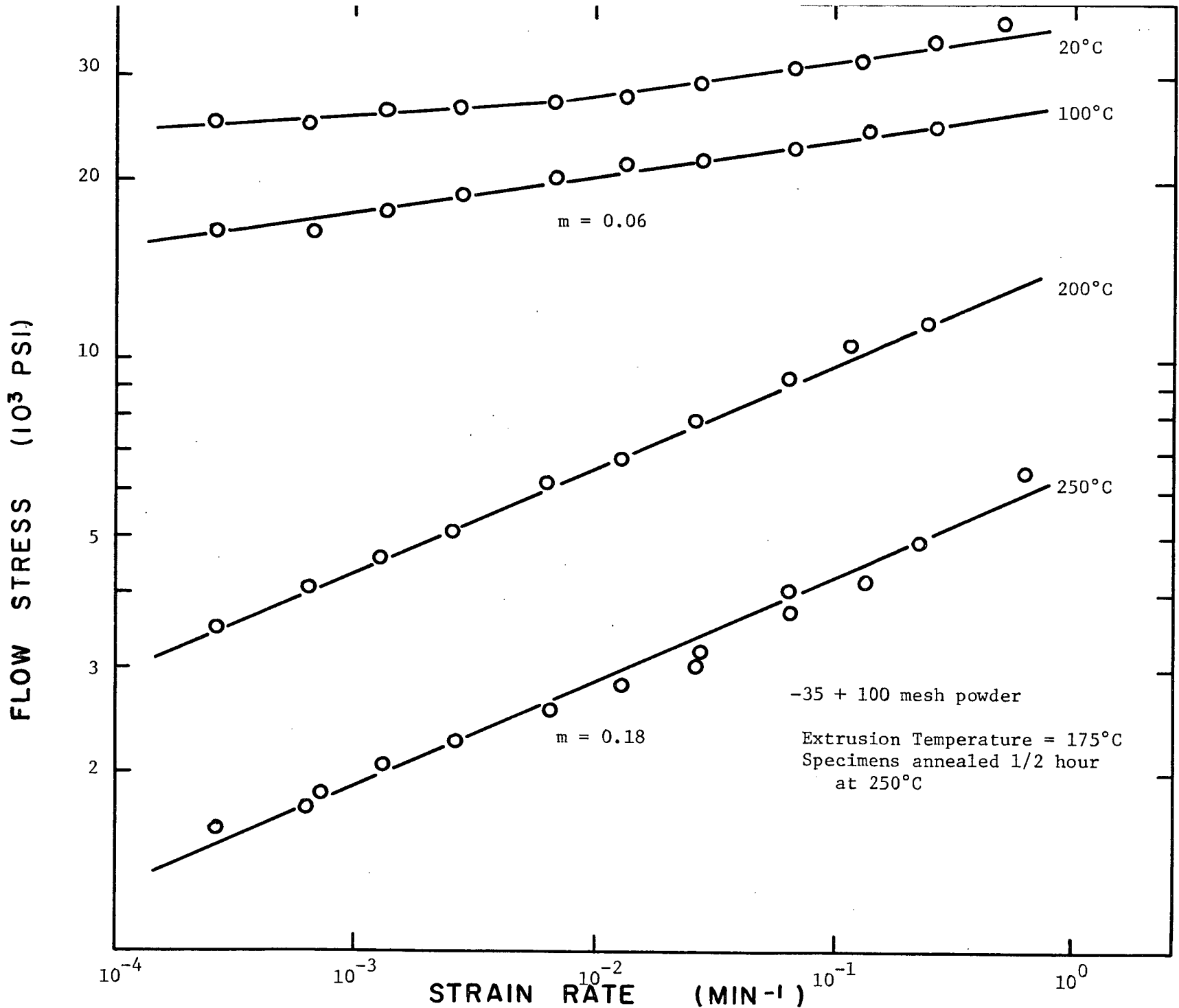


Fig. 60 The effect of temperature on the flow stress - strain-rate relationship of a thermally stabilized Zn - 0.6 wt.% Ti alloy.

reasonable to correlate the discontinuity in the yield stress - temperature relationship with an increase in m with temperature. As has been discussed, an increase in strain-rate sensitivity is generally associated with an increase in the amount of grain boundary shear which occurs during deformation. Thus it is not probable that this change in slope can be explained in terms of a change in the mode of deformation; but rather in terms of a mode which operates to a significant degree at higher temperatures. Such behaviour may be correlated with the "equicohesive" temperature.⁽⁵¹⁾ Essentially this is a temperature at which the grain boundaries are considered to become soft relative to the matrix. Although the equicohesive temperature is a function of the nature of the microstructure, it is generally around $0.5 T_H$ ($0.5 T_H$ for zinc is approximately 75°C or 350°K). If this indeed is the case, a significant increase in grain boundary shear can be expected to occur above this temperature.

4.12 Hall-Petch Analysis

4.12.1 Introduction

The expression proposed by Hall and Petch relating the yield or flow stress, σ , and the mean grain size, d , is

$$\sigma = \sigma_0 + kd^{-1/2}$$

where σ_0 and k are constants.

Although the Petch relation is often criticized because of an inherent normalizing effect on experimental data which consequently fits data mathematically which may have a poor correlation, it does allow a large volume of results to be subjected to a simple analysis.

The full significance of the grain size, slope, and intercept of the resulting plots is not fully understood. Nevertheless such an analysis is useful in qualitatively describing the relative importance of grain size and grain boundary effects and their relationship to the flow stress.

Originally the equation was formulated by the necessity to preserve continuity across grain boundaries in a single phase polycrystalline material in which plastic deformation occurred exclusively by slip. However modifications of the Petch analysis have been made in order to apply the relationship to two phase materials. (25,27,52) Successful application of this type of analysis depends upon the physical significance attached to the constants σ_0 and k .

4.12.2 Petch Equation and Hexagonal Metals

The constant σ_0 is thought to be a form of internal friction stress related to the energy required to move a dislocation on a slip plane in the absence of the influence of grain boundaries. If such is the case, σ_0 will depend on variables such as solid solution constituents, initial dislocation structure, etc.

In the second term of the equation, k has been associated with the "strength" of the grain boundary. (53) The actual physical significance attached to the term "strength" of the boundary is not clearly defined, but it is generally assumed to be associated with the ability of a boundary to act as a barrier to dislocation motion and to transmit the stress associated with the resulting dislocation pile-up to an adjacent grain in order to induce plastic flow in that grain. It has also been associated with the ability of a boundary to act as a dislocation source. (53)

As the number of available slip systems in hexagonal metals is very low in comparison with cubic metals, the values of k for hexagonal metals

are generally much higher. This suggests that orientation conditions across a grain boundary will affect the observed value of k substantially, as will any mechanism which affects the formation of dislocation pile-ups.

Thus when considering zinc or zinc alloys, the Petch relation may be considered as giving the stress required for the formation of dislocation pile-ups with resulting stress concentrations of a sufficient magnitude to activate a sufficient number of slip systems to satisfy the criteria for plastic flow. This definition is made under the assumption that grain boundary shear does not contribute to a significant degree to the overall plastic deformation of the material. It follows that if a significant amount of grain boundary shear does indeed occur, then a change in the Petch slope corresponding to the degree of shear should be observed.

4.12.3 Modifications of the Petch Analysis

Lund and Tromans⁽²⁵⁾ modified the Petch equation to:

$$\sigma_{0.2} = \sigma_0 + k_1 b^{-1/2} - k_2 d^{-1}$$

The purpose of the d^{-1} term was to include a provision for deformation resulting from grain boundary shear and/or migration. It was assumed that second phase particles were as effective as barriers to dislocation movement as were grain boundaries.

The validity of including a function to account for the extent to which grain boundary sliding and migration influence the flow stress is questionable when a multiphase material is under consideration. The amount of grain boundary shear which contributes to the overall plastic strain can not be considered to be proportional to the grain boundary area per unit volume unless all boundaries are free of secondary phases. The amount of sliding and/or migration will be a function of the amount, size, dispersion

and mechanical properties of the second phase particles.

4.12.4 Petch Analysis and Zinc-Titanium Alloys

A Petch analysis was carried out employing data obtained from a series of zinc-titanium alloys of variable composition, intermetallic size and dispersion. The analysis was done at 20°C and at -100°C.

Grain sizes were determined by a line intercept method. The procedure was thought to be reasonably accurate when the grains were equiaxed. However the grain size of material which was stringered and therefore consisted of block-shaped grains was established by taking line intercept measurements at 45° to the extrusion (and tensile) direction. It was thought that since the Petch analysis requires the mean grain diameter as a measure of the average possible slip distance, this dimension would most closely approximate the required distance. The results of this analysis are shown in Fig. 61.

4.12.4.1 Flow at -100°C

At -100°C, grain boundaries in zinc or zinc alloys will be "hard" and thus plastic deformation will be the result of slip. Lund and Tromans modified the Petch relation to suggest that the presence of dislocation barriers other than grain boundaries will affect the size and density of boundary pile-ups. This effect should be manifested by a change in the observed value of k when data are obtained under conditions such that deformation occurs exclusively by slip.

However Risebrough and Lund⁽²⁷⁾ report that at -100°C Zn-Ti, Zn-Cr, Zn-ZnO, Zn-Cr-Ti and pure Zn exhibit the same flow stress - grain size dependence and Petch obeyance is observed.

0.2% OFFSET YIELD STRESS (10^3 PSI)

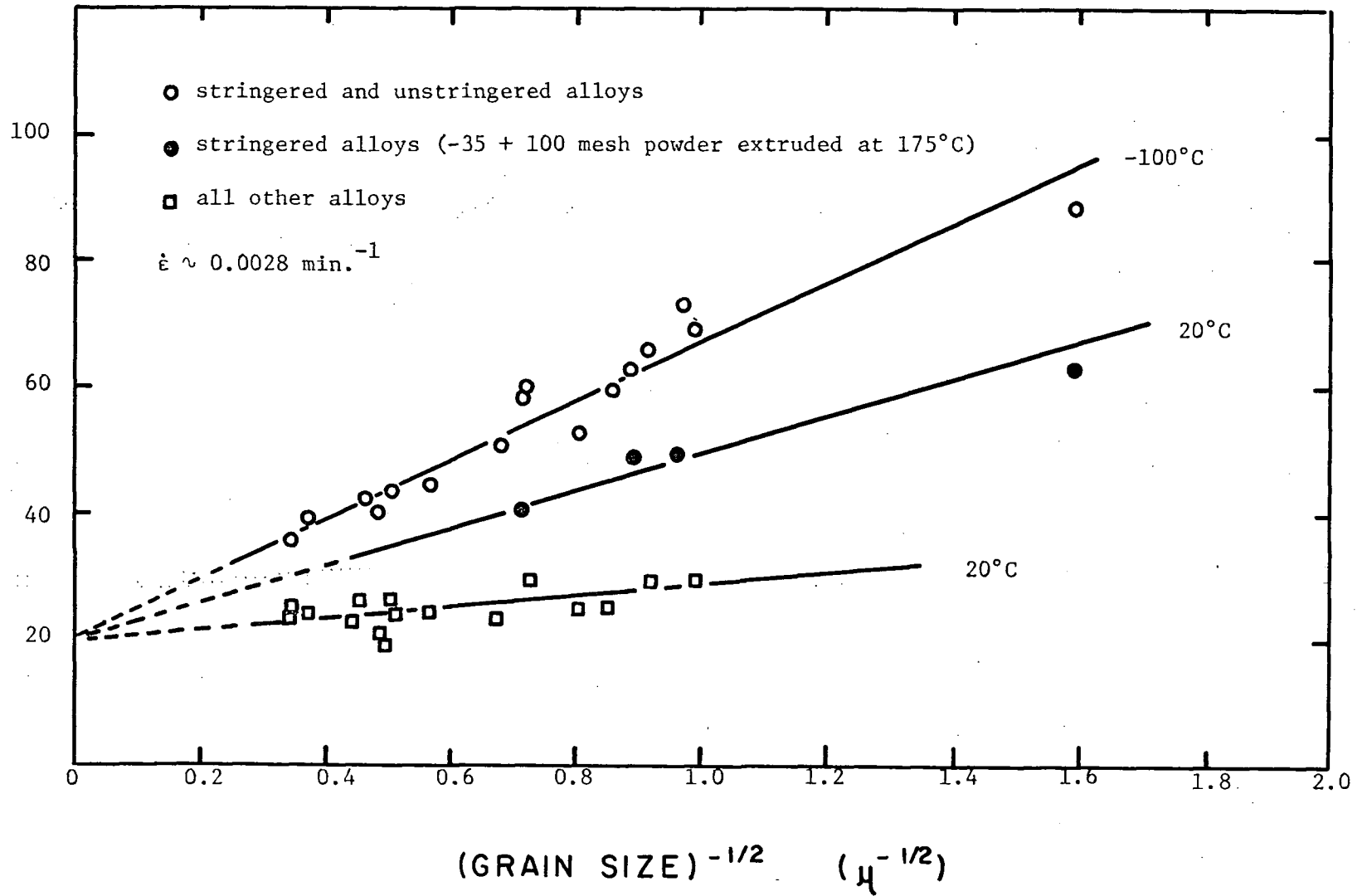


Fig. 61 The Hall-Petch plot for zinc-titanium alloys.

At this temperature, the value of the constants were:

$$\sigma_0 \sim 13,000 \text{ psi} \qquad k \sim 50,000 \text{ psi } (\mu)^{1/2}$$

These values compare reasonably with the values obtained in this study:

$$\sigma_0 \sim 20,000 \text{ psi} \qquad k \sim 47,000 \text{ psi } (\mu)^{1/2}$$

The size, dispersion, and concentration of the intermetallic do not appear to have a significant effect on the mechanical properties of these alloys at this temperature.

Therefore the strength is primarily a function of the grain size. The flow stress values obtained under these conditions can be considered to be an indication of the ultimate strengthening of zinc which could be accomplished with complete immobilization of the grain boundaries.

4.12.4.2 Flow at 20°C

4.12.4.2.1 Stringered Alloys

Plastic flow of the zinc-titanium alloys studied is characterized by two significantly different k values at 20°C. The flow stress of material fabricated from powder by extrusion at a low temperature (175°C) follows a linear relationship when plotted against the reciprocal square root of the mean grain size. It is then apparent that the flow stress is a function of the grain size only and is quite insensitive to the amount of intermetallic compound present. As has been previously discussed, extruding at 175°C gives rise to a well-defined stringered structure in which the grains are small and columnar in shape.

Lowering the titanium content results in an increased stringer spacing and width and a slightly enlarged grain size. The columnar grain

shape is generally maintained although small colonies of more equiaxed grains were observed at lower intermetallic concentrations. The $Zn_{15}Ti$ stringers in all cases consist of extremely fine particles effectively pinning the grain boundaries oriented parallel to the extrusion (and tensile) direction.

Perpendicular boundaries are devoid of second phase. Because of the high degree of pinning of boundaries and because of the unsuitable orientation of both pinned and "clean" boundaries, shear or migration is not considered to play a major role in overall plastic deformation of the material.

Since room temperature corresponds to a high effective temperature ($T_H = 0.42$), grain boundary shear and/or migration should be expected to have a great influence on the flow stress. Therefore curtailing grain boundary effects by the formation of a suitable microstructure should result in an increase in flow stress similar to the result of decreasing the effective temperature, and consequently rather high values of k are expected. For material with this type of microstructure, $\sigma \sim 20,000$ psi and $k \sim 28,000$ psi (μ)^{1/2}

4.12.4.2.2 Unstringered Alloys

Extruding or thermally treating alloys with a fine intermetallic structure at temperatures at which the $Zn_{15}Ti$ is unstable, results in rapid changes in the nature of the microstructure. Intermetallic coarsening appears to occur very rapidly, forming spheroidized particles. As coarsening proceeds, a corresponding increase in grain size and change in grain shape occurs. The larger particles of second phase remain located at the grain boundaries to a large degree with only a small percentage being situated intragranularly. Thus the grain size is controlled to a large extent by the nature of the intermetallic dispersion.

The grain sizes of material extruded using cast billets is moderately large in the as-extruded condition.

A considerable degree of scatter does exist on the Petch plot for unstringered material. This type of scatter is to be expected and is presented as such to demonstrate that a loose obedience of the Petch relationship and a significantly reduced slope ($k \sim 8000 \text{ psi}(\mu)^{-1/2}$) occurs when a stringered microstructure is not maintained.

The degree of grain boundary pinning which can be associated with the intermetallic and to a minor extent with zinc oxide is variable and depends on grain size, grain shape, composition, size and dispersion of Zn_{15}Ti , which in turn are dependent upon the thermal treatment and/or the fabrication temperature.

Generally the amount of grain boundary shear and migration (and their contribution to the flow stress) will be proportional to the unpinned grain boundary area per unit volume and the grain size.

Thus as the relative importance of boundary effects is increased, the degree of conventional Petch obedience will be reduced. At larger grain sizes, the flow stress tends to become less dependent on the presence of the hard second phase.

4.12.5 Value of σ_0

An important feature of Fig. 61 is that the extrapolated value of σ_0 appears to be constant, independent of both temperature and structure. As the grain size becomes increasingly larger, boundary deformation or recovery mechanisms become decreasingly important. Approaching the limiting case in which grain boundaries are absent, the results suggest that the

stress required to move dislocations along a slip plane must be relatively temperature insensitive, thus giving rise to a constant value of σ_0 .

5. SUMMARY

5.1 Introduction

A high homologous temperature at 20°C results in low strengths and poor creep properties for most zinc alloys. More specifically, dislocation climb, grain boundary shear and migration results in limitations upon the development of the desired mechanical properties. Thus the development of a useful zinc alloy is contingent upon the formation of a multiphase microstructure which inherently inhibits these processes. These requirements suggest that zinc is somewhat unique in that conventional dispersion hardening criteria are not strictly applicable. Additions of titanium and the use of powder metallurgical techniques have led to alloys which have improved strength and creep properties.

5.2 Deformation Characteristics

5.2.1 Strength

If deformation is carried out under conditions such that the grain boundaries are "hard", high stress levels are reached. The explanation for this strengthening effect necessarily involves the mechanisms operative during deformation.

Low temperature fabrication of powder material results in a stringered intermetallic distribution and a small, block-shaped grain size. The boundaries are pinned or oriented such that a significant degree of grain boundary shear cannot occur. At these grain sizes, twinning is not observed, thus deformation must involve the operation of non-basal slip in order to satisfy compatibility conditions.

The stress levels required to activate second order pyramidal slip are much higher than those required for either basal slip or grain boundary shear. The necessity to activate slip other than basal slip gives rise to high strengths and large values of "k" in the Hall-Petch Relationship.

Intermetallic distributions such as those which result during high temperature extrusion of powder or extrusion of cast castings lead to microstructures in which a significant amount of grain boundary shear and migration may occur. Basal slip and grain boundary shear then supply the number of deformation modes required for plastic flow, and lower strengths are observed. In the case in which grain boundary effects contribute significantly to the overall deformation, the slope of the Hall-Petch curve is low. ($\sim 8000 \text{ psi } \mu^{+1/2}$). It is possible that the critical dislocation pile-up size required to initiate non-basal slip in neighbouring grains is never reached due to annihilation by local boundary migration.

The effect of titanium concentration on the strength can be considered as a variable of secondary importance. Lower intermetallic concentrations will lead to larger stringer spacings and a reduction in strength of powders extruded at low temperatures. The effect of composition is less pronounced if the intermetallic distribution is coarse. In general, a larger grain size is associated with a coarser intermetallic distribution. This suggests that the relative proportion of stabilized and unstabilized grain boundary area remains almost constant.

The prerequisite for high strength is a fine intermetallic distribution in the as-solidified material. The fabrication must be such that this distribution must be retained in the final product. Lower temperature fabrication does not effectively fragment and distribute

coarse intermetallic particles formed at lower solidification rates or with thermal treatments.

The degree of "stringing" in the product is not a function of the initial powder size. The solidification rates are such that an equivalent fine microstructure is produced independent of powder sizes.

Less severe deformation during fabrication does result in a more poorly defined stringered structure and consequently lower strength.

The degree to which strengths are maintained at elevated temperatures is dependent on the thermal stability of the intermetallic ($Zn_{15}Ti$).

5.2.2 Strain-Rate Sensitivity

Pure zinc and zinc-aluminum alloys are associated with an S-shaped, log stress-log strain rate relationship at room temperature. Variations in "m" values are related to either a change in the controlling deformation mechanism or to a change in the degree of operation of several mechanisms. This type of relationship is observed with zinc-titanium alloys at elevated temperatures and low second phase concentrations.

At room temperature, the log stress-log strain rate relationships were linear. The changes in strain rate sensitivity observed between alloys are very small ($m = 0.02-0.07$). These values are indicative of slip controlled deformation. In alloys other than those fabricated from powder at low temperatures, grain boundary shear may make a substantial contribution to the overall deformation of the material. The strain rate sensitivity can be considered as a reflection of the controlling deformation process.

High stress levels and low strain rate sensitivities suggest

the creep properties of stringered material may be excellent. However it is difficult to predict the behaviour of these alloys at much lower (creep) strain rates.

The strain rate sensitivity is insensitive to titanium concentration but rather is determined by the nature of the second phase distribution which in turn is determined by the fabrication conditions.

At elevated temperatures, the rate sensitivity increases significantly. The observed "m" values are a function of both the microstructure and testing conditions. Experimental evidence indicates the existence of a critical temperature ($\sim 0.5T_H$) above which "m" increases markedly. Thus above this critical temperature, grain boundary shear operates to a considerable degree. Although high "m" values (up to 0.35) were obtained, extended ductility was not observed. This is due to the nature of the failure which occurred under these conditions. The activation energy suggested that deformation is controlled by a process associated with the bulk diffusion of zinc -- probably dislocation climb.

5.2.3 Dynamic Recovery

The suppression of dynamic recovery results in enhanced strengths and limited ductilities. Due to the fabrication procedures, the intermetallic particles tend to be preferentially situated on grain boundaries. This in effect limits the amount of grain boundary shear and migration which may occur. Coarsening of the second phase has an effect similar to lowering the titanium concentration and leads to large interparticle spacings along boundaries. Local migration occurs more readily as this spacing is increased as it is a function of the unpinned grain boundary area.

Since the interparticle spacing is comparable to the grain size in all alloys, it is doubtful if the intermetallic has any effect on dislocation climb within the grains.

5.2.4 Ductility and Fracture

In general higher strength material exhibits lower ductilities. This arises from stress levels in excess of the degree of work hardening which results in a condition of instability which is present at or immediately following yield. Thus in high strength material, necking is initiated at very low strains.

The stress levels reached with lower strength products lead to neck formation at higher strain values. Thus % elongation values are very low but are associated with rather large % reduction in area values. This is particularly true for extruded chill castings in which the reduction of area values were >90%. The degree to which necking occurs is governed by the microstructural modifications (grain boundary migration) which take place within the necked region. Boundary migration is probably retarded by the intermetallic and oxide distribution in products fabricated from powder.

Enhanced boundary migration and shear which occur at elevated temperatures can lead to extended ductility under conditions in which both phases in a two-phase system have equivalent mechanical properties (e.g. Zn-Al alloys). The second phase ($Zn_{15}Ti$) in zinc-titanium alloys appears to remain hard relative to the zinc matrix at all temperatures. Grain boundary shear leads to premature failure due to cavitation. Cracking is initiated at the intermetallic-matrix interphase boundary.

5.3 Thermal Stability

Experimental results suggest that fabrication alone can not develop the desired intermetallic dispersion. The initial fine microstructure present in as-atomized powder must be preserved during fabrication in order that the product has appreciable strength and reasonable strain rate sensitivity.

A certain degree of fragmentation and relocation of large primary intermetallic particles does occur during low temperature extrusion. However the degree to which this occurs does not give rise to efficient grain refinement or stabilization. Further proof of this is obtained by thermally treating powder billets prior to low temperature fabrication. Under these conditions, the mechanical properties of the resulting product approach those obtained by extrusion of cast billets.

The short diffusion paths which exist in either powder or products obtained by low temperature fabrication of powders give rise to rather rapid microstructural coarsening at moderate temperatures. The diffusion paths in cast material are sufficiently long that no significant softening occurs unless severe thermal treatments are used. These considerations place a limitation on the fabrication conditions which must be used in order to maintain a fine microstructure.

Thermal treatments are of course dependent on both time and temperature. However the fine intermetallic dispersion obtained appears to be thermally stable up to at least 150°C for short periods of time.

5.4 Other Considerations

There is evidence to suggest that it may be possible to develop a fine continuous second phase structure in cast billets. Colonies of

fine eutectic were observed to form during chill casting. An extensive solidification study of dilute zinc-titanium alloys should establish criteria for the formation of such a microstructure. This would be of considerable advantage as it may be possible to develop high strength and superior creep properties without resorting to powder metallurgical techniques.

There appears to be some controversy as to the nature of the zinc-rich portion of the zinc-titanium phase diagram. It is reasonable to assume that reconsideration of the phase relations would have to be made in conjunction with any solidification study.

6. CONCLUSIONS

The conclusions that can be made from the interpretation of the metallurgical and mechanical characteristics of dilute zinc-titanium alloys are as follows:

- (1) The eutectic composition appears to be in the range 0.4 - 0.6 wt. % Ti at the solidification rates corresponding to chill casting and atomizing.
- (2) Reduced lamellar and interdendritic spacings are formed at rapid solidification rates. Generally coarser solidification structures are observed in chill castings, however isolated areas of fine eutectic were present.
- (3) Extruded microstructures with high strength and low strain rate sensitivity are the direct result of a fine as-solidified starting material. The structure is stringered with small grain size (0.5 - 1.5 μ).
- (4) High strengths are observed when grain boundary shear and migration are inhibited by grain boundary stabilization. The degree of stabilization is associated with the orientation of the boundary with respect to the tensile axis and the distribution of second phase. Deformation occurs by both basal and non-basal slip.
Lower strengths are observed when basal slip and grain boundary shear are the operative deformation mechanisms.
- (5) The strain rate sensitivity parameter of dilute zinc-titanium alloys lies in the range 0.02 - 0.07. Varying amounts of grain boundary shear occur, nevertheless deformation is slip controlled.

- (6) Increased strain rate sensitivities (m up to 0.35) are observed at elevated temperatures. However failure due to cavitation limits ductility. The activation energy corresponds to bulk self-diffusion of zinc.
- (7) The strain rate sensitivity is not sensitive to the titanium concentration in the range 0.07 - 0.60 wt. % Ti.
Under constant fabrication conditions, the strength generally increases with increased intermetallic content.
- (8) Low % elongations and high % reduction in area values are generally observed at 20°C. These values are a function of microstructural modification within the necked region.
- (9) The tensile results obey the Hall-Petch relationship. The observed "k" values are a function of the microstructure which will result from the fabrication conditions
- $$k \approx 28,000 \text{ p.s.i.} \cdot \mu^{+1/2} \quad \text{powder extruded at } 175^\circ\text{C}$$
- $$k \approx 8,000 \text{ p.s.i.} \cdot \mu^{+1/2} \quad \text{all other alloys.}$$
- (10) The intermetallic compound is thermally stable up to 150°C for short periods of time.
- (11) The mechanical properties are not a function of initial powder size.

7. BIBLIOGRAPHY

1. A. Kelly and R. B. Nicholson, "Progress in Materials Science", 10, (Pergamon Press), 149, (1963).
2. N. J. Grant, "The Strengthening of Metals", (Reinhold, New York), 163, (1964).
3. C. G. Goetzel and R. F. Bunshah, "Powder Metallurgy", (Interscience, New York), 253, (1961).
4. M. Ashby, Z. für Metallkunde, 55, 5, (1964).
5. G. S. Ansell and F. V. Lenel, Acta Met., 8, 612, (1960).
6. N. R. Risebrough, Ph.D. Thesis, University of British Columbia, (1965).
7. G. H. Laurie and J. R. Wellington, "Zinc Extrusion", presented at Automotive Engineering Congress, Detroit, Mich., (1966).
8. J. A. Lund, D. Tromans, and S. F. Radtke, Inter. J. of Powder Met., 4, 41, (1968).
9. J. A. Lund et al., "Fundamental Investigation of Zinc Powder Metallurgy", for I.L.Z.R.O., 10, 14, 18, (1065-68).
10. P. Chaudhari, Sc. and Tech., 81, 42, (1968).
11. P. Chaudhari, I.B.M. Research Rep., RC-1946, (1967).
12. E. Underwood, J. of Met., 14, 915, (1962).
13. C. M. Packer and O. D. Sherby, A.S.M. Trans. Quart., 60, 21, (1967).
14. R. N. Stevens, Met. Rev., 11, 129, (1966).
15. R. C. Gifkins, J. of Am. Cer. Soc., 51, 69, (1968).
16. D. McLean, Rep. on Prog. in Physics, 29, 1, (1966).
17. D. McLean, Trans. A.I.M.E., 242, 1193, (1968).
18. J. J. Jonas, C. M. Sellars, and W. J. McG. Tegart, Met. Rev., 130, (1968).
19. D. L. Holt, Trans. A.I.M.E., 242, 25, (1968).
20. D. H. Avery and W. Backofen, A.S.M. Trans. Quart., 58, 551, (1965).
21. J. L. Walter and H. E. Cline, Trans. A.I.M.E., 242, 1823, (1968).

22. T. H. Alden and H. E. Cline, Trans. A.I.M.E., 239, 710, (1967).
23. T. H. Alden and H. W. Schadler, Trans. A.I.M.E., 242, 825, (1968).
24. W. H. McCarthy, J. C. Schyne and O. D. Sherby, Trans. A.S.M., 62, 117, (1969).
25. J. A. Lund and D. Tromans, A.S.M. Trans. Quart., 59, 672, (1966).
26. A. Kelly, "Fibre Reinforcement of Metals", Her Majesty's Stationery Office, London, (1965).
27. N. R. Risebrough and J. A. Lund, Trans. A.S.M., 61, 722, (1968).
28. E. H. Rennhack and G. P. Conard, Trans. A.I.M.E., 236, 694, (1966).
29. E. H. Rennhack and G. P. Conard, Trans. A.I.M.E., 236, 1441, (1966).
30. E. A. Anderson, E. J. Boyle and P. W. Ramsey, Trans. A.I.M.E., 156, 278, (1944).
31. E. Gebhardt, Z. Metallk., 33, 335, (1941).
32. W. Heine and U. Zwicker, Z. Metallk., 53, 380, (1962).
33. E. H. Rennhack, Trans. A.I.M.E., 236, 941, (1966).
34. T. W. Watson and G. H. Laurie, Cominco Internal Report, (1964).
35. Cominco, Internal Report, "The Effects of Extrusion Temperature on the Extrusion Textures of a Zn-0.16 wt.% Titanium Alloy", (1963).
36. J. L. Walker, "Liquid Metals and Solidification", (A.S.M. Cleveland, Ohio), (1958).
37. G. W. Groves and A. Kelly, Phil. Mag., 8, 877, (1963).
38. G. W. Groves, Phil. Mag., 18, 977, (1969).
39. U. F. Kocks and D. G. Westlake, Trans. A.I.M.E., 239, 1107, (1967).
40. W. J. McG. Tegart, Phil. Mag., 9, 339, (1964).
41. U. F. Kocks, Acta Met., 6, 85, (1958).
42. K. C. Donaldson, private communication.
43. K. E. Puttick, Acta. Met., 13, 1043, (1964).
44. T. H. Alden, Acta. Met., 17, 1435, (1964).
45. F. Garofalo, "Fundamentals of Creep and Creep Rupture in Metals", (MacMillan, New York), 184, (1965).

46. C. S. Barrett and T. B. Massalski, "Structure of Metals", (McGraw-Hill, New York), 47, (1966).
47. G. Woodford, Trans. A.S.M., 62, 291, (1969).
48. C. R. D'Antonio et al., Trans. A.I.M.E., 242, 2295, (1968).
49. D. M. Turner, unpublished.
50. H. Conrad, J. of Met., 16, 582, (1964).
51. J. D. Lubahn and R. P. Felgar, "Plasticity and Creep of Metals", (Wiley, New York), 291, (1961).
52. R. Armstrong et al., Phil. Mag., 7, 45, (1962).
53. J.C.M. Li, Trans. A.I.M.E., 227, 239, (1963).
54. D. V. Wilson and J. A. Chapman, Phil. Mag., 8, 1543, (1963).
55. R. C. Cook, M.A.Sc., Thesis, University of British Columbia, (1969).
56. W. A. Backofen and D. S. Fields, Trans. A.S.M., 51, 946, (1959).
57. R. L. Bell and R. W. Cahn, Phil. Mag., 239, 494, (1957).
58. H. Gleiter, Acta. Met., 17, 565, (1969).
59. M. F. Ashby et al., Trans. A.I.M.E., 245, 413, (1969).
60. H. J. McQueen, J. of Met., 20, 31, (1968).
61. J. J. Jonas, et al., Met. Rev., 130, 1, (1969).
62. H. E. Evans and R. P. Skelton, Met. Sc. J., 3, 152, (1969).
63. R. C. Gifkins et al., J. Aust. J. of Met., 11, 275, (1966).
64. R. Lagneborg, J. of Mat. Sc., 3, 596, (1968).
65. D. A. C. Williams et al., Sricp. Met., 3, 117, 1969.
66. L. Birk, "Electron Probe Microanalysis", (Interscience, New York), (1963).
67. T. H. Alden, Acta Met., 15, 469, (1967).